AD-A074 051 OHIO STATE UNIV COLUMBUS ELECTROSCIENCE LAB F/G 15/3
RADIATIVE TRANSMISSION LINE ANALYSIS.(U)
JUN 79 R J GARBACZ, J RICHMOND, B TRAN F19628-77-C-0069
UNCLASSIFIED ESL-784659-5 RADC-TR-79-158 NL

1 OF 2
AD
A074051

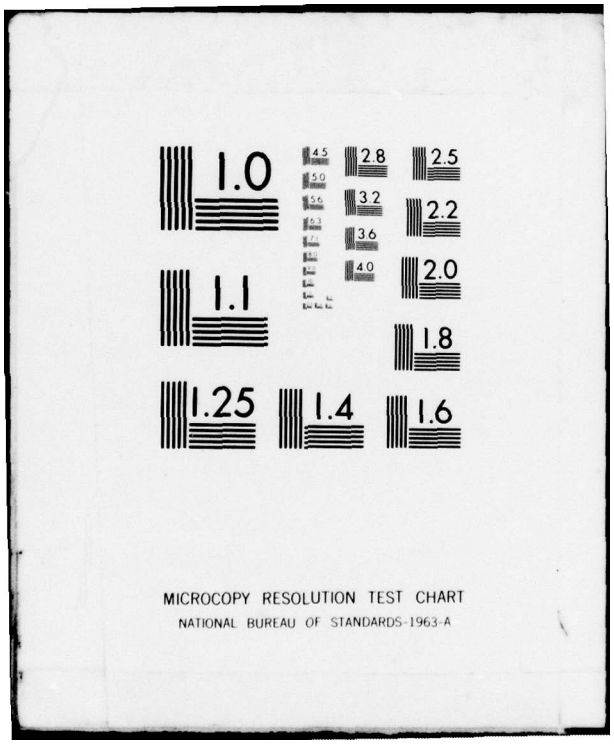
1.0
1.1
1.25
1.4
1.6
1.8
2.0
2.2
2.5
2.8
3.2
3.6
4.0
4.5
5.0
5.6
6.3
MICROCOPY RESOLUTION TEST CHART
NATIONAL BUREAU OF STANDARDS-1963-A

RADC-TR-79-158
Final Technical Report
June 1979

LEVEL II

RADIATIVE TRANSMISSION LINE ANALYSIS

The Ohio State University ElectroScience Laboratory

R. J. Garbacz
J. Richmond
B. Tran
M. Kuznetsov
F. McQuillin

ROME AIR DEVELOPMENT CENTER
Air Force Systems Command
Griffiss Air Force Base, New York 13441

This report has been reviewed by the RADC Information Office (OI) and is releasable to the National Technical Information Service (NTIS). At NTIS it will be releasable to the general public, including foreign nations.

RADC-TR-79-158 has been reviewed and is approved for publication.

APPROVED: John Antonucci

JOHN ANTONUCCI
Project Engineer

APPROVED: William R Baschnagel

WILLIAM R. BASCHNAGEL, LtCol, USAF
Asst Chief, Electromagnetic Sciences Division

FOR THE COMMANDER: John P. Huss

JOHN P. HUSS
Acting Chief, Plans Office

If your address has changed or if you wish to be removed from the RADC mailing list, or if the addressee is no longer employed by your organization, please notify RADC (EEC), Hanscom AFB MA 01731. This will assist us in maintaining a current mailing list.

Do not return this copy. Retain or destroy.

UNCLASSIFIED

SECURITY CLASSIFICATION OF THIS PAGE (When Data Entered)

REPORT DOCUMENTATION PAGE

READ INSTRUCTIONS BEFORE COMPLETING FORM

1. REPORT NUMBER: RADC-TR-79-158	2. GOVT ACCESSION NO.
3. RECIPIENT'S CATALOG NUMBER	
4. TITLE (and Subtitle): RADIATIVE TRANSMISSION LINE ANALYSIS	5. TYPE OF REPORT & PERIOD COVERED: Final Technical Report, 4 Feb 77 - 30 Sep 78
6. PERFORMING ORG. REPORT NUMBER: ESL-784659-5	
7. AUTHOR(s): R. J. Garbacz, M. Kuznetsov, J. Richmond, F. McQuillin, B. Tran	8. CONTRACT OR GRANT NUMBER(s): F19628-77-C-0069
9. PERFORMING ORGANIZATION NAME AND ADDRESS: The Ohio State University ElectroScience Laboratory, Department of Electrical Engineering, Columbus OH 43212	10. PROGRAM ELEMENT, PROJECT, TASK AREA & WORK UNIT NUMBERS: 62702F, 46001502
11. CONTROLLING OFFICE NAME AND ADDRESS: Deputy for Electronic Technology (RADC/EEC), Hanscom AFB MA 01731	12. REPORT DATE: June 1979
	13. NUMBER OF PAGES: 128
14. MONITORING AGENCY NAME & ADDRESS (if different from Controlling Office): Same	15. SECURITY CLASS. (of this report): UNCLASSIFIED
	15a. DECLASSIFICATION/DOWNGRADING SCHEDULE: N/A

16. DISTRIBUTION STATEMENT (of this Report)

Approved for public release; distribution unlimited.

17. DISTRIBUTION STATEMENT (of the abstract entered in Block 20, if different from Report)

Same

18. SUPPLEMENTARY NOTES

RADC Project Engineer: John Antonucci (RADC/EEC)

19. KEY WORDS (Continue on reverse side if necessary and identify by block number)

Goubau line	Periodic dipole
Surface waves	Array
Transmission line	Attenuation
Yagi	Propagation
Barrier sensor	Leaky coaxial cable

20. ABSTRACT (Continue on reverse side if necessary and identify by block number)

This Final Report summarizes the results of work accomplished from 4 February 1977 to 30 September 1978 on the theoretical analysis of two types of transmission lines for use as intruder sensors.

One type is the Yagi line consisting of uniformly spaced, imperfectly conducting thin rods of identical length which are suspended a uniform height above and perpendicular to a lossy flat earth. For (Cont'd)

DD FORM 1 JAN 73 1473

402 254

UNCLASSIFIED

SECURITY CLASSIFICATION OF THIS PAGE (When Data Entered)

Item 20 (Cont'd)

the major mode supported by this structure, data are displayed of attenuation constant and phase velocity associated with a variety of design parameters. For a limited number of cases radiative losses and reflections at circular bends in the line are shown, as are suggested feed and termination configurations. Some calculated field distributions are also presented, as are some estimates of the reflection expected from an idealized (metallic wire) intruder. Some experimental data taken on a scaled model are included to verify certain results calculated from theory.

A second type of line investigated theoretically is the single coaxial cable whose outer shield is perforated by circumferential rectangular slots, each one narrow in longitudinal extent, subtending an arc of arbitrary length and spaced uniformly along the line's extent. The cable has an imperfectly conducting circular center conductor separated by a lossy dielectric from the outer shield which is assumed to be perfectly conducting and infinitesimally thin. This configuration is enclosed in a circular sheath of lossy dielectric and the whole is assumed to be suspended above or buried within a lossy flat earth. For one geometry corresponding to a commercially available version of this so-called "leaky" coaxial cable (Andrew Corporation's Radiax cable) data are presented of the attenuation constants and phase velocities of the major modes found to exist on the structure. A few examples of the corresponding field configurations are also given.

As a prelude to work on the leaky coaxial cable, some effort was expended to develop the theory of the Goubau line over the flat earth as well as that of the coaxial cable with 360^{0} circumferential slots over the flat earth. In addition, although tangential to the main thrust of the contract, theory was developed for the leaky coaxial cable centered in a cylindrical tunnel through earth. This latter theory could easily be changed to accommodate a cable located eccentrically in a tunnel.

The report concludes with a discussion of the utility of the lines as intruder sensors and suggestions for future work.

CONTENTS

Evaluation

1. This contract was to investigate guided wave structures of about one mile long which might be used as intruder sensors. The guided wave transmission line was to operate in the presence of a lossy earth. The predominant structure examined was the Yagi Transmission line. It consisted of uniformly spaced imperfectly conducting thin rods (dipoles) of equal length held above and perpendicular to a lossy earth. The effect of bends were included in the study. The attenuation, phase velocity and surface wave field were determined as a function of the various parameters of the line. The effect of a simulated intruder was also determined.

2. It was found that a Yagi line was not sensitive enough to detect an intruder, although, improvements do seem possible.

3. Generally, much was learned of the Yagi line and the influence of its parameters. Enough knowledge has been attained so as to be able to consider making use of the line in conjunction with other structures. The treatment here is quite thorough and permits speculation for future work.

John Antonucci

JOHN ANTONUCCI
Project Engineer

I. INTRODUCTION

In the not-distant future it is expected that critical permanent areas, such as nuclear power plants, nuclear waste sites, dams, water supplies, prisons, etc., as well as semi-permanent areas such as forward located airstrips, docking sites, etc., which are vulnerable to noncooperative intruders, will require protection by one or several means, from physical barriers to electronic sensors. With this potential need in mind, the present contract was undertaken to investigate and evaluate a few electromagnetic guided wave structures which appear to be suitable for use as intruder sensors for barriers of length up to one mile. Of necessity, any such structure must operate in the presence of lossy earth and theory of the resulting attenuation of the guided wave must take this source of loss into consideration. Additionally, it was suggested that the guided field structure should be sensitive to an intruder within a longitudinally oriented region approximately 2 meters wide and 3 meters high and be such that it cannot be penetrated from beneath without detection. Frequency of operation was specified to lie in the range 50-500 MHz, particularly below 100 MHz where data indicate a broad resonance in standing human scatterers. This report summarizes the results of theoretical analyses of two types of guided wave structures - the Yagi transmission line and the "leaky" coaxial cable. Peripheral results are also presented for the Goubau line.

The Yagi (or Yagi-Uda) transmission line consists of uniformly spaced, imperfectly conducting thin rods of identical length suspended a uniform height above and perpendicular to a lossy flat earth[1-7]. For the major mode supported by this structure, data are presented of attenuation constant and phase velocity associated with a variety of design parameters. For a limited number of representative cases radiation losses and reflections at 90^{o} circular bends in the line are shown, as are suggested feed and termination configurations. Some calculated

field distributions are also presented, as are estimates of the reflection expected from an idealized (metallic wire) "intruder". Limited experimental data taken on a scaled model are included to verify certain results calculated from theory. Improvements in the theory are also suggested and discussed.

The leaky coaxial cable is being investigated by several groups[18-26] as a potential intruder sensor and their experimental results indicate that it is a promising candidate. At the start of the present contract we or the sponsor know of no theoretical model developed for the particular type of cable investigated here from which numerical results could be calculated for propagation constants and field structure. It was considered useful that such a theoretical model be available to help explain some of the observed characteristics of leaky coaxial cable and, should it be incorporated into sensor systems, to provide some guidance in the design of the cable itself and its deployment geometry. Thus, some effort was expended in the latter half of the present contract to develop a theory for the single leaky coaxial cable in the presence of a lossy flat earth. Although this cable is usually used in a parallel pair configuration, time considerations forced us to leave this interesting extension undone.

The geometry considered consists of a single coaxial cable whose imperfectly conducting circular center conductor is separated by a lossy dielectric from the outer shield which is assumed to be perfectly conducting and infinitesimally thin. This outer shield, rather than braided, is perforated by circumferential rectangular slots, each are narrow in longitudinal extent, subtending an arc of arbitrary length and spaced uniformly along the line's extent. This configuration is enclosed in a circular sheath of lossy dielectric and the whole is assumed to be suspended above or buried within a lossy flat earth. For one geometry corresponding to a commercially available version of this line (Andrew Corporation's Radiax line (27)) data are presented of the attenuation constants and phase velocities of the major modes found to exist on

the structure. A few examples of the corresponding field configurations are also given. As a special case which is interesting in its own right, the leaky coaxial cable was assumed to reside along the centerline of a cylindrical tunnel through lossy earth. If necessary the theory can readily be modified to accommodate an eccentric cable and thus form the basis for designing an open communication system in tunnels - a subject of interest in recent literature[28-38].

The report closes with a discussion of the utility of the lines considered here as intruder sensors and suggestions for future work.

II. THE YAGI TRANSMISSION LINE

A. Synopsis of Theoretical Approaches

Although most theoretical work under this contract centered on the straight Yagi line of infinite extent because this geometry presented a tractable boundary value problem in classical format, certain questions posed by the sponsor, such as those involving radiative losses at bends, feed and termination configurations, and reflection from an intruder, could best be answered for a finite Yagi line using a computer-oriented approach such as that provided by the method of moments. In this section we summarize, in varying detail, the two approaches.

1. The Infinite Line

In this section expressions are developed for the surface-wave fields and the transcendental equation whose root determines the complex propagation constants of the surface wave supported by an infinitely long Yagi line in free space and over the flat earth.[1,2]

Figure 1 illustrates a periodic array of dipoles in free space. Each dipole is a straight wire with length $\ell = 2h$, radius "a" and conductivity σ. Each wire is parallel with the z axis, and s denotes the

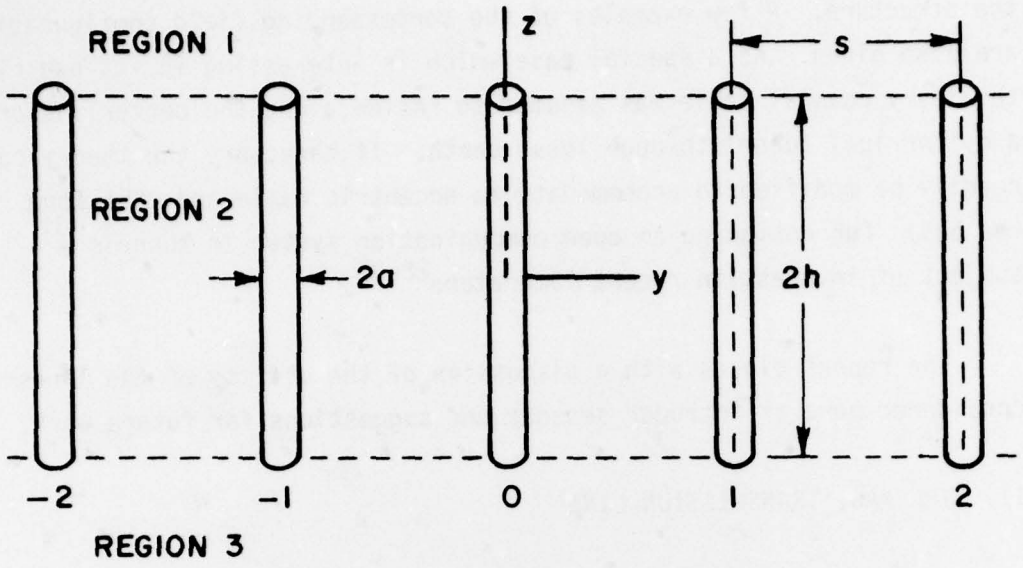

Figure 1. Periodic array of dipoles in free space.

spacing between the axes of neighboring wires. The time dependence $e^{i\omega t}$ is understood. The surface impedance Z_s is defined in terms of the field on the surface of dipole number 0 as follows:

$$E_x(a,x) = Z_s\, H_\phi(a,z) \qquad \text{for } -h < z < h \quad . \tag{1}$$

Ampere's law relates H_ϕ to the current distribution, so that Equation (1) can be written as follows:

$$E_z(a,x) = Z_s\, I_0(x)/(2\pi a) \tag{2}$$

where $I_0(z)$ represents the current distribution on dipole 0. A valid relation can be obtained by multiplying both sides of Equation (2) by $I_0(z)$ and integrating. This leads to the following relaxed boundary condition:

$$\int_{-h}^{h} I_0(z)\, E_z\, E_z(z)\, dz = \frac{Z_s}{2\pi a} \int_{-h}^{h} I_0^2(z)\, dz \tag{3}$$

$$E_z = E_z^i + E_z^r \tag{4}$$

$$E_z^i = E_o + \sum_{n=1}^{\infty} (E_n + E_{-n}) \tag{5}$$

where E_n denotes the free-space field of dipole n and E_z^r denotes the field reflected from the flat earth.

Let I_{on} denote the current at the center of dipole n. When a surface wave propagates on the dipole array, the dipole currents are given by

$$I_{on} = I_{oo}\, e^{n\gamma s} \tag{6}$$

where γ denotes the propagation constant for the surface wave. From Equations (1)-(6), the terminal voltage at dipole 0 is

$$V(\gamma) = Z_o + Z_o^r + 2 \sum_{n=1}^{\infty} Z_n \cosh(n\gamma s) = 0. \tag{7}$$

The term Z_o^r vanishes for a dipole array in free space. The mutual impedance between dipoles 0 and n in free space is defined by

$$Z_n = \frac{-1}{I_{oo}\, I_{on}} \int_{-h}^{h} I_o(z)\, E_n(z)\, dz\ . \tag{8}$$

If the dipole length ℓ does not exceed $\lambda/2$, a suitable trial function for the current distribution on dipole n is

$$I_n(z) = I_{on} \frac{\sin k(h - |z|)}{\sin kn} \tag{9}$$

where $k = \omega\sqrt{\mu_o \varepsilon_o}$. Corresponding to equations (8) and (9), the mutual impedance Z_n is given by Schelkunoff and Friis[39] for parallel filamentary sinusoidal dipoles with spacing $\rho = |ns|$. The self impedance of dipole 0 (in free space) is

$$Z_o = Z_{oo} + \frac{[kh - \sin(kh)\cos(kh)]\, Z_s}{2\pi\, ka \sin^2(kh)} \qquad (10)$$

where Z_{oo} denotes the self impedance of a perfectly conducting dipole in free space. To calculate Z_{oo}, we consider the mutual impedance of filamentary sinusoidal dipoles with spacing $\rho = a$. The term Z_o^r represents the contribution to $V(\gamma)$ arising via reflection from the flat earth, and it is considered later.

In Equation (7), $V(\gamma)$ denotes the voltage appearing across the short-circuited terminals of dipole 0 with a terminal current I_{oo} of one ampere. This voltage must vanish, and Equation (7) is the transcendental equation for the system. The propagation constant γ for the surface wave is determined by searching for a root of $V(\gamma)$. As usual, we let $\gamma = \alpha + j\beta$. For a perfectly conducting array over a lossless dielectric half-space, the attenuation constant α vanishes and the series in Equation (7) converges slowly. When the dipoles and/or the earth have finite conductivity, α is positive and the series diverges. To improve this situation, we add and subtract (in Equation (7)) the following asymptotic form of the mutual impedance:

$$Z_n \tilde{=} (D/n)\, e^{-jkns} \qquad (11)$$

$$D = \frac{j\,(1 - \cos kh)^2}{\pi ks \sin^2 kh} \qquad (12)$$

where $\eta = \sqrt{\mu_o/\varepsilon_o}$. This leads to the following transcendental equation:

$$V(\gamma) = Z_o + Z_o^r - D\,\ell n[1 - \exp(\gamma s - jks)] - D\,\ell n[1 - \exp(-\gamma s - jks)]$$
$$+ 2 \sum_{n=1}^{\infty} [Z_n - (D/n)e^{-jkns}] \cosh(n\gamma s) = 0. \qquad (13)$$

When α and Z_o^r vanish, Equation (13) reduces precisely to the transcendental equation used earlier[14] for a perfectly conducting dipole array

in free space. For this and other reasons, it is convenient to refer to "analytic continuation" as the basis for Equation (13). When α = 0, the series in Equation (13) converges rapidly and the following number of terms is sufficient[14]:

$$N = 1 + 17\ h/s\ . \tag{14}$$

When α is positive, we still use Equations (13) and (14). Newton-Raphson iteration is convenient for locating the root of Equation (13).

In deriving Equation (13) we used the following:

$$\sum_{1}^{\infty} \frac{e^{nz}}{n} = -\ \ell n(1 - e^{z}) \tag{15}$$

where z denotes a complex constant. Equation (15) can be found in the literature for the special cases where z is imaginary or negative real. In the general case it can be derived formally by integrating (with respect to z) both sides of the following summation formula:

$$\sum_{1}^{\infty} e^{nz} = e^{z}/(1 - e^{z})\ . \tag{16}$$

If the hyperbolic function in Equation (7) is written as the sum of two exponentials, then Equation (7) contains the sum of a divergent series and a convergent series. The divergent series is given by

$$V_1(\gamma) = \sum_{1}^{\infty} Z_n\ e^{n\gamma s}\ . \tag{17}$$

From Equations (11), (15) and (17),

$$V_1(\gamma) = -\ D\ \ell n\ [1 - e^{(\gamma - jk)s}] + \sum_{1}^{\infty} [Z_n - (D/n)e^{-jkns}]e^{n\gamma s}. \tag{18}$$

When α is positive, the series eventually diverge in Equations (17) and (18), although they appear to be converging when n is small. Therefore, results obtained with the transcendental Equation (13) are not

considered reliable until they are confirmed by other methods. Confirmation has been obtained by several methods.

In method 1, we use Equations (11) and (17) to obtain

$$V_1 = \sum_{1}^{M} Z_n e^{n\gamma s} + D \sum_{M+1}^{\infty} \frac{e^{(\gamma - jk)ns}}{n} \tag{19}$$

where M is large enough to justify the asymptotic form. If αs and $(\beta - k)$s are small, the last series in Equation (19) is nicely approximated by an integral as follows:

$$V_1 \simeq \sum_{1}^{M} Z_n e^{n\gamma s} + D \int_{M+\frac{1}{2}}^{\infty} \frac{e^{(\gamma - jk)sx}}{x} \, dx \, . \tag{20}$$

This integral is recognized as the exponential integral $E_1(z)$ where $z = -(M+\frac{1}{2})(\gamma - jk)s$. Of course, the integral in Equation (20) diverges, and we may replace it with $E_1(z)$ only if we are willing to accept the implied deformation of the path of integration. When αs and $(\beta - k)$s are small, the results obtained with method 1 (Equation (20)) agree closely with those obtained with analytic continuation (Equation (13)).

When method 1 begins to fail, method 2 becomes effective. In method 2 we consider a large but finite linear array of parallel dipoles with uniform length and spacing. We insert a one-volt generator at the center of the dipole at one end of the array, invert the impedance matrix and thus solve for the currents on all the dipoles. Since the impedance matrix has the Toeplitz form, it takes only a few seconds to carry out this operation for an array of 200 dipoles. Now the current I_{on} is known at the center of each dipole. On the dipoles near an end of the array, the current on one dipole may bear little relation to the currents on the neighboring dipoles. For a small group of dipoles at the center of the array, however, it is reasonable to assume the currents are related as follows:

$$I_{on} = C_1 e^{n\gamma_1 s} + C_2 e^{-n\gamma_1 s} + C_3 e^{n\gamma_2 s} + C_4 e^{-n\gamma_2 s} \quad . \qquad (21)$$

Thus we are postulating two modes propagating in each direction along the array. There are four unknown coefficients C_i and two unknown propagation constants. By using the recursion relations for the exponential and hyperbolic functions, it turns out that we can easily solve for γ_1 and γ_2 if the currents I_{on} are known on any group of six consecutuve dipoles. In this manner we calculated γ_1 and γ_2 for an array of 190 dipoles with various lengths and spacings. In all cases where we were able to fund a root of Equation (13), it turned out that γ_1 was associated with the surface wave of interest here. Furthermore, when αs and $(\beta-k)s$ are not too small, method 2 yields values of γ_1 showing close agreement with those obtained with analytic continuation. The values of γ_2 indicate a wave propagating essentially with the speed of light and with a comparatively large attenuation constant. Although this wave is not well understood, it may be the free-space radiation emanating from each end of the finite array. Waves of this type would presumably propagate at the speed of light and would not possess a true attenuation constant. Instead, they would behave like $(1/R)e^{-jkR}$ where R denotes the distance from a "radiation center". Over the range of six consecutive dipoles at the center of the array, however, the function 1/R can be approximated by the function $e^{-\gamma R}$.

It was found that method 2 fails if the last two terms are deleted in Equation (21). This indicates that two distinct modes are prominent even in the central region of an array of 190 dipoles.

Finally, conservation of energy was employed to check the attenuation constant obtained via Equation (13). The check proceeded as follows. We considered a surface wave propagating in the negative y direction on a periodic array of dipoles in free space as in Figure 1. Using the field expressions presented here, we integrated the Poynting vector over the plane surface $y = y_1$ to determine the time-average power transmitted in the (-y) direction. Conservation of energy requires that

$$P_t(s/2) - P_t(-s/2) = P_d \qquad (22)$$

where $P_t(y)$ denotes the time-average power transmitted and P_d denotes the time-average power dissipated in dipole 0. Using the value of β obtained via Equation (13), we calculated the various quantities in Equation (22) and used Newton-Raphson iteration to adjust α until Equation (22) was satisfied. It was found that the value of α obtained in this manner agreed closely with that obtained via Equation (13).

In view of the results obtained with method 1, method 2 and conservation of energy, we concluded that the method of analytic continuation (Equation (13)) is valid even though its derivation is questionable.

As is done in Equation (4), it is convenient to express the surface-wave field as the sum of the incident field (generated by the dipole currents radiating in unbounded free space) and the reflected field arising via reflection from the air-earth interface. We are now prepared to develop suitable expressions for the incident field.

It must be kept in mind that we require incident field expressions in a form that will permit application of the boundary conditions at the air-earth interface. The Poisson sum formula may be thought to be useful for this purpose. Difficulties arise however when one attempts to apply the Poisson sum formula to the field of the surface wave. Although the field of one sinusoidal dipole has a simple closed form, a divergent series results from summing over all the dipoles in the array. However, Floquet's theorem suggests an alternative approach.

To simplify the field expressions, let us replace the round wires with thin metal strips lying in the yz plane. Then the volumetric current density for dipole n is given by

$$J_n = \hat{z}\, e^{\gamma ns}\, \delta(x)\, P(y-nx)\, I_o(z)/w \quad \text{amperes/m}^2 \tag{23}$$

where γ denotes the propagation constant for the surface wave on the array of dipoles over the flat earth, and P(y-ns) denotes a pulse function with unit height and width w, centered at y = ns. So that the field of the strips will closely resemble the field of the round wires, we choose w = 4a for the width of the strips. If w is much smaller than s, we can replace $e^{\gamma ns}$ with $e^{\gamma y}$ in Equation (23) because the two functions are essentially equal in the small region where P(y-ns) does not vanish. Using the Fourier transform, we can express Equation (23) as follows:

$$\vec{J}_n = \frac{\hat{z}\, I_o(z)\, e^{\gamma y}}{\pi^2\, w} \int_{-\infty}^{\infty} \frac{\sin(pw/2)}{p}\, e^{-jpns}\, e^{jpy}\, dp \int_0^{\infty} \cos(fx)\, df. \tag{24}$$

By summing on n and using Equations (3-41) and (3-44) in Reference 40, we obtain the current density of the periodic array of strip dipoles:

$$J_z = \frac{I_o(z)e^{\gamma y}}{s} \sum_{m=-\infty}^{\infty} S_m(y) \int_0^{\infty} \cos(fx)df \tag{25}$$

$$S_m(y) = \frac{\sin(m\pi w/s)}{m\pi w/s}\, e^{j2m\pi y/s} \tag{26}$$

where $I_o(z)$ is given by Equation (9) and $S_o(y) = 1$.

Using Equation (25), it is not difficult to show that the free-space field of the periodic array of dipoles is:

$$E_x^i = - A\, e^{\gamma y} \sum_{m=-\infty}^{\infty} S_m(y) \int_0^{\infty} f \sin(fx)\, Q(z)\, df \tag{27}$$

$$E_y^i = A\, e^{\gamma y} \sum (\gamma + j2m\pi/s)\, S_m(y) \int \cos(fx)\, Q(z)\, df \tag{28}$$

$$E_z^i = \begin{cases} -A\, e^{\gamma y} \sum S_m(y) \int (k^2+g^2)\, \dfrac{\cos(fx)}{g}\, P(z)\, df, \text{ in Regions 1,3} & (29a) \\ 2kA\, e^{\gamma y} \sum S_m(y) \int \left[e^{-g|z|}\cos(kh) - e^{-gh}\cosh(gz)\right] \dfrac{\cos f(x)}{g}\, df, \text{ in Region 2} & (29b) \end{cases}$$

$$A = \frac{j\, I_{oo}\eta}{2\pi\, ks\, \sin kh} \tag{30}$$

$$g^2 = f^2 - (\gamma + j2m\pi/s)^2 - k^2 \tag{31}$$

$$P(z) = \int_{-h}^{h} \sin k(h - |z'|)\, e^{-g|z-z'|}\, dz' \tag{32}$$

$$Q(z) = \int_{-h}^{h} \mathrm{sgn}(z-z')\, \sin k(h - |z'|)\, e^{-g|z-z'|}\, dz'. \tag{33}$$

In regions 1 and 3 of Figure 1, where $|z| > h$,

$$P(z) = 2k\, e^{-g|z|}\, (\cosh gh - \cos kh)/(k^2 + g^2) \tag{34}$$

$$Q(z) = P(z)\, \mathrm{sgn}(z)\ . \tag{35}$$

In region 2, where $|z| < h$,

$$P(z) = 2\left[g \sin k(h-|z|) + k \cosh(g|z|)e^{-gh} - k \cos(kh)e^{-g|z|}\right]/(k^2+g^2) \tag{36}$$

$$Q(z) = 2k\left[\cos k(h-|z|) - \sinh(g|z|)e^{-gh} - \cos(kh)e^{-g|z|}\right] \frac{\mathrm{sgn}(z)}{k^2+g^2}\ . \tag{37}$$

The magnetic field intensity is found from curl $\bar{E}$, and it is observed that $H_z^i = 0$. It has been verified that the given field satisfies the appropriate wave equation in each region and continuity of the tangential field components across the boundaries between adjacent regions.

Now that suitable expressions are available for the incident field, we are in a position to consider the fields reflected from the air-earth interface.

Figure 2 illustrates a periodic array of vertical dipoles over the flat earth. The field incident on the air-earth interface is given by Equations (27-35). Everywhere in region I (the upper half-space), the reflected field is:

$$E_x^r = e^{\gamma y} \sum S_m \int \frac{fg\ RC\ \sin(fx)\ e^{-gz}\ df}{k^2 + g^2} \tag{38}$$

$$E_y^r = -\ e^{\gamma y} \sum (\gamma + j2m\pi/s) S_m \int \frac{g\ RC\ \cos(fx)\ e^{-gz}\ df}{k^2 + g^2} \tag{39}$$

$$E_z^r = e^{\gamma y} \sum S_m \int RC\ \cos(fx) e^{-gz}\ df \tag{40}$$

$$C = \frac{-j\ \eta I_{oo}\ (\cosh gh - \cos kh)}{\pi\ gs\ \sin kh}\ . \tag{41}$$

Everywhere in region II (the lower half-space), the transmitted field is

$$E_x^t = -\ e^{\gamma y} \sum S_m \int \frac{fg\ TC\ \sin(fx) e^{qz}\ df}{q^2 - \gamma_2^2} \tag{42}$$

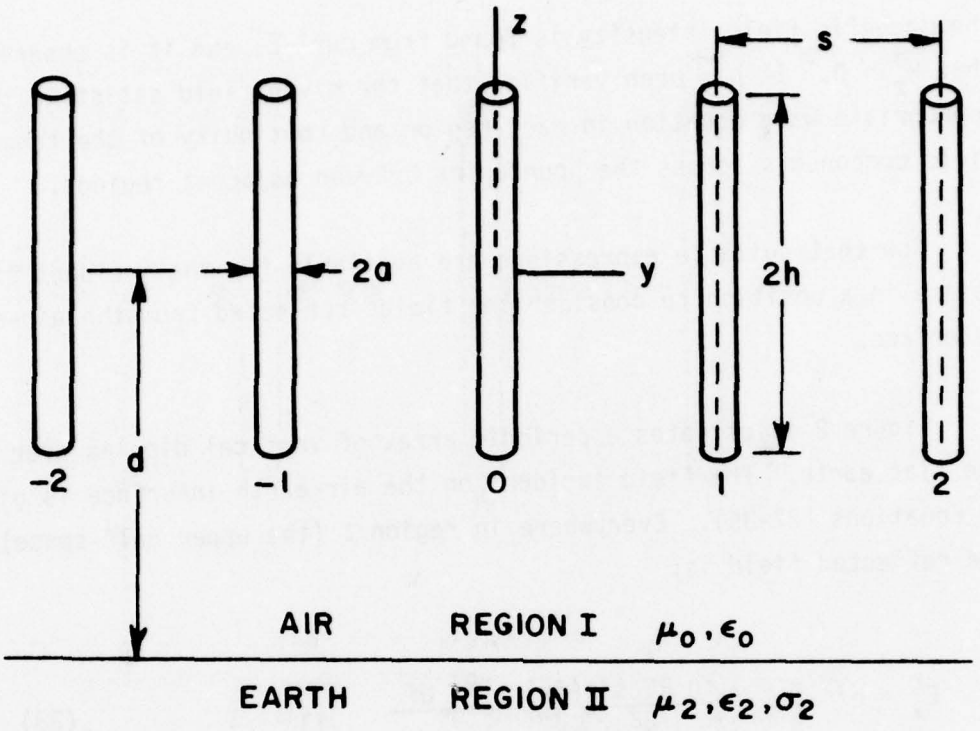

Figure 2. Periodic array of vertical dipoles over the flat earth.

$$E_y^t = e^{\gamma y} \sum (\gamma + j2m\pi/s)\, S_m \int \frac{q\, TC \cos(fx) e^{qz}\, df}{q^2 - \gamma_2^2} \tag{43}$$

$$E_z^t = e^{\gamma y} \sum S_m \int TC \cos(fx) e^{qz}\, df \tag{44}$$

$$q^2 = \gamma_2^2 - (\gamma + j\, 2m\pi/s)^2 + f^2 \tag{45}$$

$$\gamma_2^2 = j\omega\mu_2\sigma_2 - \omega^2\mu_2\epsilon_2 \,. \tag{46}$$

It is found that $H_z^r = 0$ and $H_z^t = 0$. The tangential components of $\vec{E}$ and H must be continuous across the air-earth interface. By enforcing these boundary conditions, we determine the reflection coefficient R and the transmission coefficient T:

$$R = \frac{(g\varepsilon_c - q\varepsilon_o)e^{-2gd}}{g\varepsilon_c + g\varepsilon_o} \tag{47}$$

$$T = \frac{2\, g\varepsilon_o\, e^{-gd}\, e^{qd}}{g\varepsilon_c + q\varepsilon_o} \tag{48}$$

$$\varepsilon_c = \varepsilon_2 - j\sigma_2/\omega\ . \tag{49}$$

Now that expressions are available for the field reflected from the air-earth interface, we are in a position to evaluate the term Z_o^r *in the transcendental equation.*

The reflected field makes the following contribution to the voltage V( ) in Equations (7) and (13):

$$Z_o^r = \frac{-1}{I_{oo} \sin kh} \int_{-h}^{h} \sin k(h-|z|) E_z^r(0,0,z)\, dz\ . \tag{50}$$

From Equations (40) and (50),

$$Z_o^r = \frac{-2k}{I_{oo} \sin kh} \sum_{m=-\infty}^{\infty} S_m(0) \int_o^{\infty} \frac{(\cosh gh - \cos kh)RC\, df}{k^2 + g^2}\ . \tag{51}$$

Specific numerical results derived from the above theory are given in Section IIB.

2. The Finite Line

The foregoing theory is suited for ideally periodic structures i.e., those of infinite extent. If, however, we wish to investigate the effects of bends in the line, or of various terminations and feeds, or of an obstacle placed near the line, it is appropriate to apply the method of moments[41-42] to a Yagi line of finite extent. By the method of moments we mean nothing more than a computer-oriented technique whereby the integral equation, derived from Maxwell's equations subject to the appropriate boundary conditions at the dipoles, is approximated by a set of simultaneous linear algebraic equations whose unknowns are the currents induced on the dipoles by some given primary (voltage) source. In this method, each dipole is considered to be divided into N segments and a piecewise-sinusoidal current of unknown amplitude is assumed on each segment. These current amplitudes form the unknowns. Written in matrix form, the problem reduces to one of inverting the kernal matrix (usually an impedance matrix) by some algorithm suited to the digital machine, whereby one obtains numerical values for the current distributions on each dipole.

Under this contract we considered by the above technique only Yagi lines in free-space; the earth can be incorporated if one is willing to accept considerable complications in the formulation of the fields. Up to 200 dipoles were considered, but most computations were made with fewer than 100 dipoles and in some cases as few as 30 dipoles.

The primary source usually consisted of a voltage source at the center of a dipole, or several sources in adjacent dipoles phased to correspond to the phase velocity of the propagating surface wave.

Specific numerical results involving bends in the Yagi line, intruder effects and feed and termination designs are given in Section IIB.

B. Some Calculated Results

Because the Yagi line has so many parameters available to the designer (one of the reasons we selected this structure) it was difficult under this contract alone to amass all the data necessary to form a complete picture of the line's behavior. In this section we present certain calculated data, based upon the approaches just described, to give some idea of the line's potential as an intruder sensor. Some of the computer codes employed are given in References 1 and 2, should more data be desired; other computer codes (specifically, those involving the finite line) are not documented explicitly.

Figures 3 and 4 are contour plots of the relative phase velocity and attenuation constant of the primary mode supported by the infinitely long Yagi line of copper rods of radius 0.001 operating at 300 MHz in free space. Figures 5-8 present the same data in a different form. Comparing Figures 5-8 with Figures 9-12 will give some feeling for the effects of reducing the dipole radii from 0.001λ to 0.00067λ, all other parameters being fixed.

All the above figures show the same trends: (1) the surface wave slows down with increasing dipole length and with decreasing dipole spacing, all other parameters being fixed, (2) slowing down the wave either by increasing dipole length or by decreasing dipole spacing increases the attenuation constant due to increased copper loss, (3) slowing down the wave binds the surface wave more tightly to the structure. The last fact may be deduced from Equations (27)-(37) and based upon these equations we have calculated and plotted fields for a few cases. Figures 13-18 present magnitude of the electric field component E_z parallel to the dipoles as a function of the transverse distance from the dipoles along the line y=0, z=0 (i.e., in the plane of a dipole). The dipoles are copper rods of radius 0.001λ, the frequency is 300 MHz, and the four curves on each figure correspond to dipole lengths of $2h/\lambda = 0.36, 0.40, 0.42$ and 0.44. Dipole spacings considered are $s/\lambda = 0.30,$

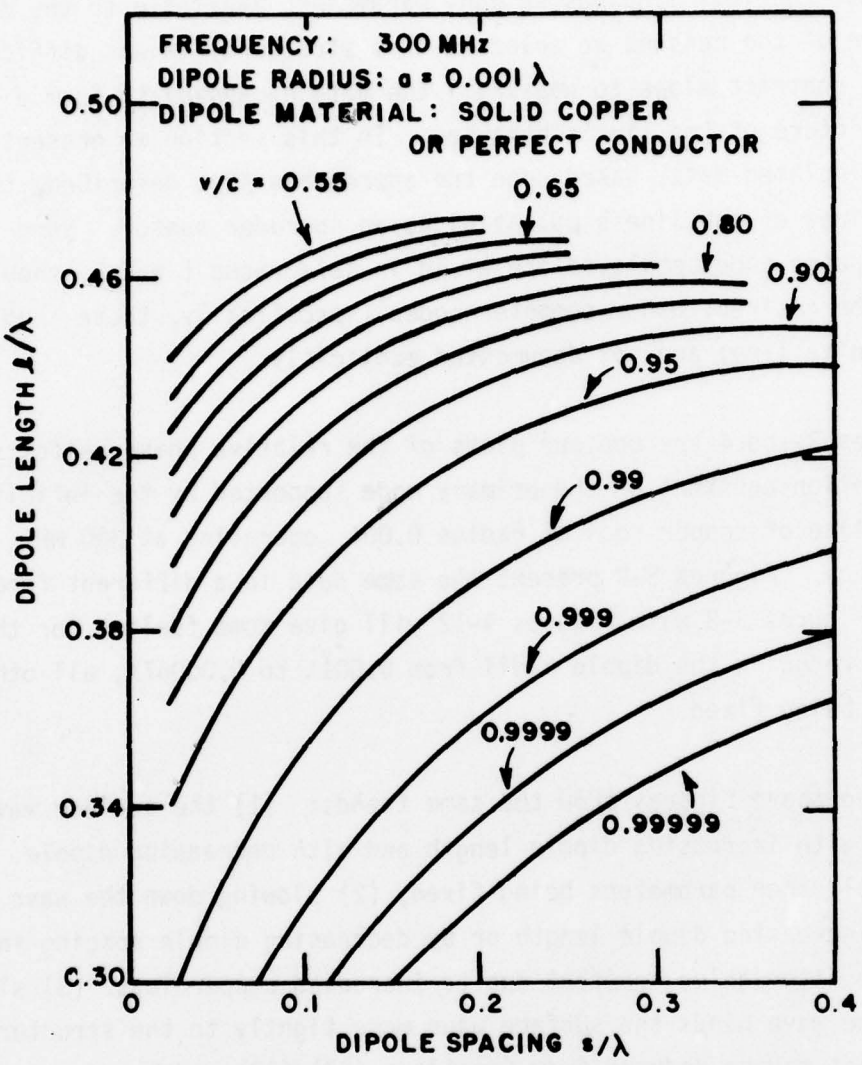

Figure 3. Contours of constant phase velocity for surface wave on periodic array of dipoles in free space.

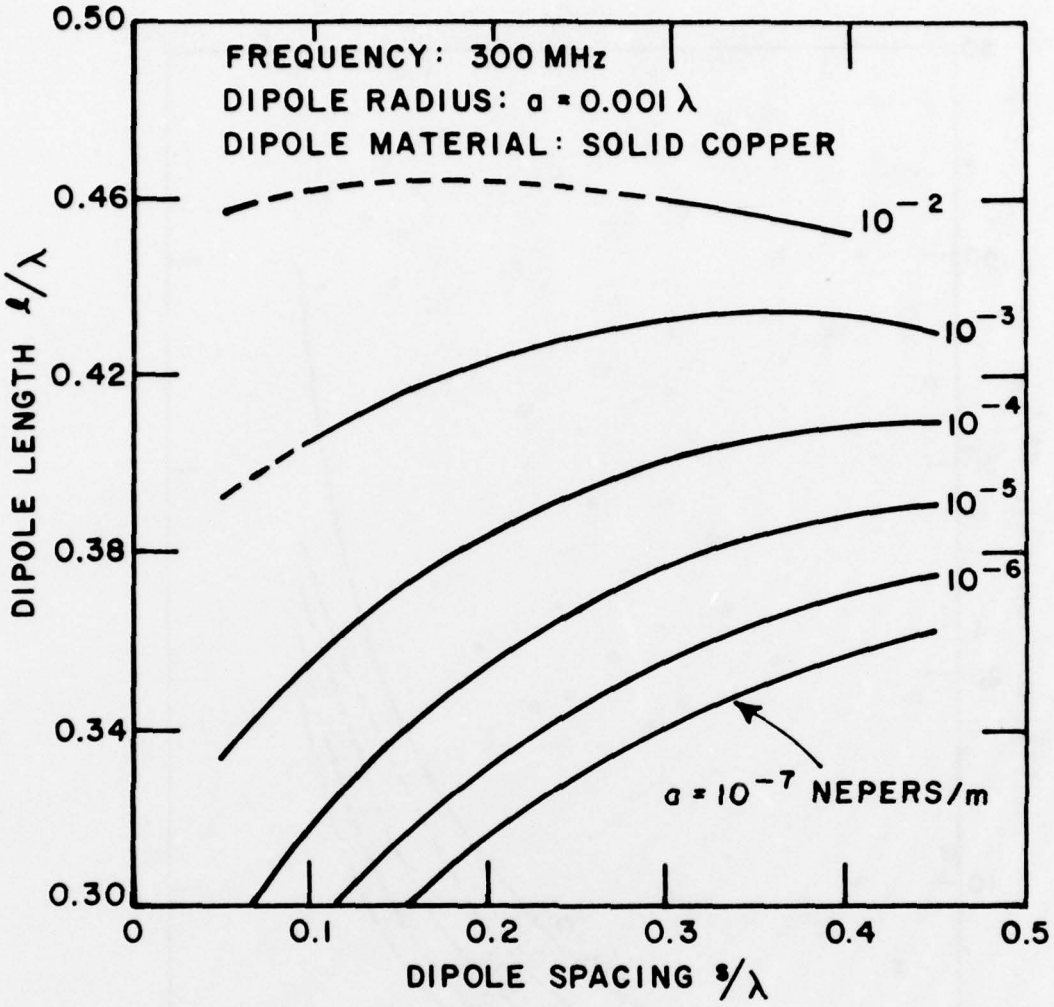

Figure 4. Contours of constant attenuation for surface wave on periodic array of dipoles in free space.

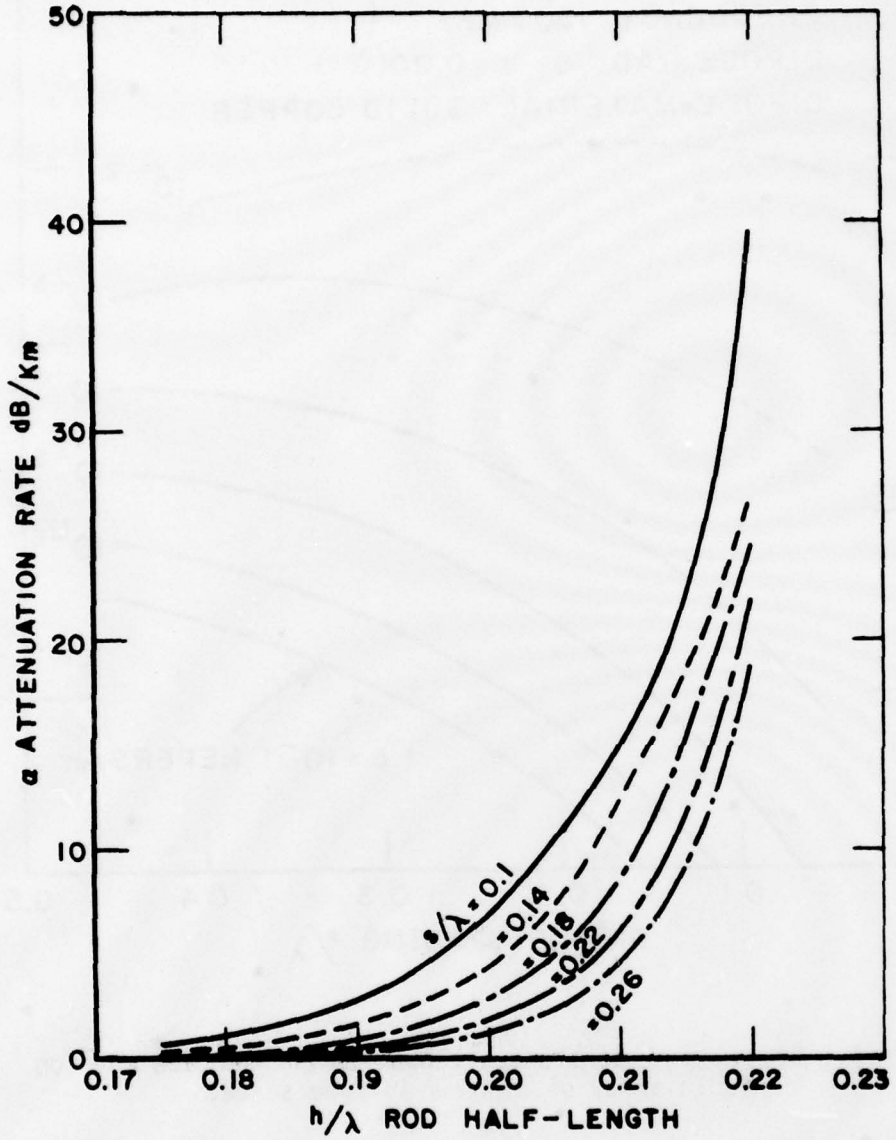

Figure 5. Attenuation constant versus dipole length for copper dipoles with a = 0.001 wavelength. f = 300 MHz.

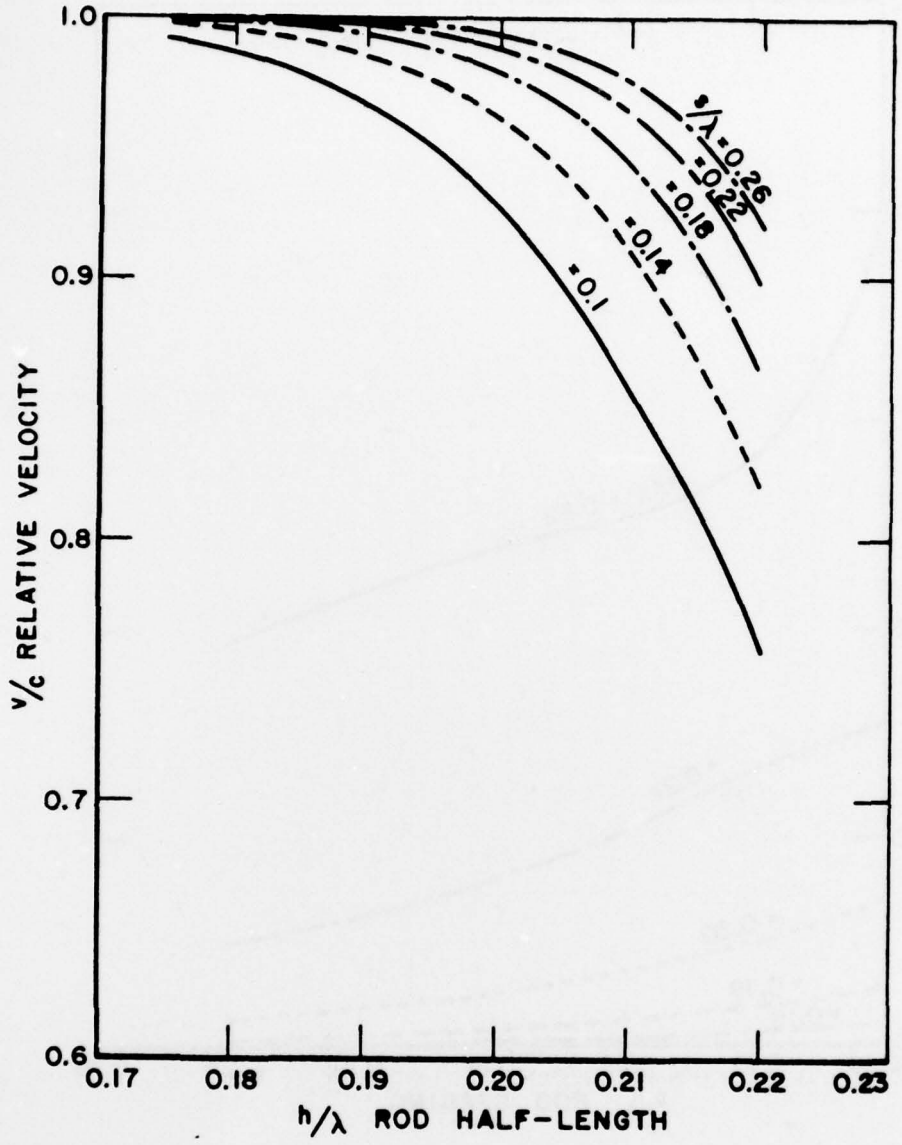

Figure 6. Phase velocity versus dipole length for copper dipoles with a = 0.001 wavelength. f = 300 MHz.

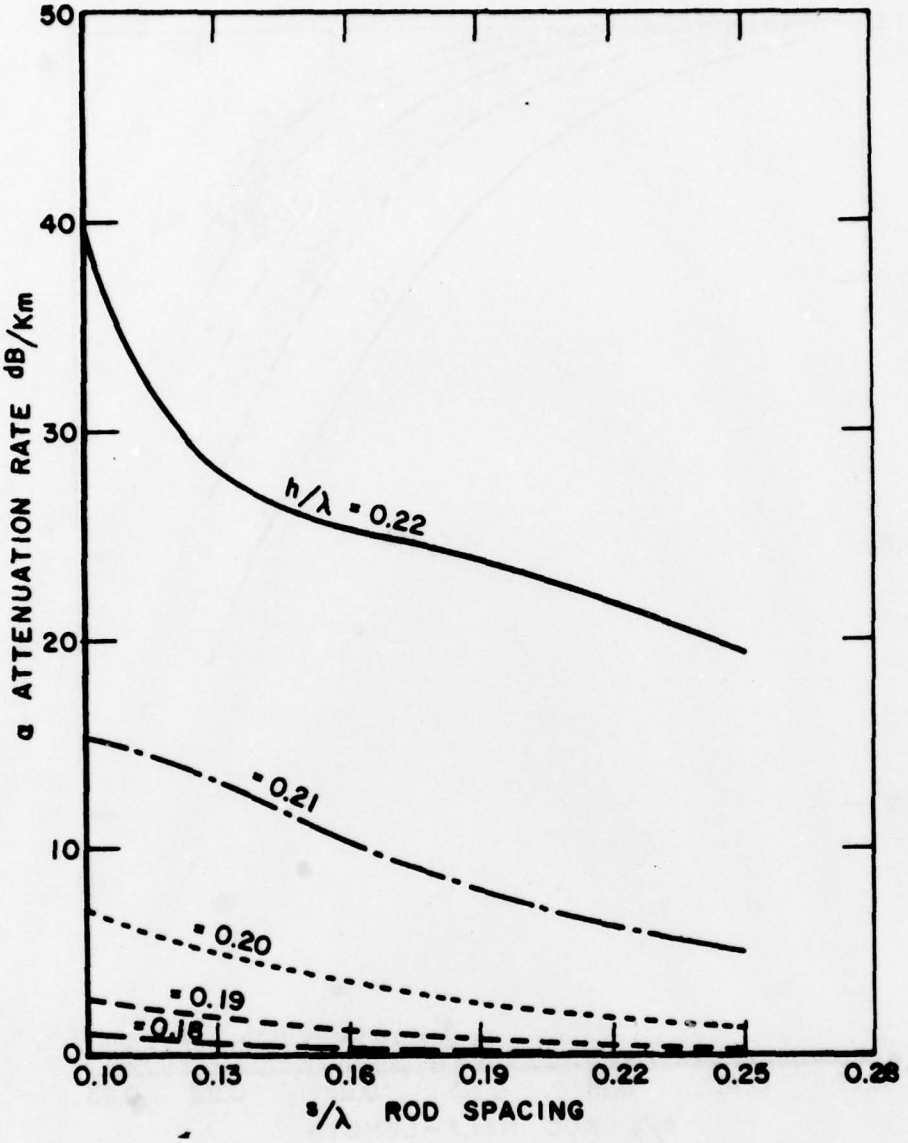

Figure 7. Attenuation constant versus dipole length for copper dipoles with a = 0.001 wavelength. f = 300 MHz.

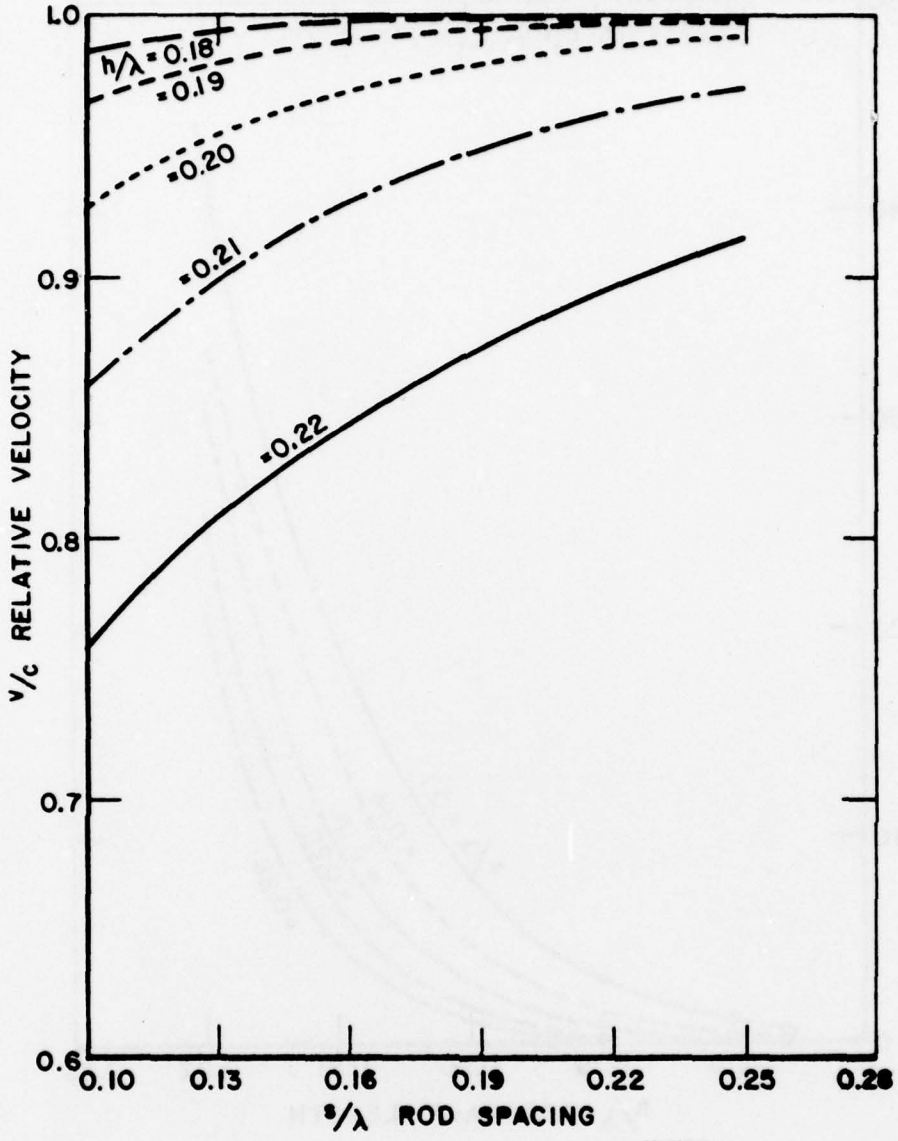

Figure 8. Phase velocity versus dipole length for copper dipoles with a = 0.001 wavelength. f = 300 MHz.

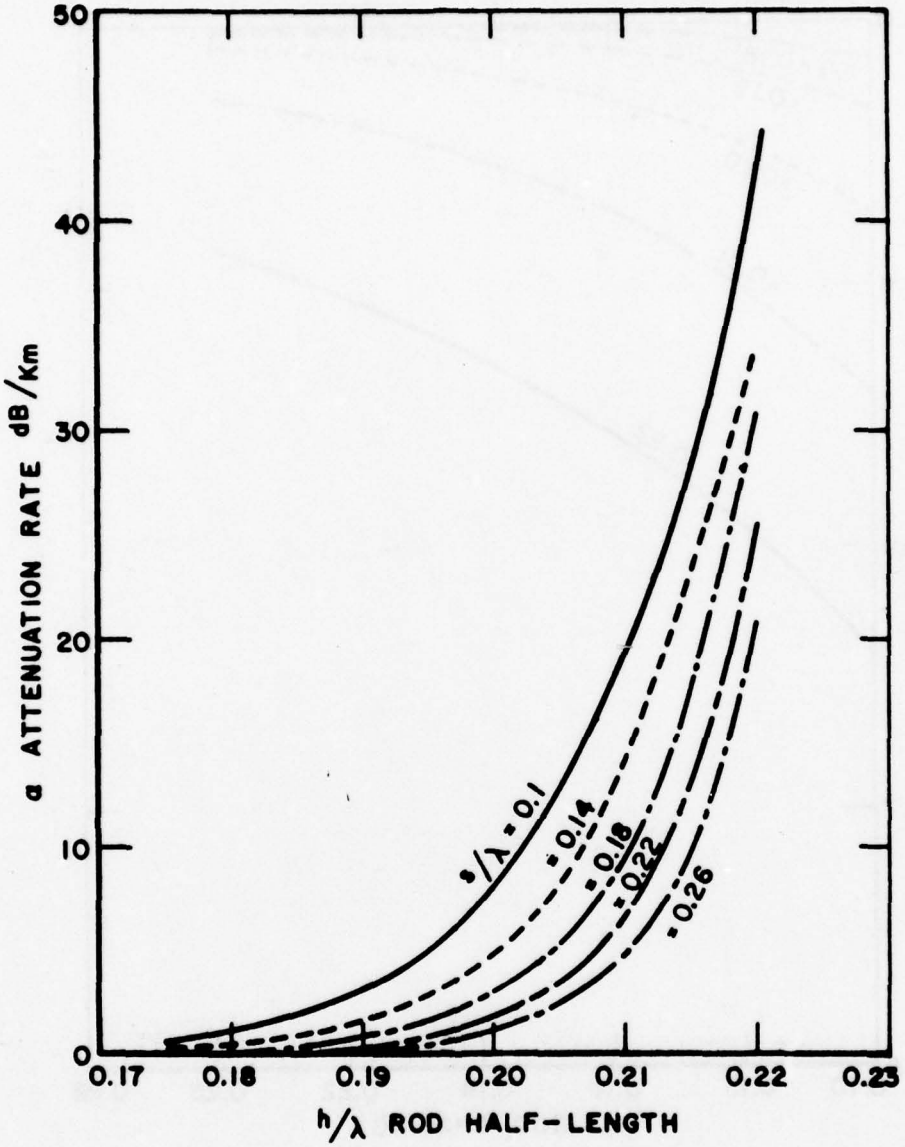

Figure 9. Attenuation constant versus dipole length for copper dipoles with a = 0.000667 wavelength. f = 300 MHz.

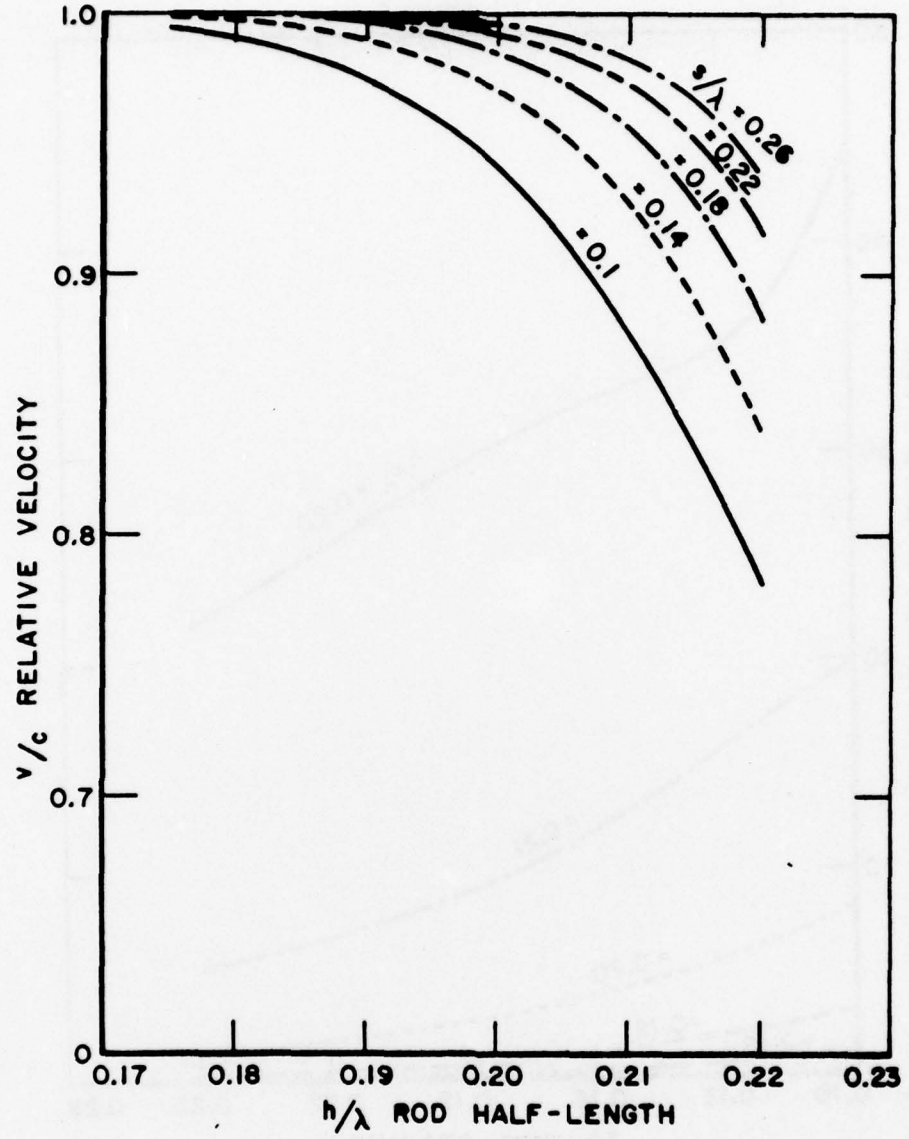

Figure 10. Phase velocity versus dipole length for copper dipoles with a = 0.000667 wavelength. f = 300 MHz.

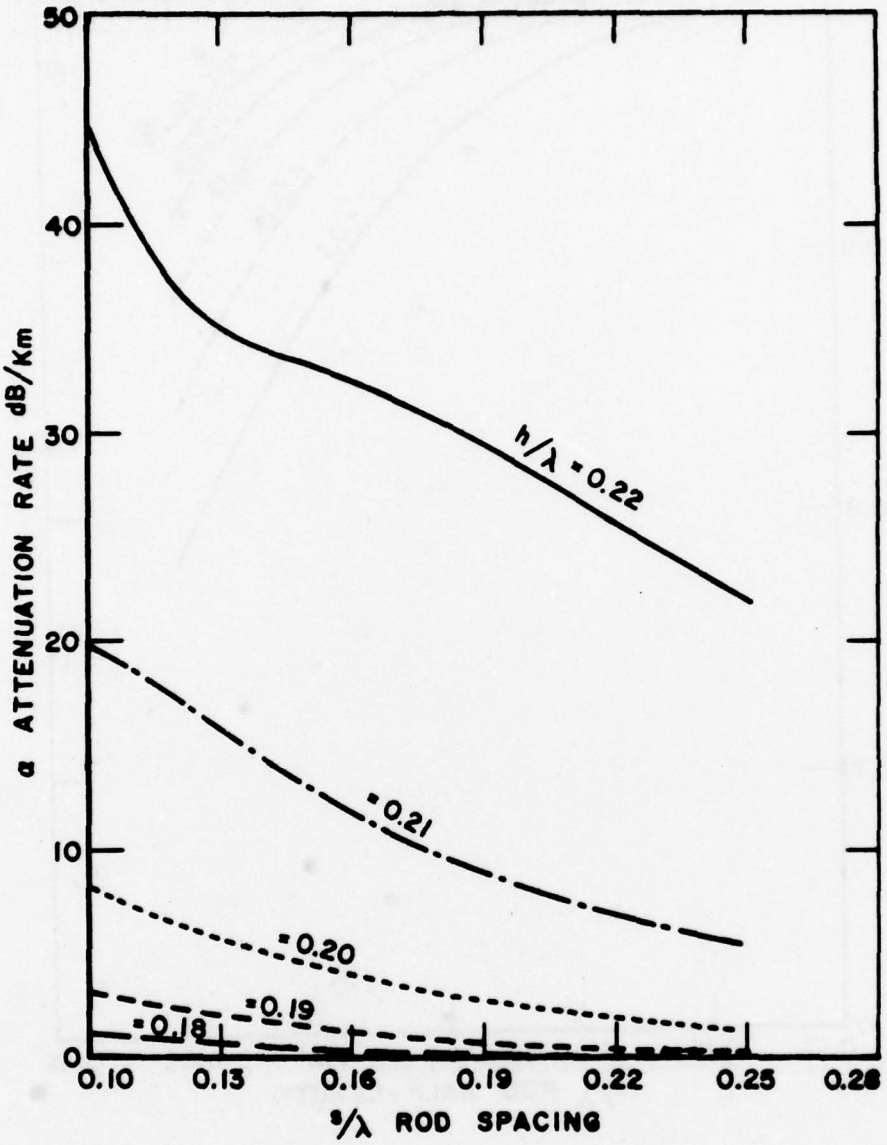

Figure 11. Attenuation constant versus dipole length for copper dipoles with a = 0.000667 wavelength. f = 300 MHz.

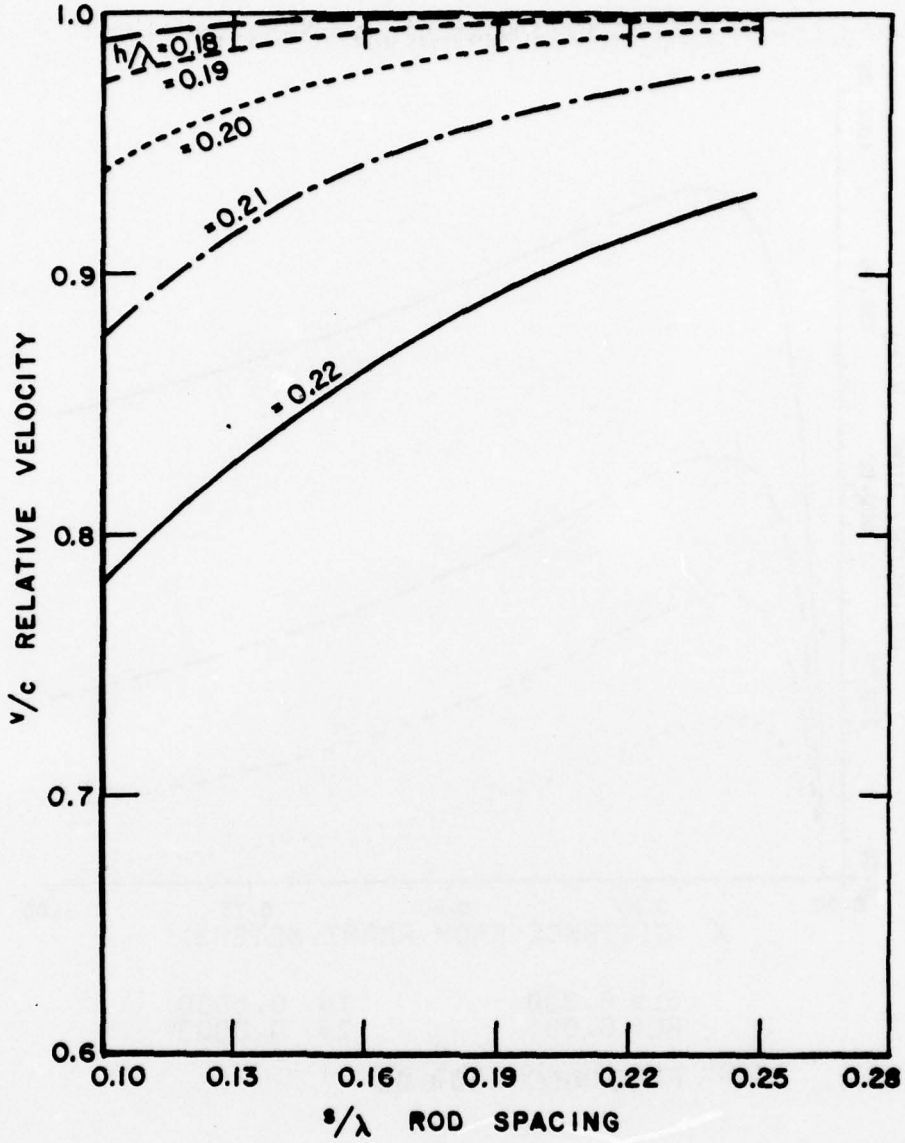

Figure 12. Phase velocity versus dipole length for copper dipoles with a = 0.00067 wavelength. f = 300 MHz.

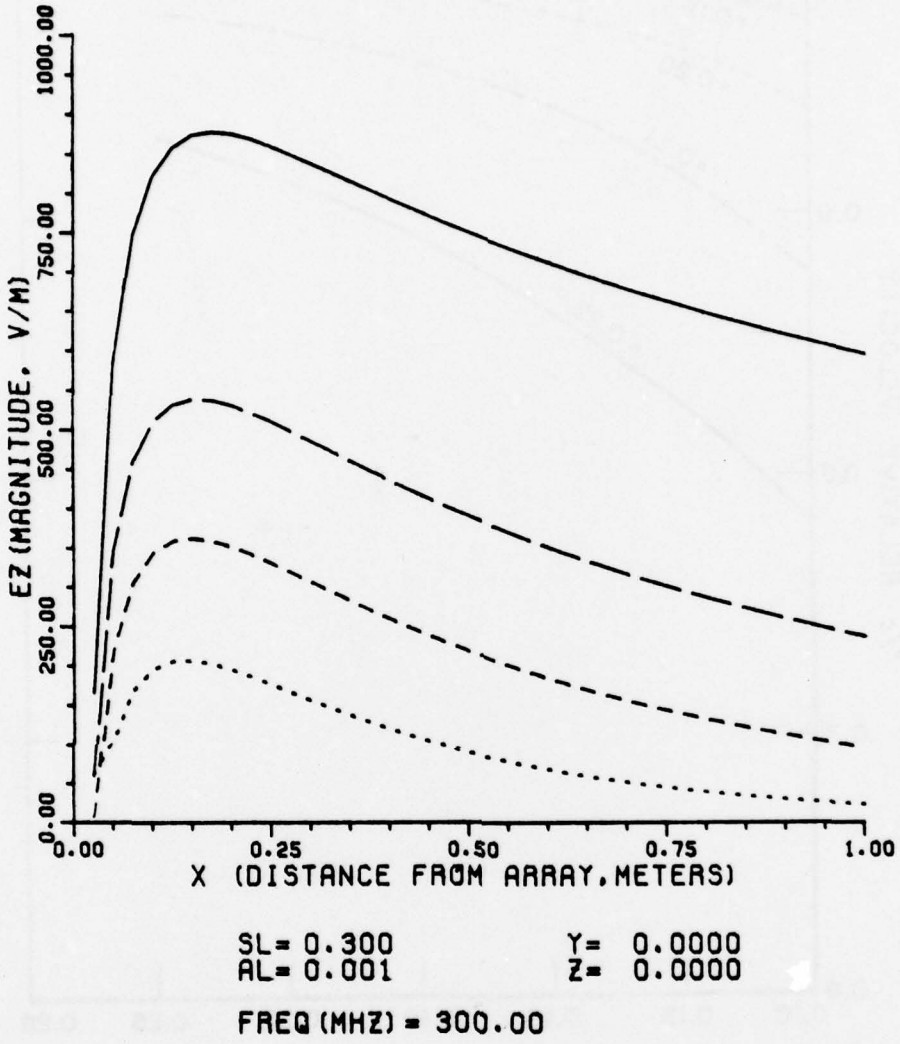

Figure 13. z-component of E-field in a transverse cut in plane of a dipole, normalized such that current at center of each dipole is 1 Amp. $a/\lambda = 0.001$, $s/\lambda = 0.30$, f=300 MHz.

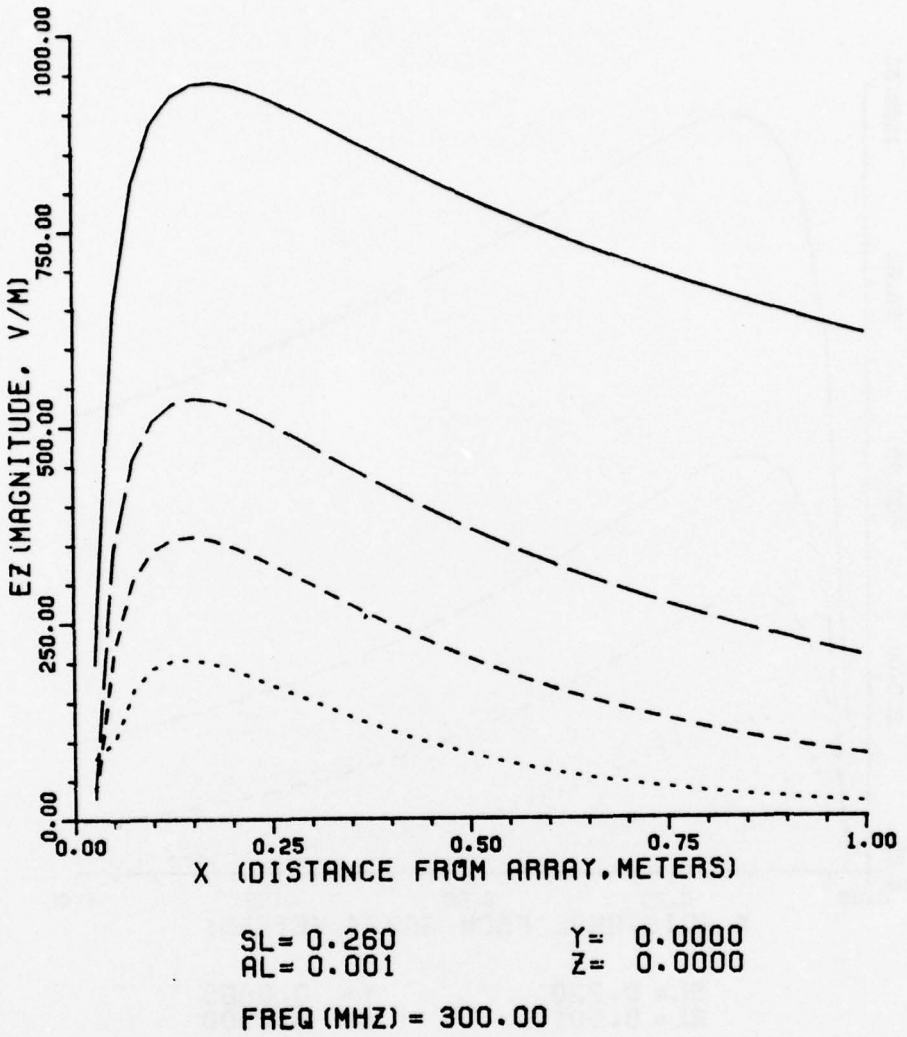

Figure 14. z-component of E-field in a transverse cut in plane of a dipole, normalized such that current at center of each dipole is 1 Amp. $a/\lambda=0.001$, $s/\lambda=0.26$, f=300 MHz.

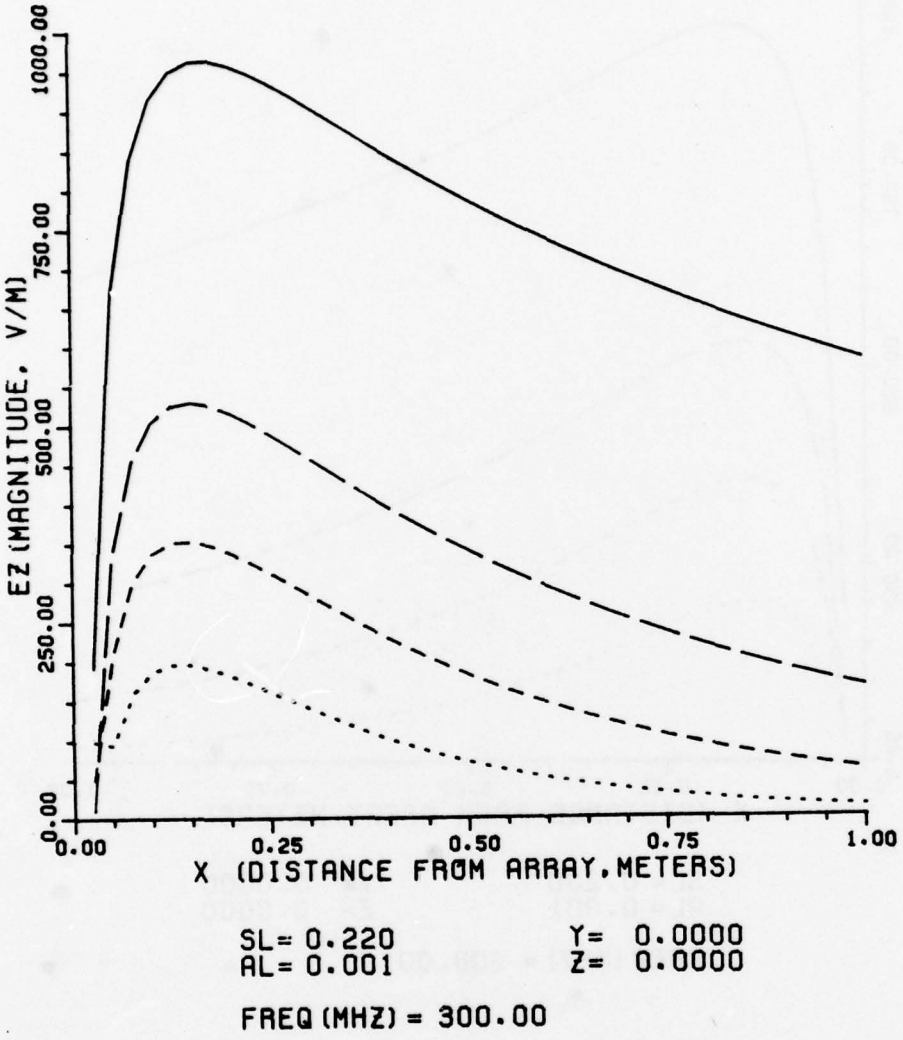

Figure 15. z-component of E-field in a transverse cut in plane of a dipole, normalized such that current at center of each dipole is 1 Amp. $a/\lambda = 0.001$, $s/\lambda = 0.22$, f=300 MHz.

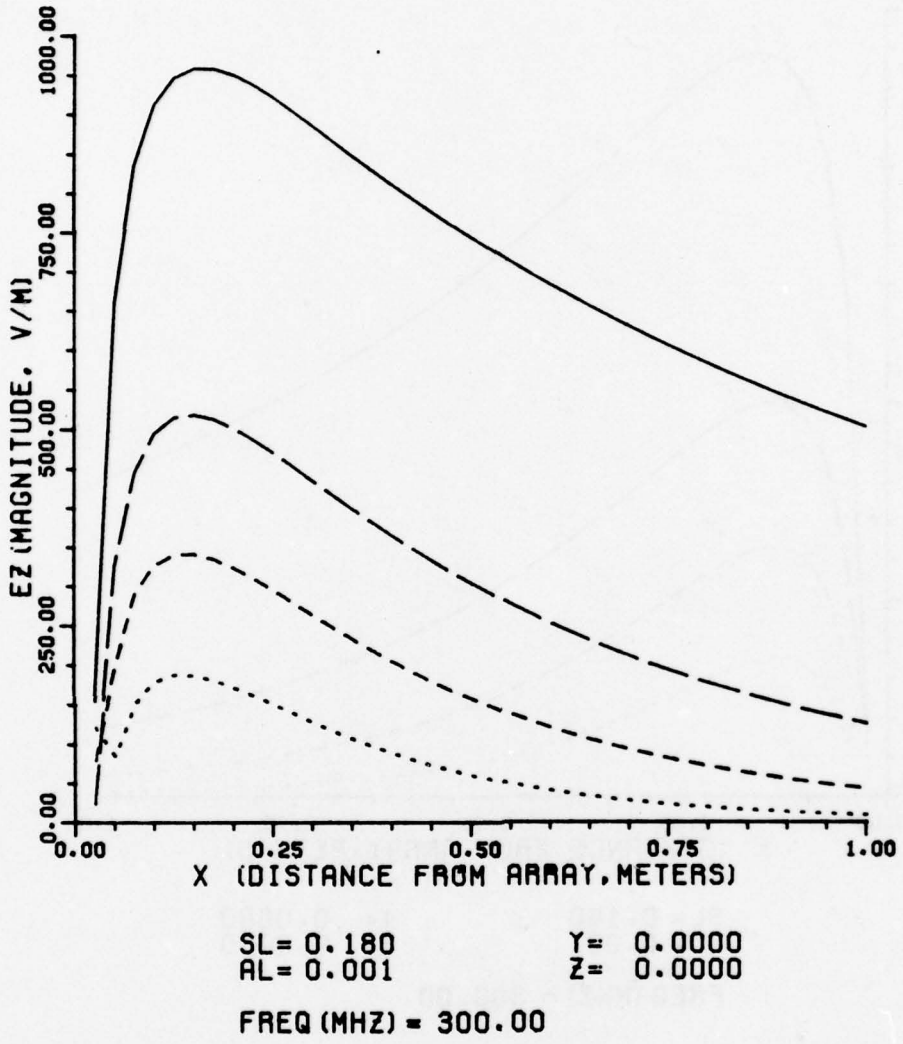

Figure 16. z-component of E-field in a transverse cut in plane of a dipole, normalized such that current at center of each dipole is 1 Amp. a/λ=0.001, s/λ=0.18, f=300 MHz.

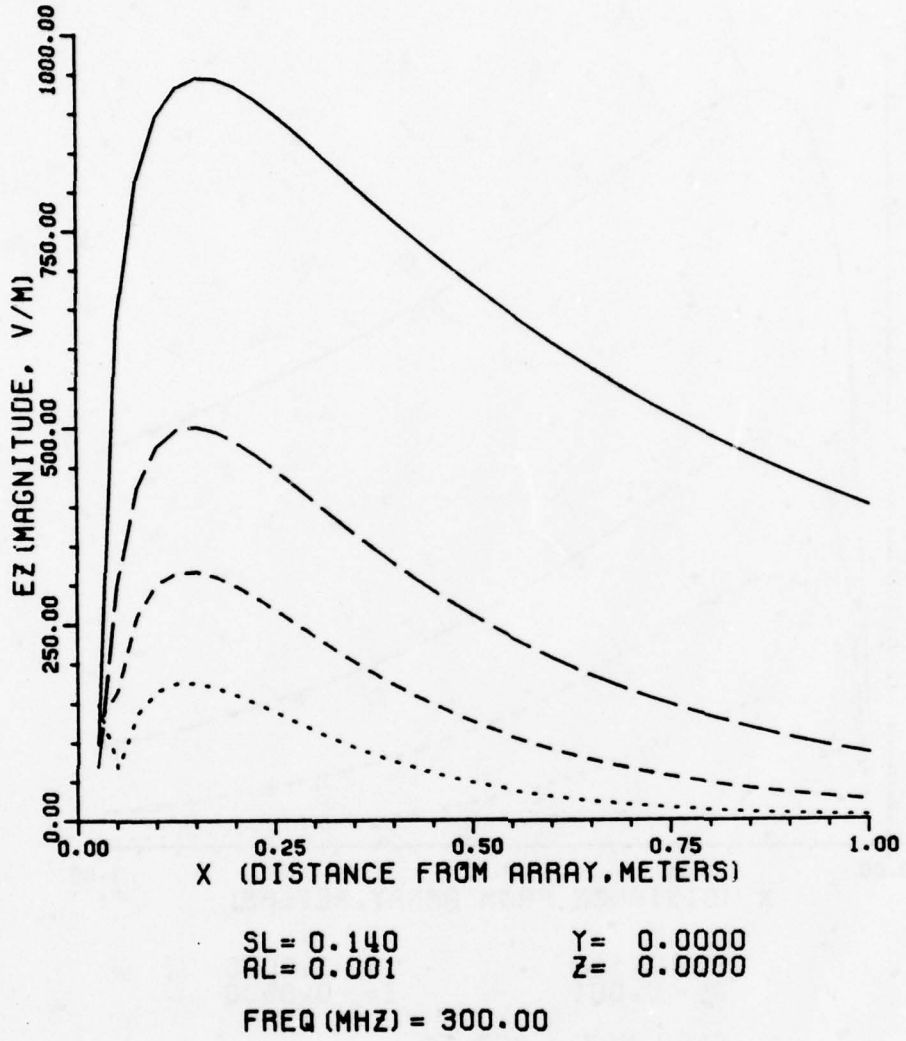

Figure 17. z-component of E-field in a transverse cut in plane of a dipole, normalized such that current at center of each dipole is 1 Amp. $a/\lambda = 0.001$, $s/\lambda = 0.14$, f=300 MHz.

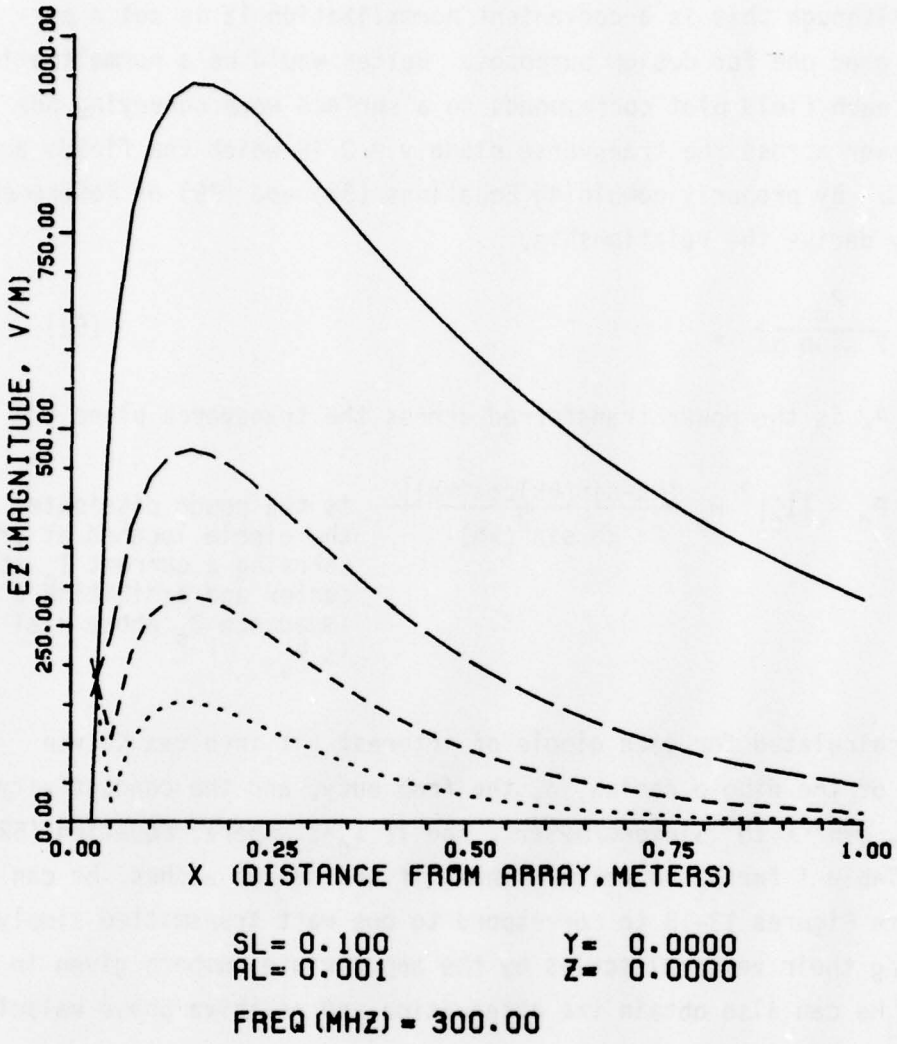

Figure 18. z-component of E-field in a transverse cut in plane of a dipole, normalized such that current at center of each dipole is 1 Amp. a/λ=0.001, s/λ =0.10, f=300 MHz.

0.26, 0.22, 0.18, 0.14, and 0.10. Each field plot is normalized to correspond to 1 ampere of current flowing at the center of the reference dipole. Although this is a convenient normalization it is not a particularly good one for design purposes. Better would be a normalization such that each field plot corresponds to a surface wave conveying one watt of power across the transverse plane y = 0 in which the fields are calculated. By properly combining Equations (32) and (35) of Reference 1, one may derive the relationship,

$$P_t = \frac{P_d}{2 \sinh \alpha s} \quad , \tag{52}$$

where P_t is the power transferred across the transverse plane y=0

$$P_d = |I_o|^2 R_s \frac{[kh-\sin(kh)\cos(kh)]}{2\pi\, ka \sin^2(kh)}$$ is the power dissipated in the dipole located at y=0 and carrying a current I_o at its center and exhibiting a surface impedance Z_s whose real part is R_s.

If R_s is calculated for each dipole of interest (it involves Kelvin functions of the dipole radius, a, the frequency, and the conductivity of copper, σ=57 x 10^6 Siemens/meter), and if I_o=1 ampere, Equation (52) leads to Table I for P_t in watts. Thus, if the reader wishes, he can renormalize Figures 13-18 to correspond to one watt transmitted simply by dividing their vertical scales by the appropriate numbers given in Table I. He can also obtain the attenuation and relative phase velocity for each case depicted.

Figures 19-22 present field plots similar to the ones discussed above, normalized to 1 ampere flowing at the center of the reference dipole, but at a frequency of 100 MHz. The dipoles were of copper (field calculations for aluminum dipoles are not included because they differ very slightly from that for copper) and of two diameters, 2.05 cm and 4.08 cm (corresponding to s/λ = 0.0034 and 0.0068, respectively). The

Table I

Power transferred, power dissipated, attenuation and relative velocity on a free space copper Yagi line at 300 MHz. Reference current of 1 Ampere, $a/\lambda=0.001$

ℓ/λ	s/λ	P_t(watts)	P_d(watts)	$\alpha\left(\frac{\text{nepers}}{\text{m}}\right)$	v/c
.360	.100	4060.	.11	.000130	.9862
.360	.140	6338.	.11	.000059	.9952
.360	.180	11611.	.11	.000025	.9984
.360	.220	23572.	.11	.000010	.9995
.360	.260	50968.	.11	.000004	.9998
.360	.300	113413.	.11	.000002	.9999
.400	.100	745.	.12	.000827	.9268
.400	.140	831.	.12	.000529	.9611
.400	.180	1017.	.12	.000336	.9787
.400	.220	1297.	.12	.000216	.9881
.400	.260	1691.	.12	.000140	.9933
.400	.300	2225.	.12	.000092	.9961
.420	.100	407.	.13	.001633	.8568
.420	.140	344.	.13	.001382	.9097
.420	.180	358.	.13	.001031	.9430
.420	.220	401.	.13	.000753	.9627
.420	.260	460.	.13	.000556	.9749
.420	.300	521.	.13	.000426	.9826
.440	.100	148.	.14	.004848	.7560
.440	.140	162.	.14	.003171	.8207
.440	.180	157.	.14	.002543	.8635
.440	.220	139.	.14	.002345	.8959
.440	.260	133.	.14	.002085	.9197
.440	.300	128.	.14	.001874	.9359

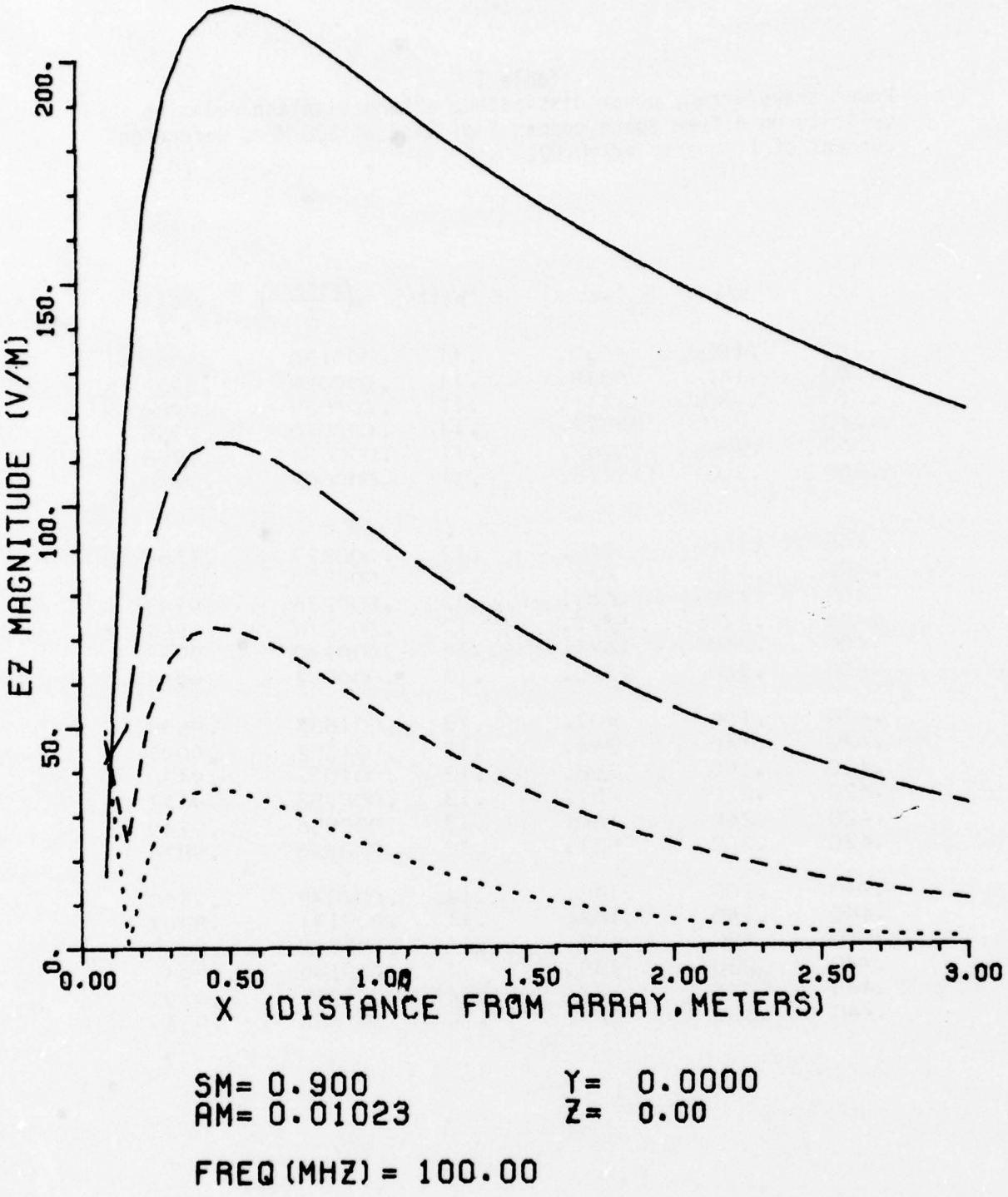

Figure 19. z-component of E-field in a transverse cut in plane of a dipole, normalized such that current at center of each dipole is 1 Amp. a/λ=0.00341, s/λ=0.3, f=100 MHz.

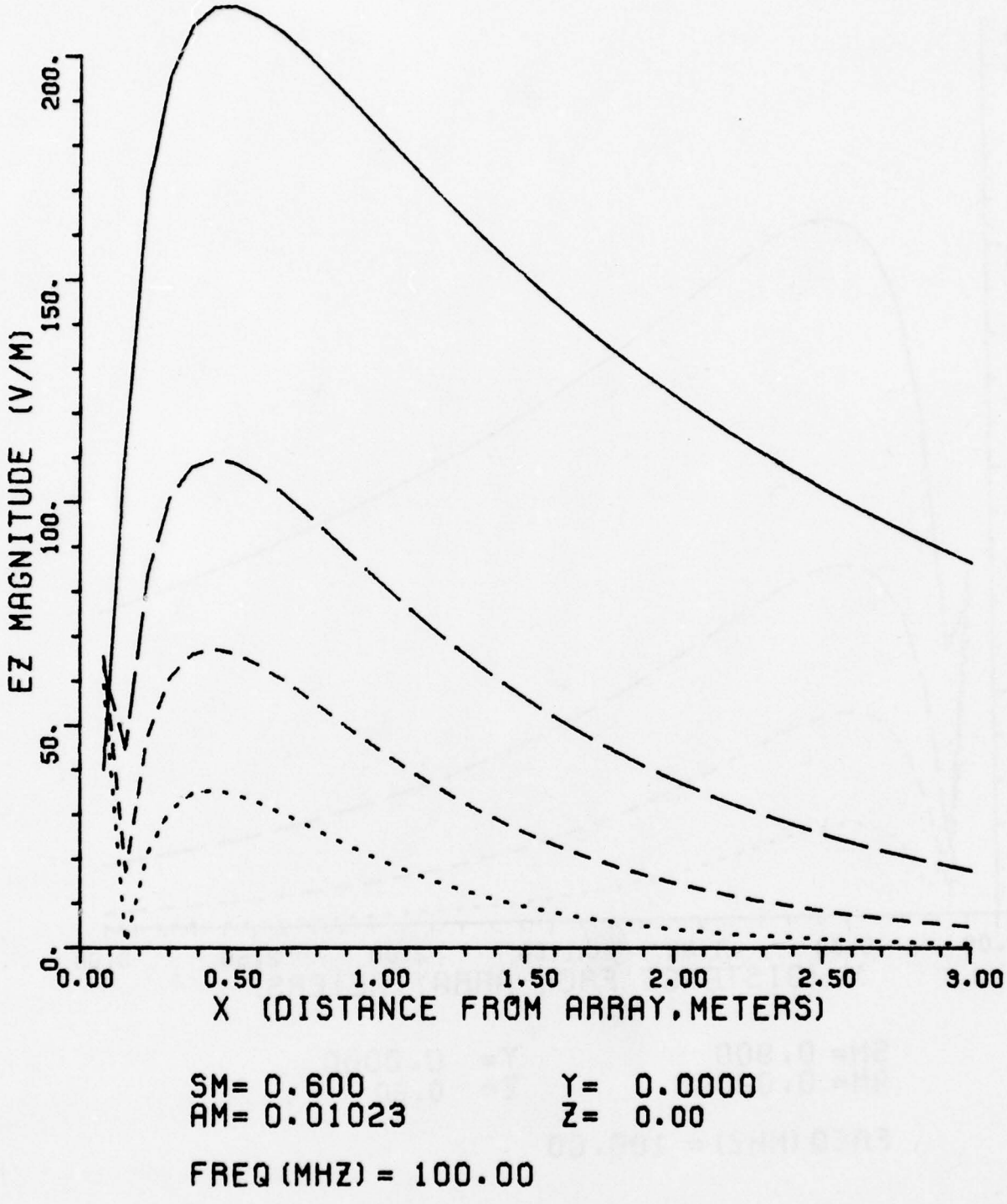

Figure 20. z-component of E-field in a transverse cut in plane of a dipole, normalized such that current at center of each dipole is 1 Amp. $a/\lambda=0.00341$, $s/\lambda=0.2$, f=100 MHz.

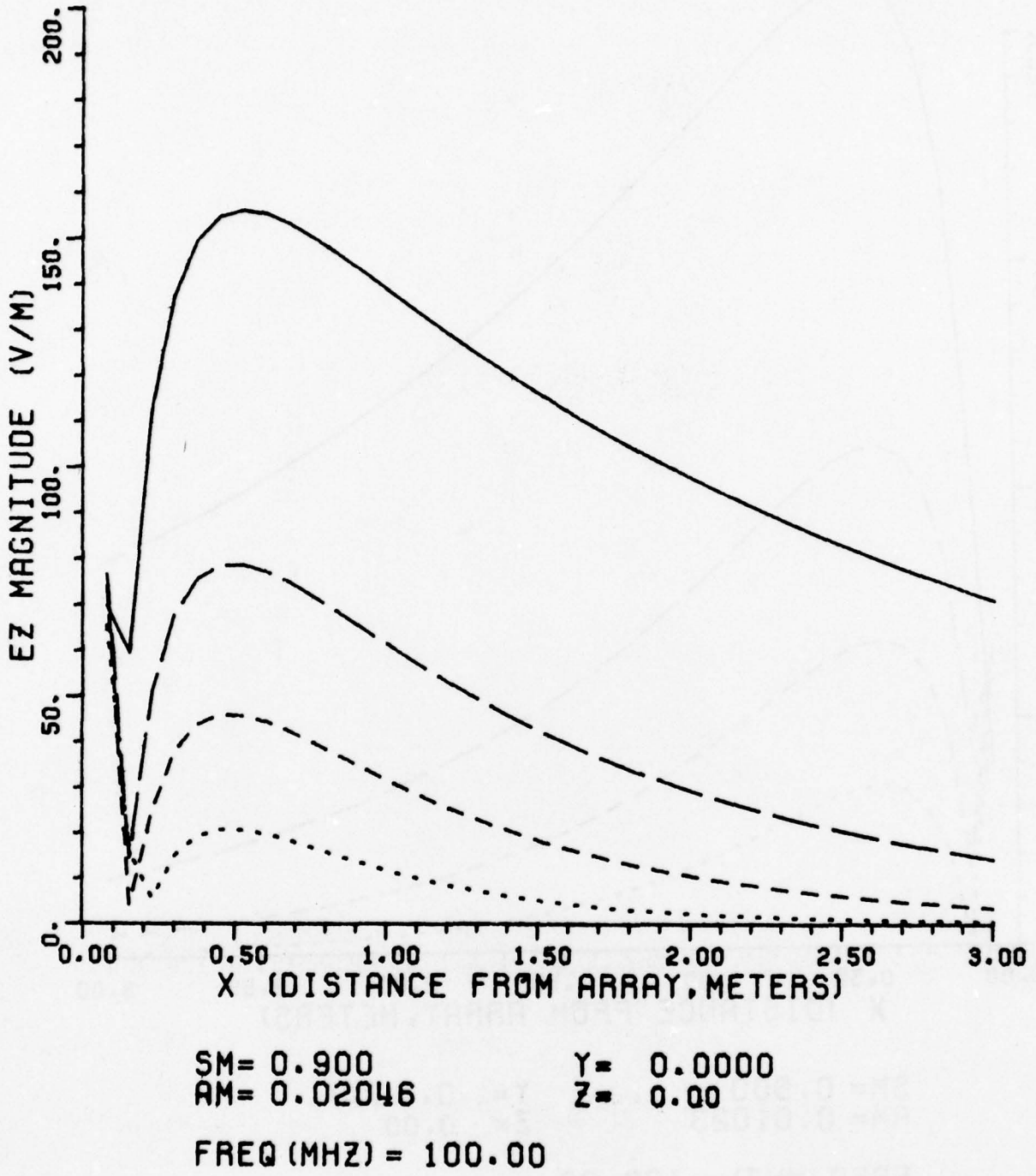

Figure 21. z-component of E-field in a transverse cut in plane of a dipole, normalized such that current at center of each dipole is 1 Amp. a/λ=0.00682, s/λ=0.3, f=100 MHz.

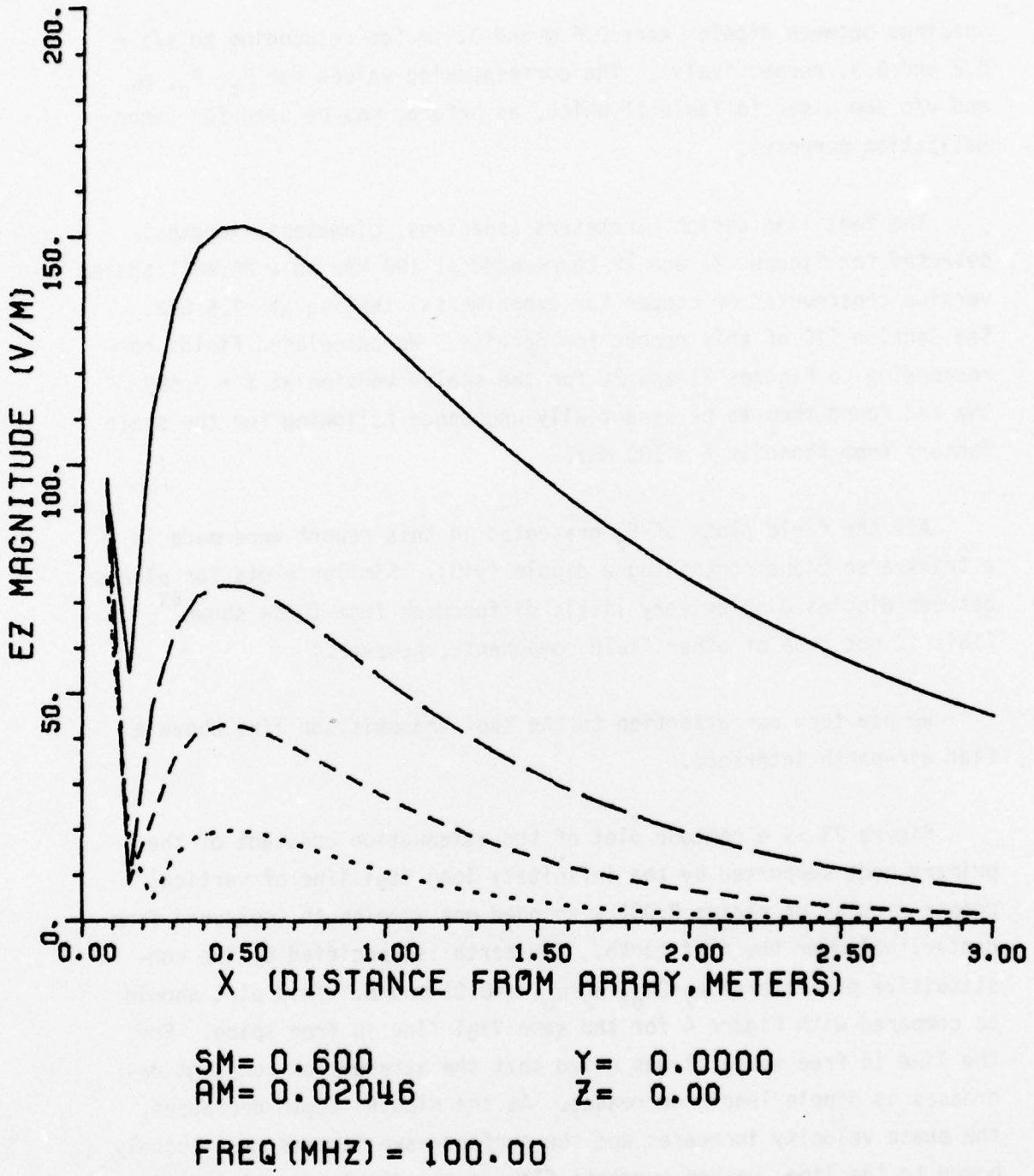

Figure 22. z-component of E-field in a transverse cut in plane of a dipole, normalized such that current at center of each dipole is 1 Amp. $a/\lambda=0.00682$, $s/\lambda=0.2$, f=100 MHz.

spacings between dipoles were 0.6 m and 0.9 m (corresponding to s/λ = 0.2 and 0.3, respectively). The corresponding values for P_t, P_d, α, and v/c are given in Table II which, as before, may be used for renormalization purposes.

The Yagi line design parameters (spacings, diameters, lengths) selected for Figures 21 and 22 correspond at 100 MHz to a 25.98:1 scaled version constructed of copper for experimental testing at ~2.5 GHz. See Section IIC of this report for details. We calculated fields corresponding to Figures 21 and 22 for the scaled version at f = 2.598 GHz and found them to be essentially unchanged (allowing for the scale factor) from those at f = 100 MHz.

All the field plots of E_z presented in this report were made in a transverse plane containing a dipole (y=0). Similar plots for planes between dipoles display very little differences from those shown[43]. (This is not true of other field components, however.)

We now turn our attention to the Yagi transmisison line above a flat air-earth interface.

Figure 23 is a contour plot of the attenuation constant of the primary mode supported by the infinitely long Yagi line of vertical copper dipoles of radius 0.001 suspended one wavelength (measured from centerline) over the flat earth. The earth is specified by the constituitive parameters* $\varepsilon_2=2\varepsilon_o$, $\mu_2=\mu_o$, σ=0.01 mho/m. This plot should be compared with Figure 4 for the same Yagi line in free space. For the line in free space it was noted that the attenuation constant decreases as dipole length decreases. As the dipole length decreases, the phase velocity increases and the surface-wave becomes more loosely bound to the line, weaker currents flow on the dipoles and less power is dissipated in each dipole when the power transmitted via the surface-

*Some data on Earth media electrical characteristics are given in Reference 44.

Table II

Power transferred, power dissipated, attenuation and relative velocity on free space copper Yagi lines at 100 MHz. Reference current of 1 Ampere, a/λ =0.0034 and 0.0068.

a/λ=.341000E -2

ℓ/λ	s/λ	P_t(watts)	P_d(watts)	$\alpha\left(\frac{\text{nepers}}{\text{m}}\right)$	v/c
.360	.200	2700.	.02	.000005	.9945
.360	.300	8001.	.02	.000001	.9992
.400	.200	357.	.02	.000049	.9569
.400	.300	494.	.02	.000023	.9838
.420	.200	151.	.02	.000124	.8999
.420	.300	148.	.02	.000084	.9498
.440	.200	60.	.02	.000335	.8029
.440	.300	51.	.02	.000266	.8592

a/λ=.682000E -2

.360	.200	949.	.01	.000008	.9853
.360	.300	1840.	.01	.000003	.9964
.400	.200	172.	.01	.000050	.9214
.400	.300	192.	.01	.000030	.9633
.420	.200	92.	.01	.000102	.8457
.420	.300	69.	.01	.000091	.9042
.440	.200	44.	.01	.000231	.7278
.440	.300	18.	.01	.000377	.7812

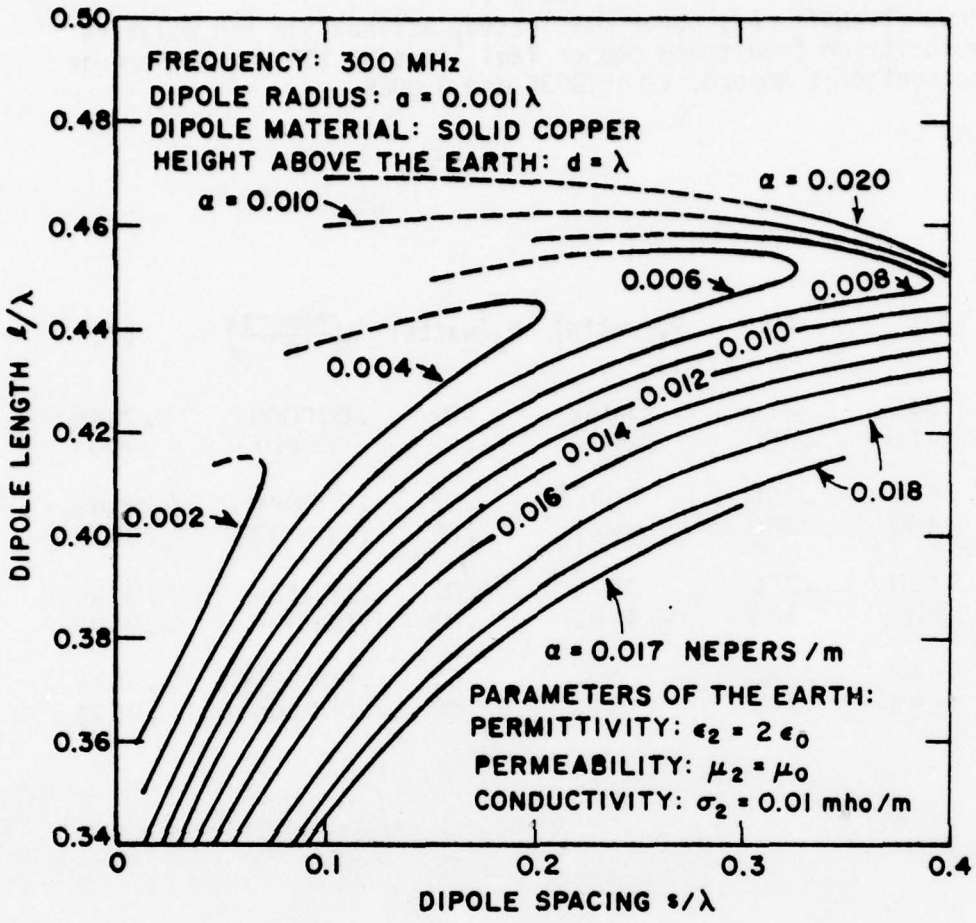

Figure 23. Contours of constant attenuation for surface wave on periodic array of vertical dipoles over the flat earth.

wave is held fixed. For dipole lengths receding from $\lambda/2$, this same type of behavior is observed in Figure 23 for the Yagi line over the flat earth. But here, as the dipole length decreases further, the attenuation constant increases again. The surface-wave becomes more loosely bound, the surface-wave field penetrates more strongly into the earth and more power is dissipated there. Thus, for each value of spacing s and height d, there is an optimum dipole length that minimizes α.

As one increases the height d above the earth, the attenuation constant decreases rapidly and the surface-wave characteristics approach those of the array in free space.

We have not constructed a contour plot of relative phase velocity for the Yagi line over flat earth. Evidently it would be almost identical to that shown in Figure 3 for the free space case, differing significantly only in the region where the phase velocity is nearly equal to the velocity of light.

Figures 24-26 show the influence on α and v/c of raising the Yagi line. Figures 27-29 present similar data which show the effect of decreasing the dipole radius from 0.001λ to 0.0067λ.

Figures 30-33 present field plots of E_z of the same copper Yagi pertinent to Figures 21 and 22 but spaced varying distances above a lossy earth interface. The frequency is 100 MHz, normalization in all cases is to one ampere at the center of the local dipole, and all plots are in the plane of the dipole (y=0). Rather than plotting E_z as a function of transverse distance x along a line (y=0, z=0) as was done in Figures 21 and 22 for the free space case, we here have plotted E_z as a function of z along three lines, (y=0, x=0.375 m), (y=0, x=0.75 m) and (y=0, x=1.5 m) extending from the ground upward. Figure 30 is for the center line-to-ground distance d=2.4 m, which is essentially unchanged from the free space case. Figures 31-33 are for progressively smaller

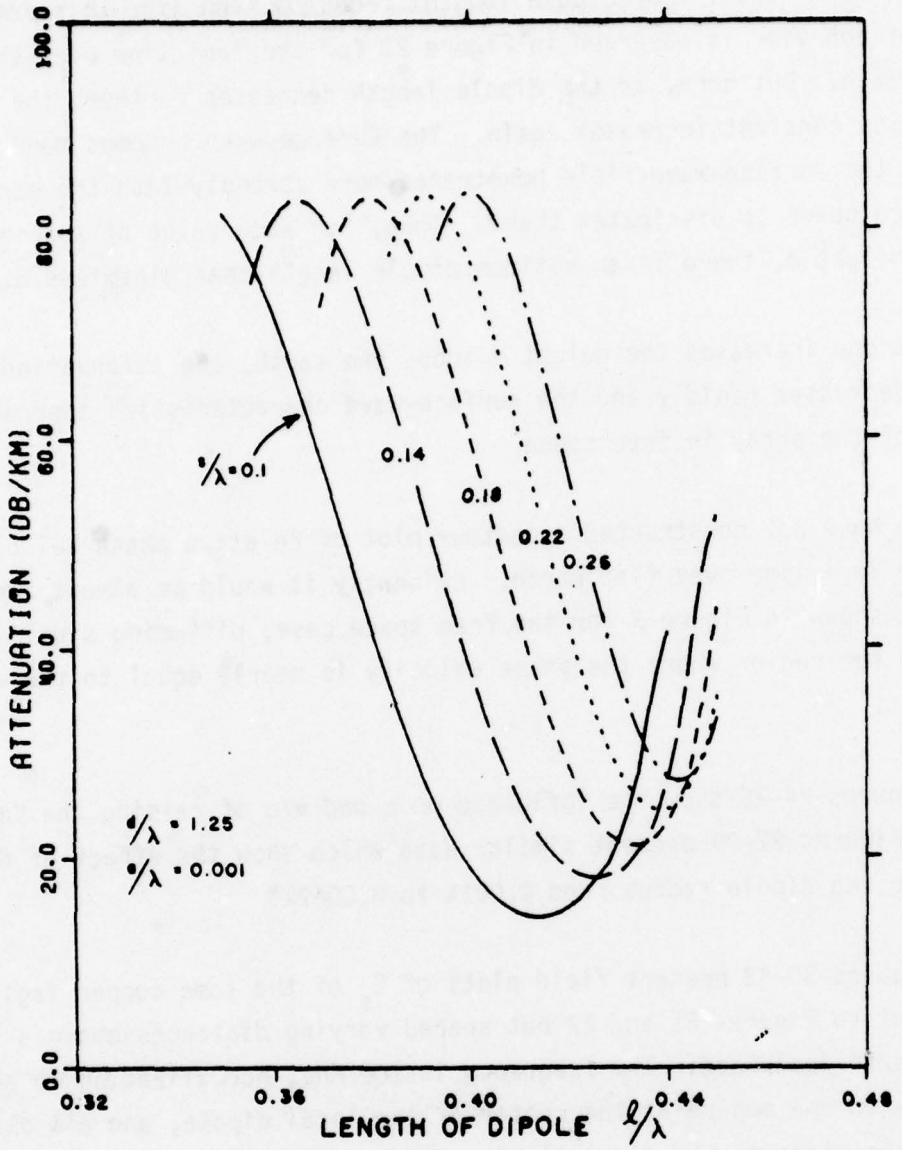

Figure 24. Attenuation constant versus dipole length for copper dipoles over earth ($\mu_2=\mu_0, \varepsilon_2=2\varepsilon_0, \sigma_2=0.01$ mho/m). f=300 MHz.

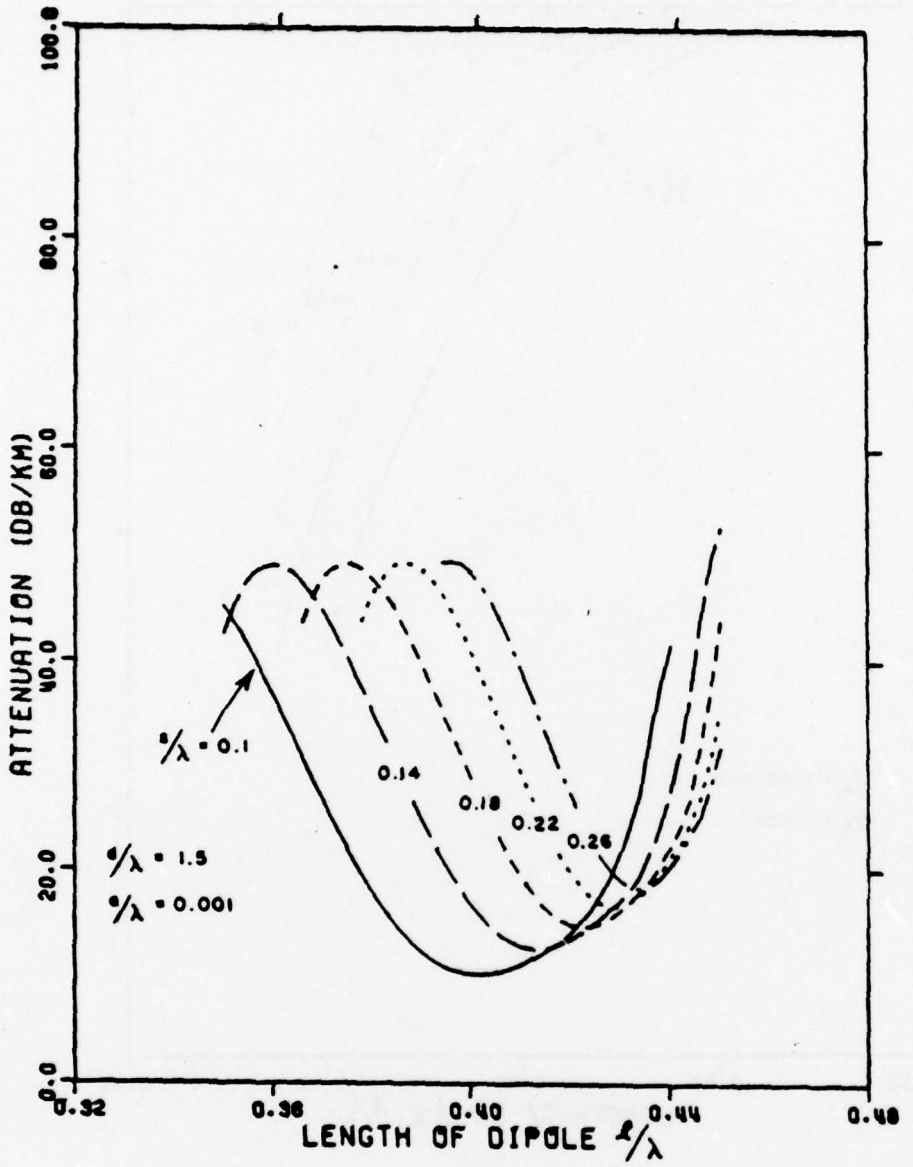

Figure 25. Attenuation constant versus dipole length for copper dipoles over earth ($\mu_2=\mu_0, \varepsilon_2=2\varepsilon_0, \sigma_2=0.01$ mho/m). f=300 MHz.

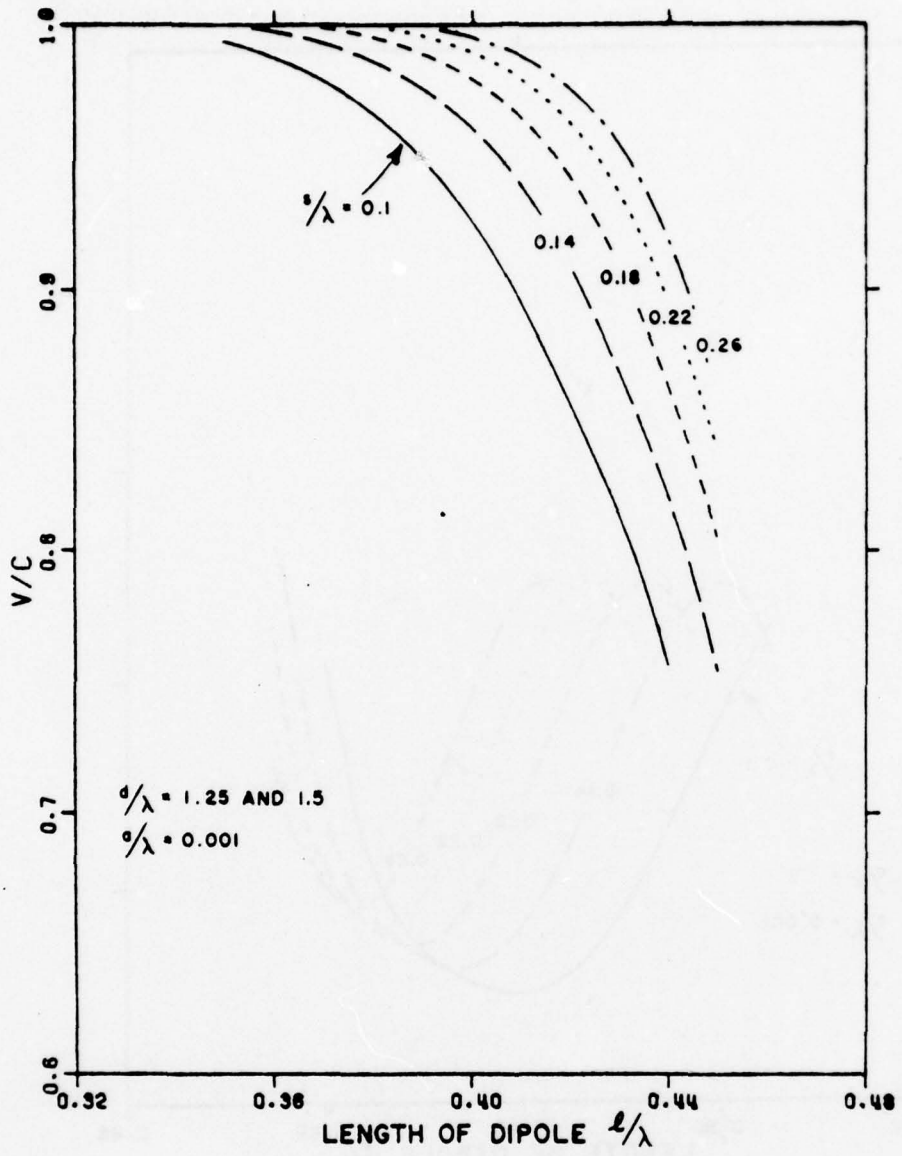

Figure 26. Phase velocity versus dipole length for copper dipoles over earth ($\mu_1=\mu_o, \varepsilon_2=2\varepsilon_o, \sigma_2=0.01$ mho/m). f=300 MHz.

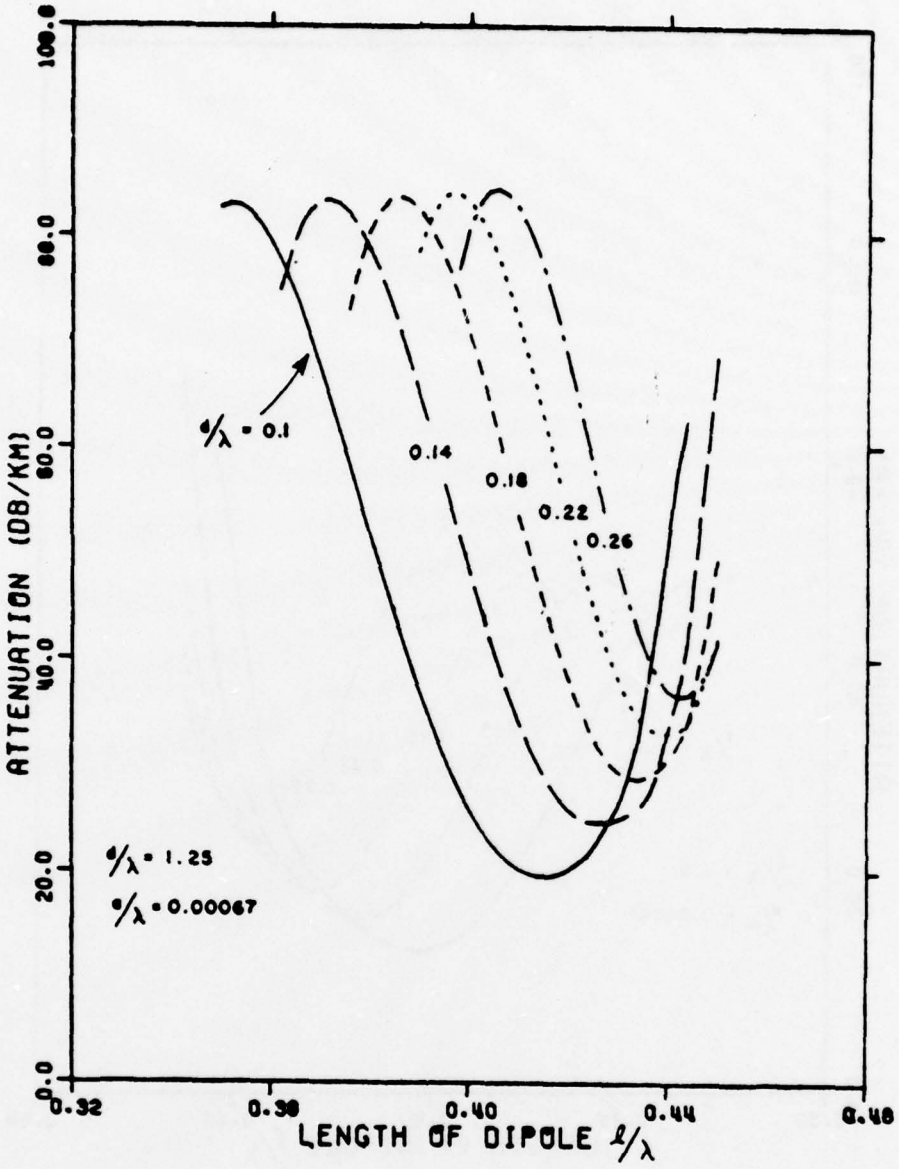

Figure 27. Attenuation constant versus dipole length for copper dipoles over earth ($\mu_2=\mu_0, \varepsilon_2=2\varepsilon_0, \sigma_2=0.01$ mho/m). f=300 MHz.

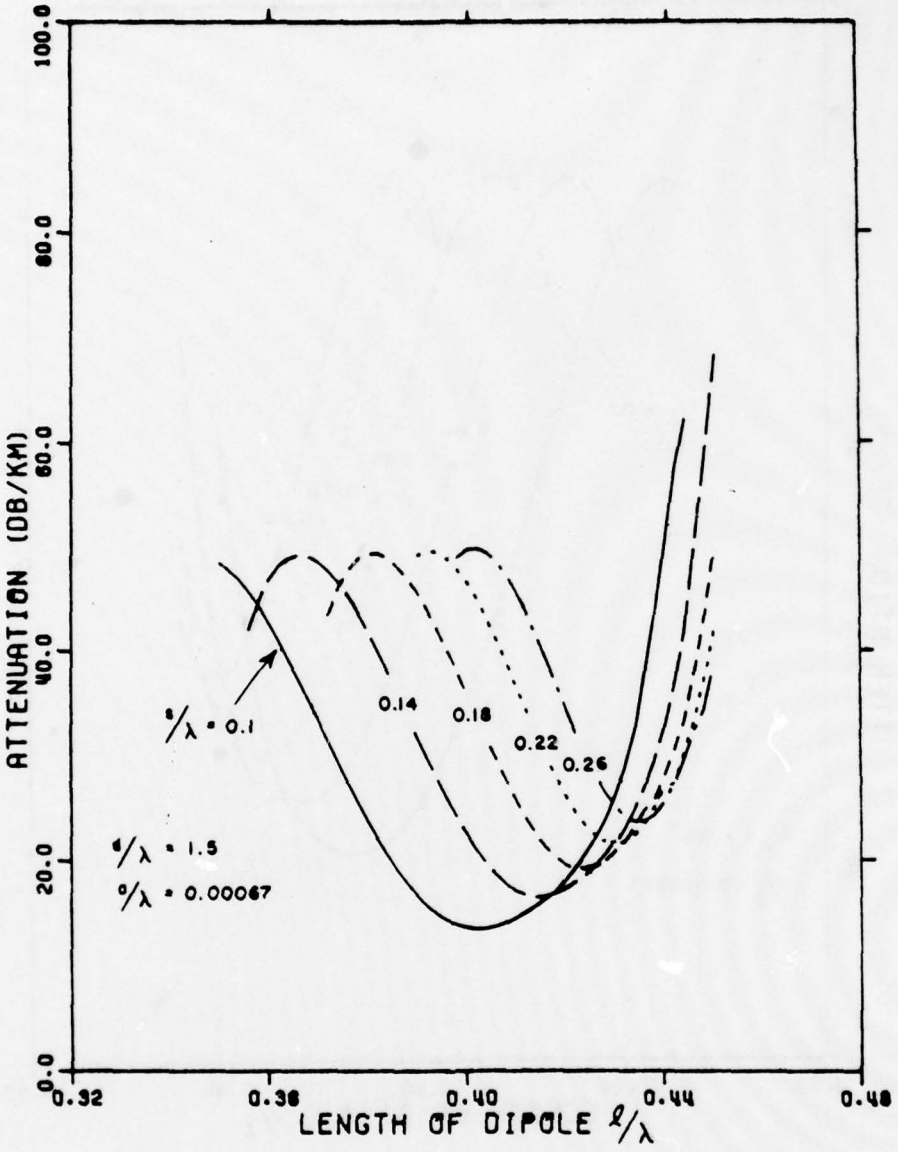

Figure 28. Attenuation constant versus dipole length for copper dipoles over earth ($\mu_2=\mu_0, \varepsilon_2=2\varepsilon_0, \sigma_2=0.01$ mho/m). f=300 MHz.

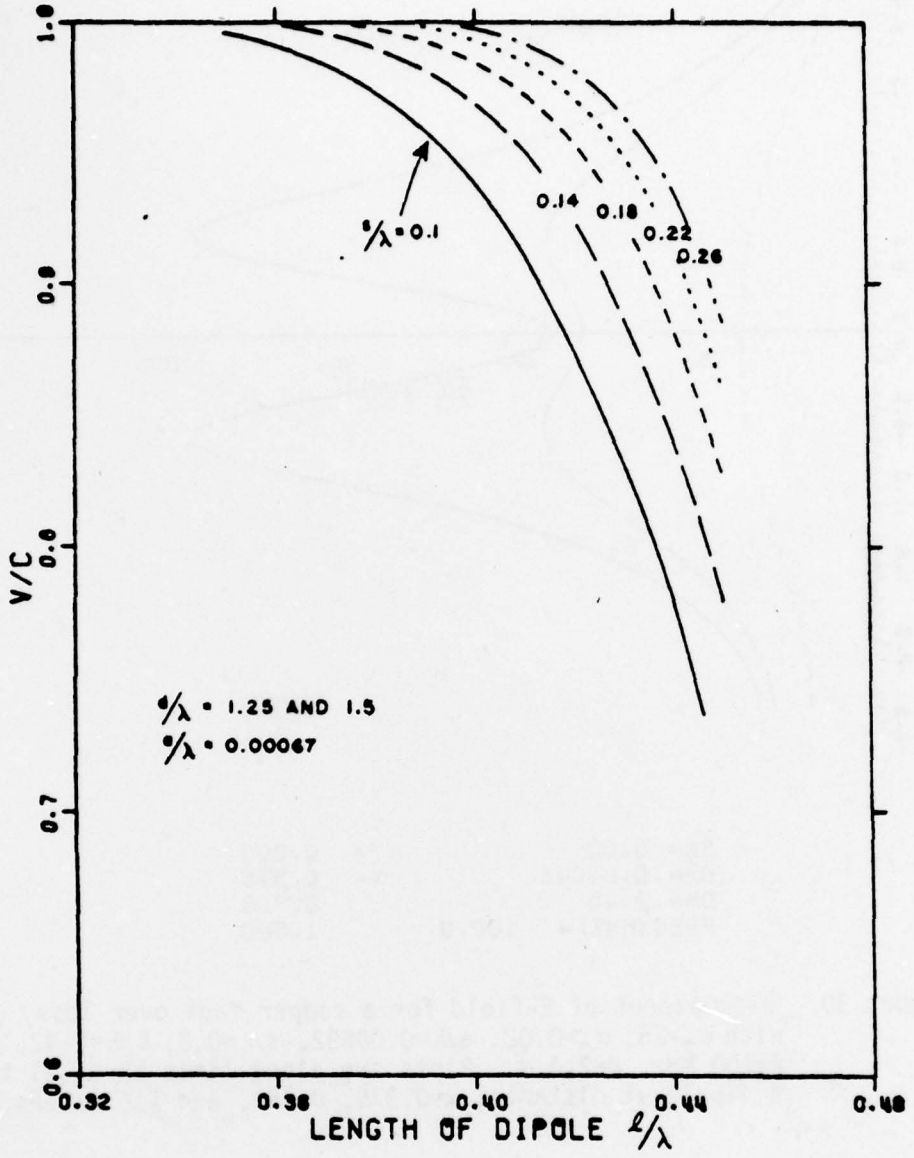

Figure 29. Phase velocity versus dipole length for copper dipoles over earth ($\mu_1=\mu_0, \varepsilon_2=2\varepsilon_0, \sigma_2=0.01$ mho/m). f=300 MHz.

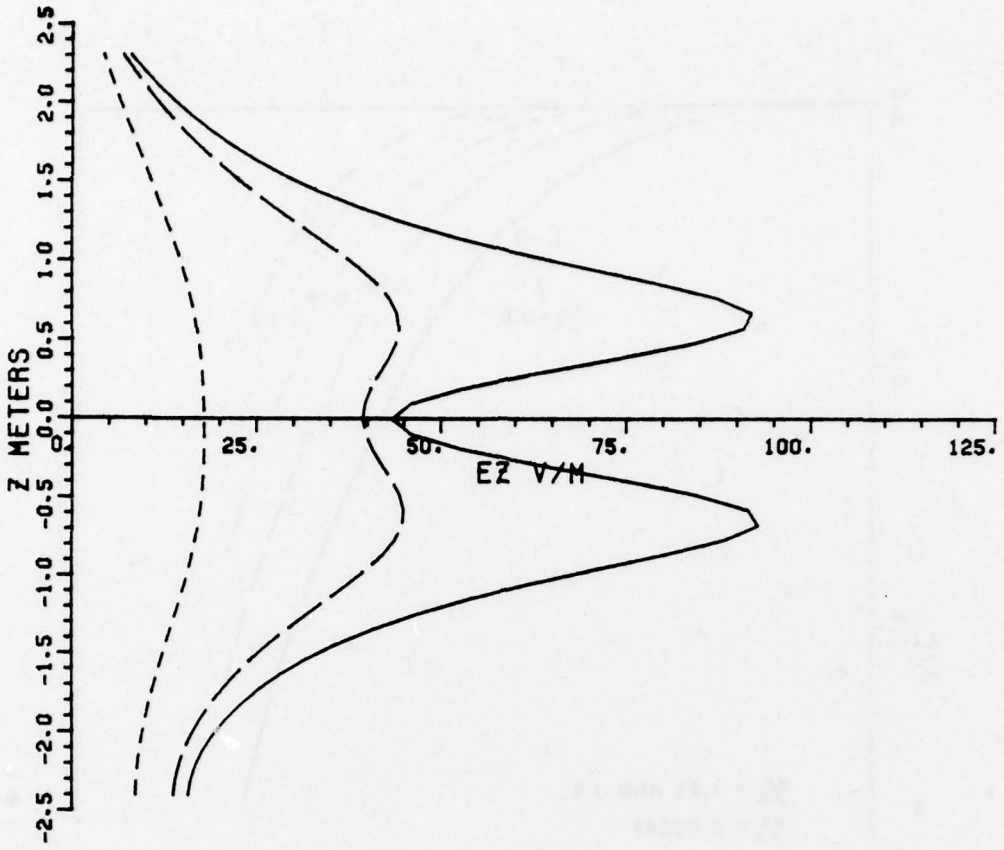

SM= 0.90
AM= 0.02048
DM= 2.40
FREQ(MHZ)= 100.0

Y= 0.000
X= 0.375
0.750
1.500

Figure 30. z-component of E-field for a copper Yagi over lossy ground with ϵ_2=16, σ_2=0.02, a/λ=0.00682, s/λ=0.3, ℓ/λ=0.42, f=100 MHz, d=2.4 m. Plots are along lines parallel to a dipole at distances x=0.375, 0.750, and 1.5 meters.

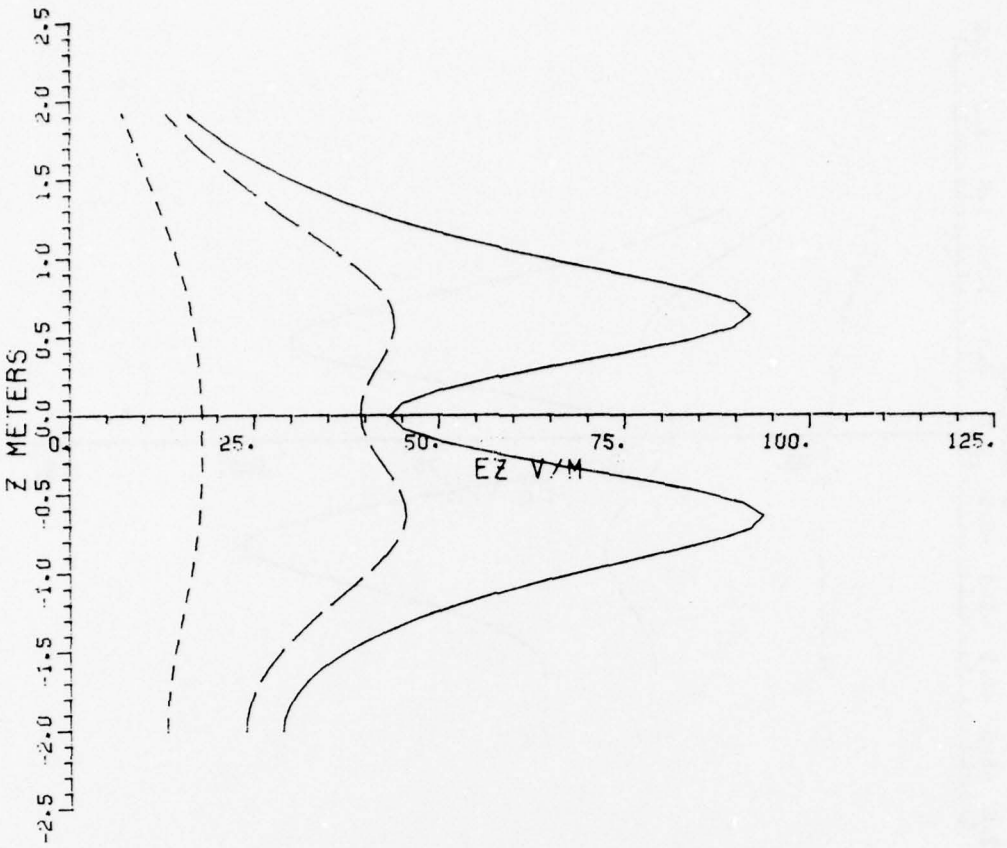

SM= 0.90
AM= 0.02046
OM= 2.00
FREQ(MHZ)= 100.0

Y= 0.000
X= 0.375
0.750
1.500

Figure 31. z-component of E-field for a copper Yagi over lossy ground with ϵ_2=16, σ_2=0.02, a/λ=0.00682, s/λ=0.3, ℓ/λ=0.42, f=100 MHz, d=2.0 m. Plots are along lines parallel to a dipole at distances x=0.375, 0.750, and 1.5 meters.

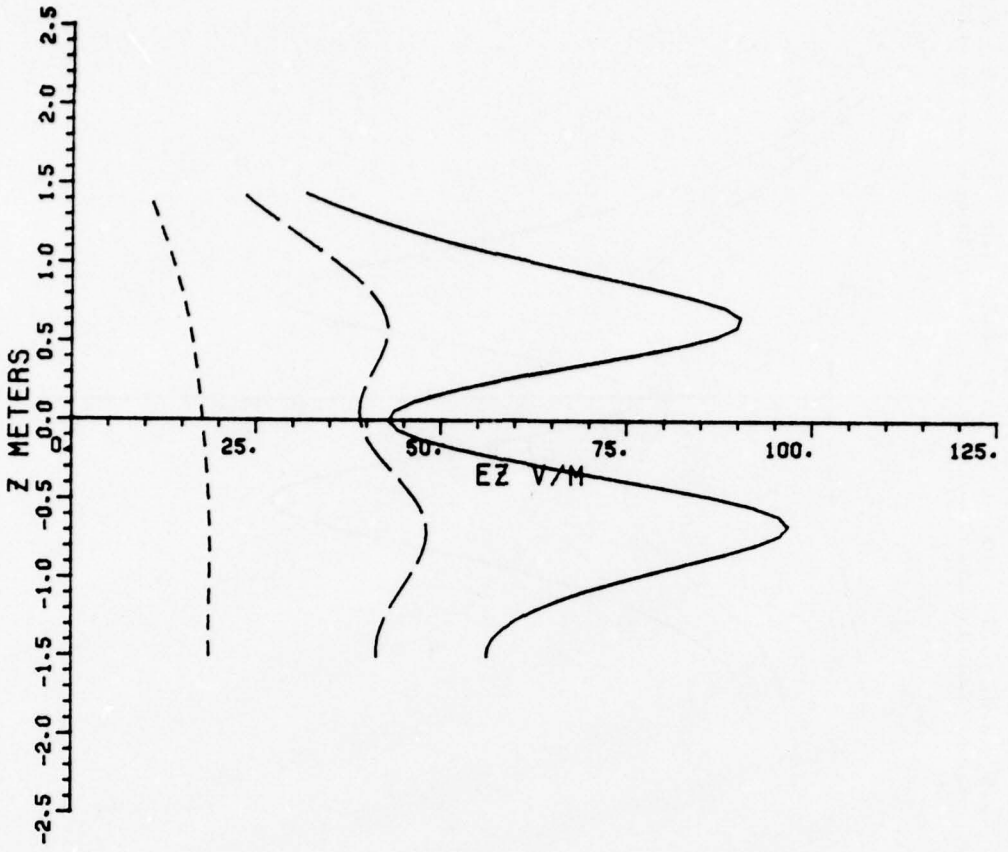

SM= 0.90
AM= 0.02046
DM= 1.50
FREQ(MHZ)= 100.0

Y= 0.000
X= 0.375
0.750
1.500

Figure 32. z-component of E-field for a copper Yagi over lossy ground with ε_2=16, σ_2=0.02, a/λ=0.00682, s/λ=0.3, ℓ/λ=0.42, f=100 MHz, d=1.5 m. Plots are along lines parallel to a dipole at distances x=0.375, 0.750, and 1.5 meters.

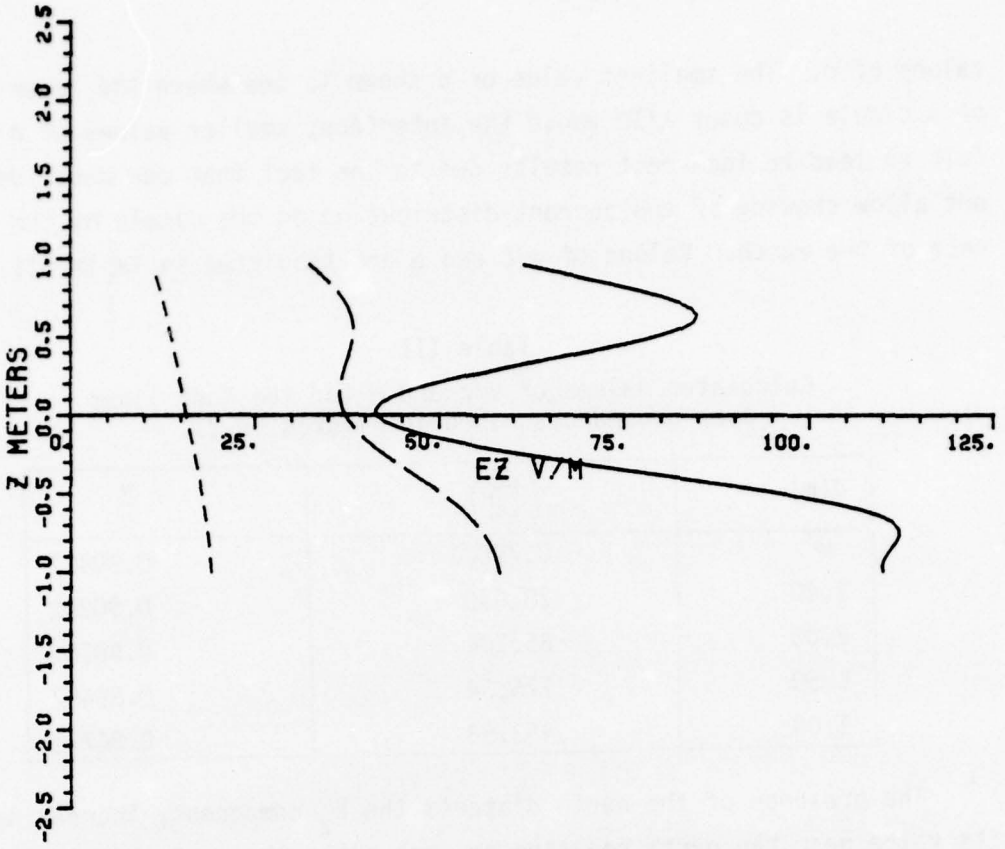

SM= 0.90
AM= 0.02048
DM= 1.00
FREQ(MHZ)= 100.0

Y= 0.000
X= 0.375
0.750
1.500

Figure 33. z-component of E-field for a copper Yagi over lossy ground with ε_2=16, σ_2=0.02, a/λ=0.00682, s/λ=0.3, ℓ/λ=0.42, f=100 MHz, d=1.0 m. Plots are along lines parallel to a dipole at distances x=0.375, 0.750, and 1.5 meters.

values of d. The smallest value of d shown is one where the lower tip of a dipole is about $\lambda/10$ above the interface; smaller values of d are felt to lead to incorrect results due to the fact that our model does not allow skewing of the current distribution on the dipole by the presence of the earth. Values of v/c and α are tabulated in Table III.

Table III

Calculated values of v/c and α for the Yagi lines over ground described in Figures 30-33.

d(m)	$\alpha\left(\frac{dB}{km}\right)$	$\frac{v}{c}$
∞	0.79026	0.90417
2.40	28.950	0.90292
2.00	65.104	0.90107
1.50	175.34	0.89402
1.00	453.58	0.86771

The presence of the earth distorts the E_z component, increasing its value near the earth relative to that along the centerline (y=0, z=0). This is good from the standpoint of providing detection of an intruder trying to roll beneath the line, but bad from the standpoint of attenuation due to earth losses. Unfortunately we have no calculations of earth losses comparable to P_d of Table II, and therefore have not provided numbers to renormalize Figures 30-38 to one watt of transferred power.

Another aspect of the Yagi line (or of any open transmission line for that matter) is the effect of a curve upon the surface wave propagating along the line. Invariably the discontinuity caused by the curve will cause a reflection which, together with radiation of energy as the wave proceeds around the curve, will result in a reduction of energy transmitted by the surface wave propagating beyond the curve. A high transmission loss is undesirable and it is of interest to know if and how one can design a line to convey the surface wave around a curve with tolerable loss. We had a tentative look at this problem.

Figure 34 represents a top view of a Yagi line of 90 dipoles in free space, dipoles number 1-30 and 61-90 forming straight input and output sections, respectively, the remainder forming a 90^{o} circular arc. The dipoles all have a spacing $S=0.3\lambda$, length $\ell=0.44\lambda$ and a radius $a=0.001\lambda$. Dipole No. 1 is excited with 1 ampere, causing, as described previously, surface waves and "strange" waves to travel from the source to the end of the line (outgoing waves) and from the end of the line back to the source (reflected waves). By solving for all the currents on the 90 dipoles by the method of moments technique we can choose sets of 6 dipoles, first in the straight input section, then in the curve, and finally in the straight output section. Each of these will yield the amplitudes of the currents and propagation constants of the surface waves and strange waves proceeding in both directions in each of these three regions. Figure 35 shows the results for the outgoing and reflected surface waves only (the outgoing and reflected strange waves are, respectively, one and two orders of magnitude below the reflected surface wave and are not presented here). The solid curve C_o represents the (eye-interpolated) curve passing through the current amplitudes associated with the outgoing surface wave. Clearly, these currents experience a substantial drop in their procession around the curve, indicating substantial transmission loss due to radiation (wave attenuation due to copper loss is negligible by comparison). The dashed curve C_r represents the (eye-interpolated) curve passing through the current amplitudes associated with the reflected surface wave; an identical percentage transmission loss is experienced by this wave as it proceeds around the curve, as would be expected from the symmetric geometry of the whole line. The two curves marked $C_o + C_r$ and $C_o - C_r$ are simply the sum and difference of C_o and C_r. The heavy dots represent the actual current amplitudes as obtained by the method-of-moments before resolution into surface and strange modes. The fact that a few points fall outside the region bounded by $C_o + C_r$ and $C_o + C_r$ is evidence that strange modes exist but are small. It may be commented here that the velocities of the strange modes were found to exceed the speed of light - as would be expected if they were due to direct radiations from the ends of the line,

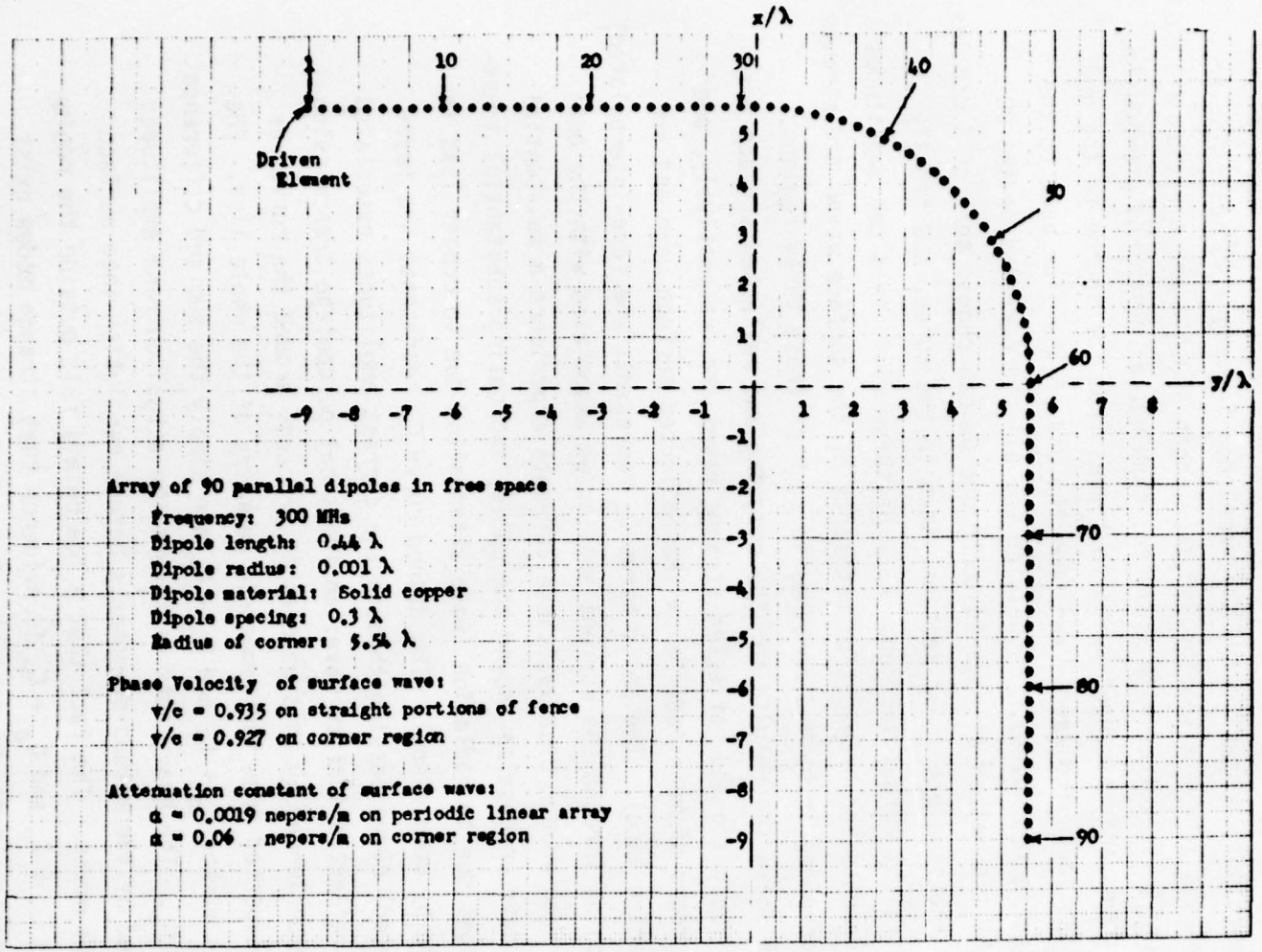

Figure 34. Transmission around a 90^{o} arc of a finite Yagi line.

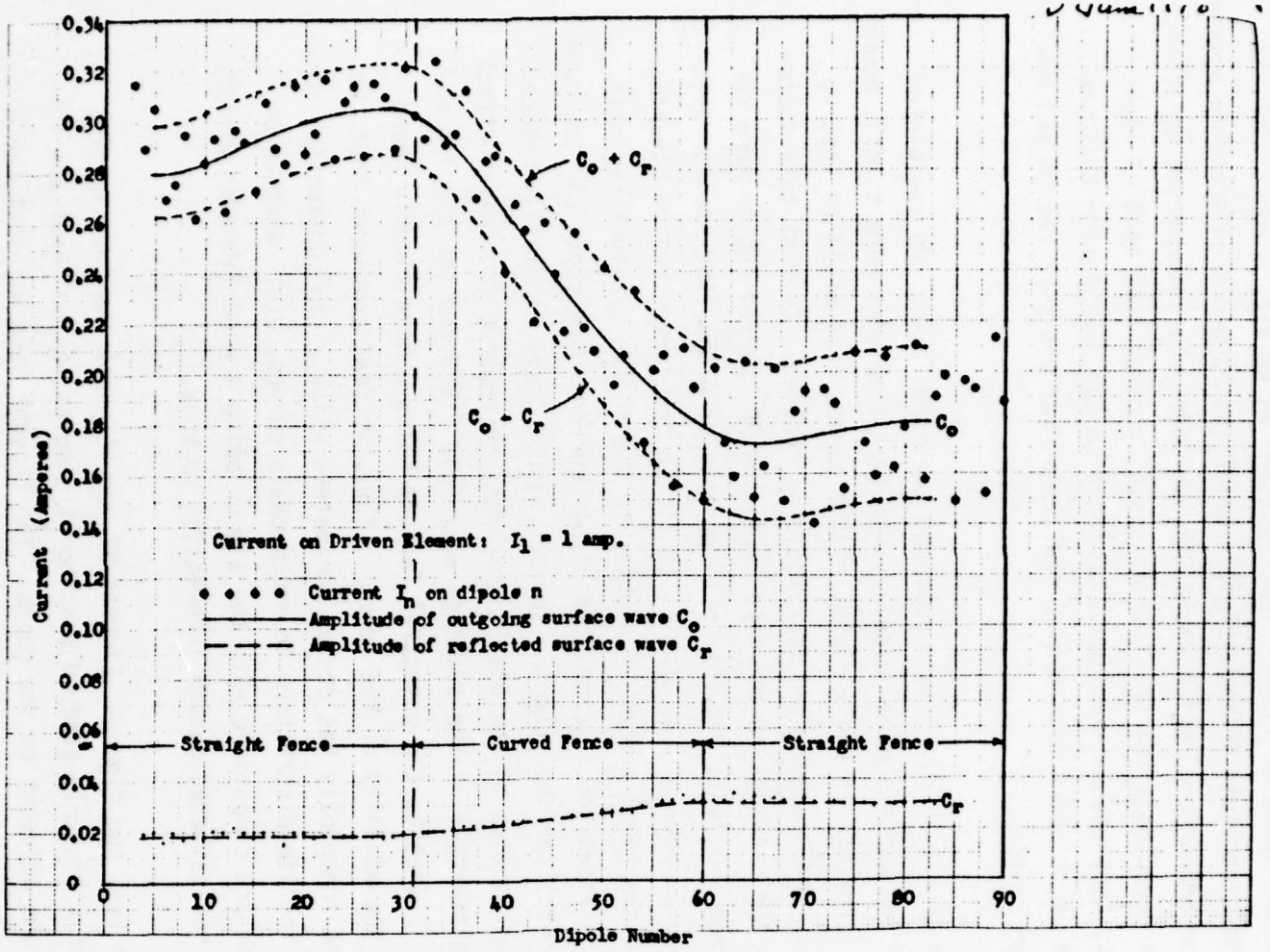

Figure 35. Transmission around a 90^o arc of a finite Yagi line.

that radiation proceeding in straight lines to all points in the curved Yagi at the speed of light. Then testing, as we did, along a line skew to these directions of radiation, wavelengths larger than actually present would be encountered which would, in our model, be interpreted as strange waves proceeding along the Yagi at speeds greater than that of light. In fact, this observation lends credence to our speculation that the strange waves are indeed due to radiation from the feed region and reflection region.

In Figure 35 all dipole spacings are held fixed. We speculated that if the surface wave guided by the Yagi line were more tightly bound to the structure in the vicinity of the curve, less would be lost to radiation and transmission loss would be reduced. To test this speculation, the spacings of the dipoles in the 90^{o} curved region were reduced from $S=0.3\lambda$ to $S=0.15\lambda$ in increments of 0.05λ (the smaller spacings require more of the dipoles to lie in the curved region, leaving fewer of the total number of dipoles to lie in the straight regions). Figure 36 shows the interpolated dipole current magnitudes (in the curved region only) for the outgoing surface wave. There is clearly reduced transmission loss as the dipole spacings are reduced (a similar effect would be expected if the spacings were held fixed and the dipoles increased in length, the essential feature being a more tightly bound wave in the vicinity of the curve). Thus, we feel confident that the Yagi line inherently has design parameters which allow substantial control of the field structure to accommodate curves, etc. Whether or not these are compatible with the aim of being a good intruder sensor, we have not gathered enough information to know.

The last two figures, Figures 37 and 38, show the (negligible) effect of a linearly tapered spacing of dipoles in the input and output regions adjacent to the curve. The thought here was that the discontinuity caused by the curve and sudden reduction in dipole spacing might cause a non-negligible reflection of the outgoing surface wave as it enters the curved region. The tapers were intended to mitigate

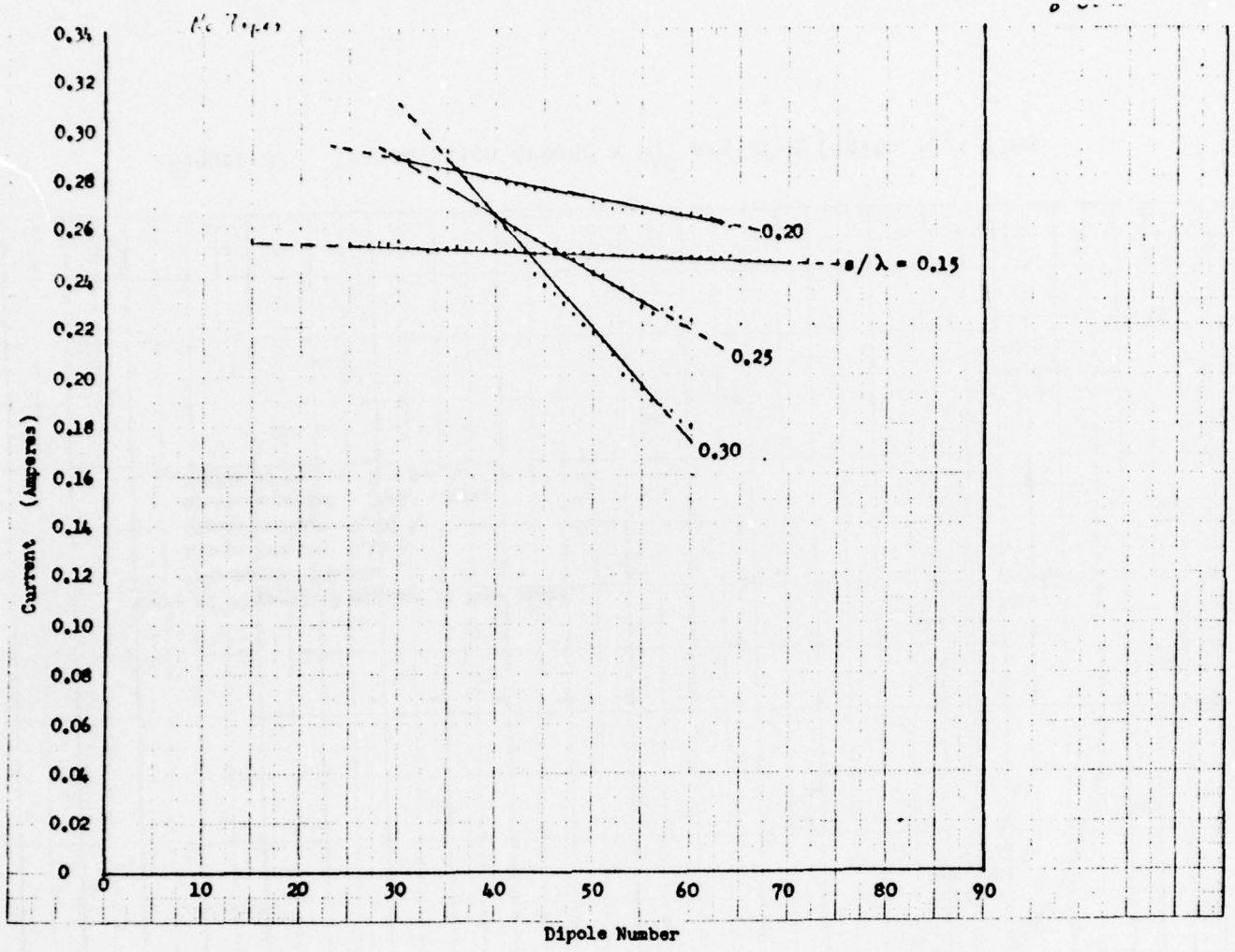

Figure 36. Transmission around a 90^{0} arc of a finite Yagi line.

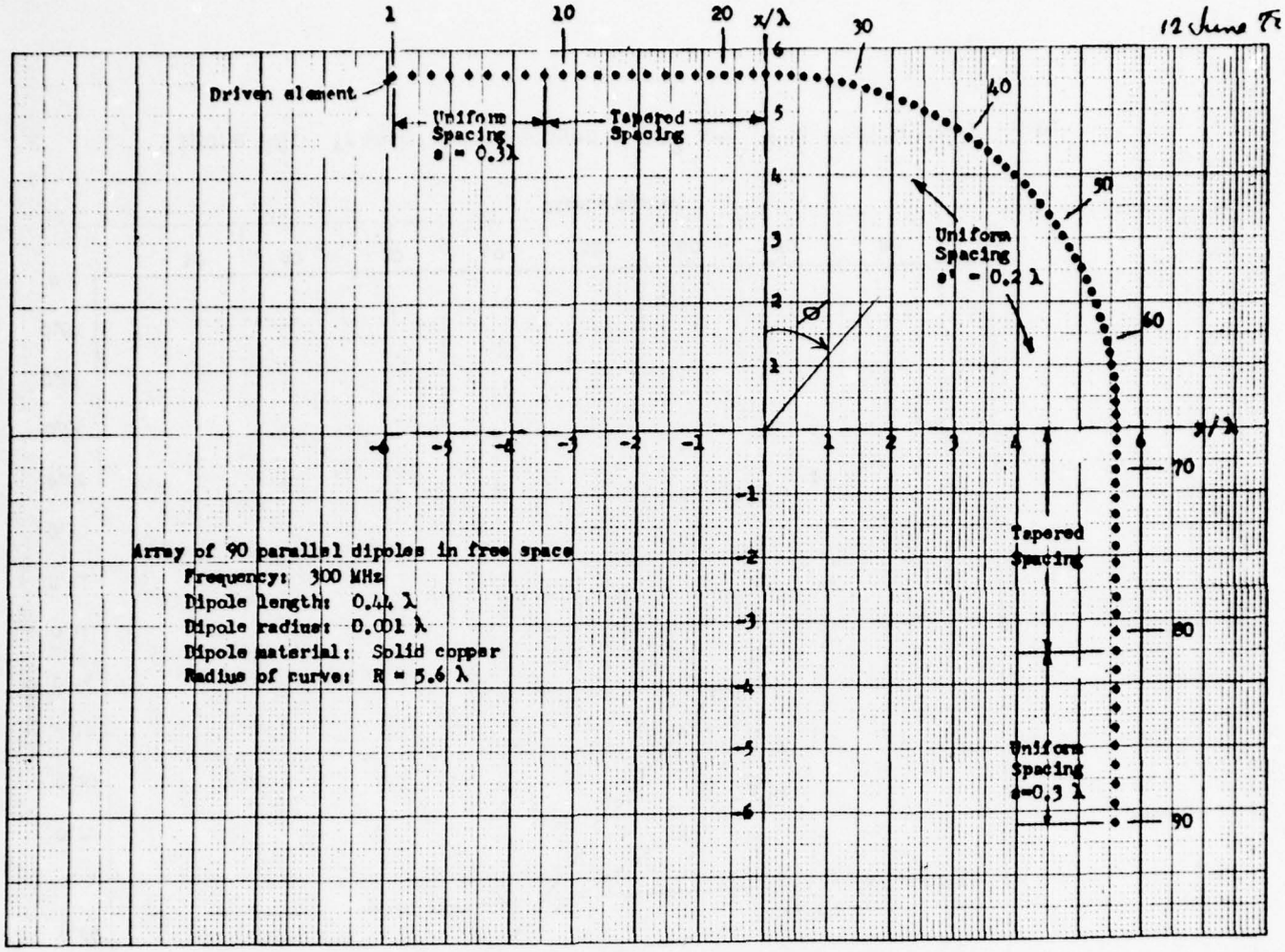

Figure 37. Transmission around a 90^{0} arc of a finite Yagi line.

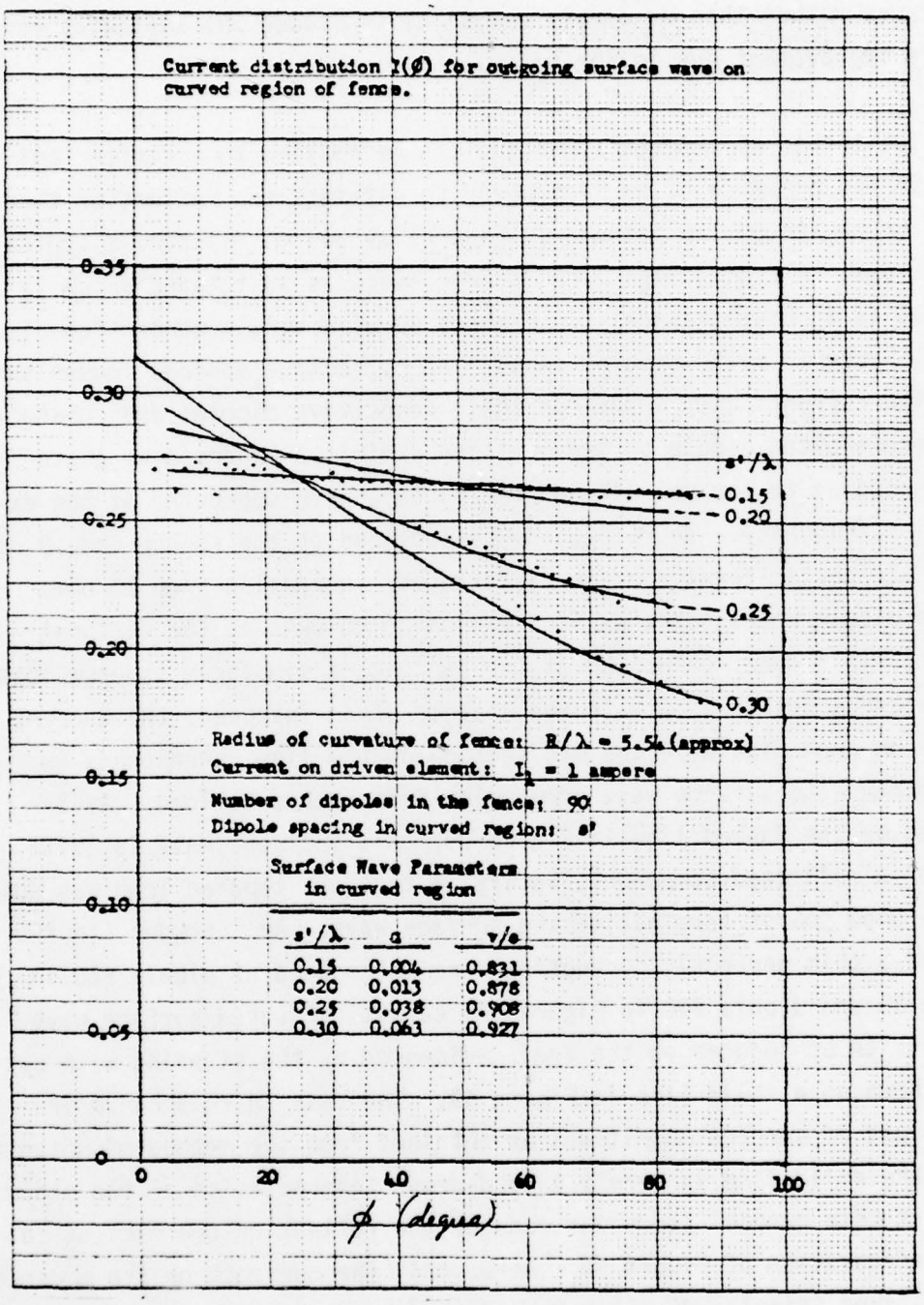

Figure 38. Transmission around a 90^{0} arc of a finite Yagi line.

this reflection. Figure 38 (currents plotted vs the angle ϕ around the curve rather than vs dipole number as in Figure 36) indicates very little improvement due to the taper.

The method of moments technique can be applied to a finite Yagi line in the presence of an "intruder" to estimate the reflection that would be caused by the intruder. Figures 39 and 40 illustrate typical situations. A finite Yagi line in free space is postulated which is excited in a chosen manner - in Figures 39 by a single center-fed dipole, or in Figure 40 by 10 dipoles center fed by voltage sources chosen such that the currents they induce on their respective dipoles are constant from one excited dipole to the next and exhibit a progressive phase corresponding to the velocity of the surface wave supported at the excitation frequency. To reduce any reflections at the source end, 8 dipoles are center-terminated in resistances, increasing from 10 ohms at the dipole nearest the excited region to 80 ohms at the farthest dipole. To reduce reflection at the far end, a similarly tapered lossy load arrangement is used. In the absence of an intruder, the current $I_0 e^{-\gamma y}$ on each dipole in the mid section of the line corresponds to the appropriate surface wave proceeding from source to load. As indicated by the dashed line in Figure 39, this incident wave is quite free of a reflected component, verifying that our tapered load was doing a very good job of terminating the surface wave. An intruder (in the form of a thin perfectly conducting wire introduced at dipole #20 in Figure 39 and dipole #40 in Figure 40) causes reflected surface wave currents to be induced on the Yagi, evidenced by the standing wave pattern shown as a solid line in Figure 39. The dots in this curve are the values of current magnitudes as obtained from the method of moments while the solid line is merely a hand-drawn interpolation of the standing wave. A more careful study was made of the reflection coefficient in the configuration of Figure 40. Here, only the currents on the midsection of the lines (dipoles 25-35) are presented because it is in this region that we expect to see a combination of incident and reflected waves.

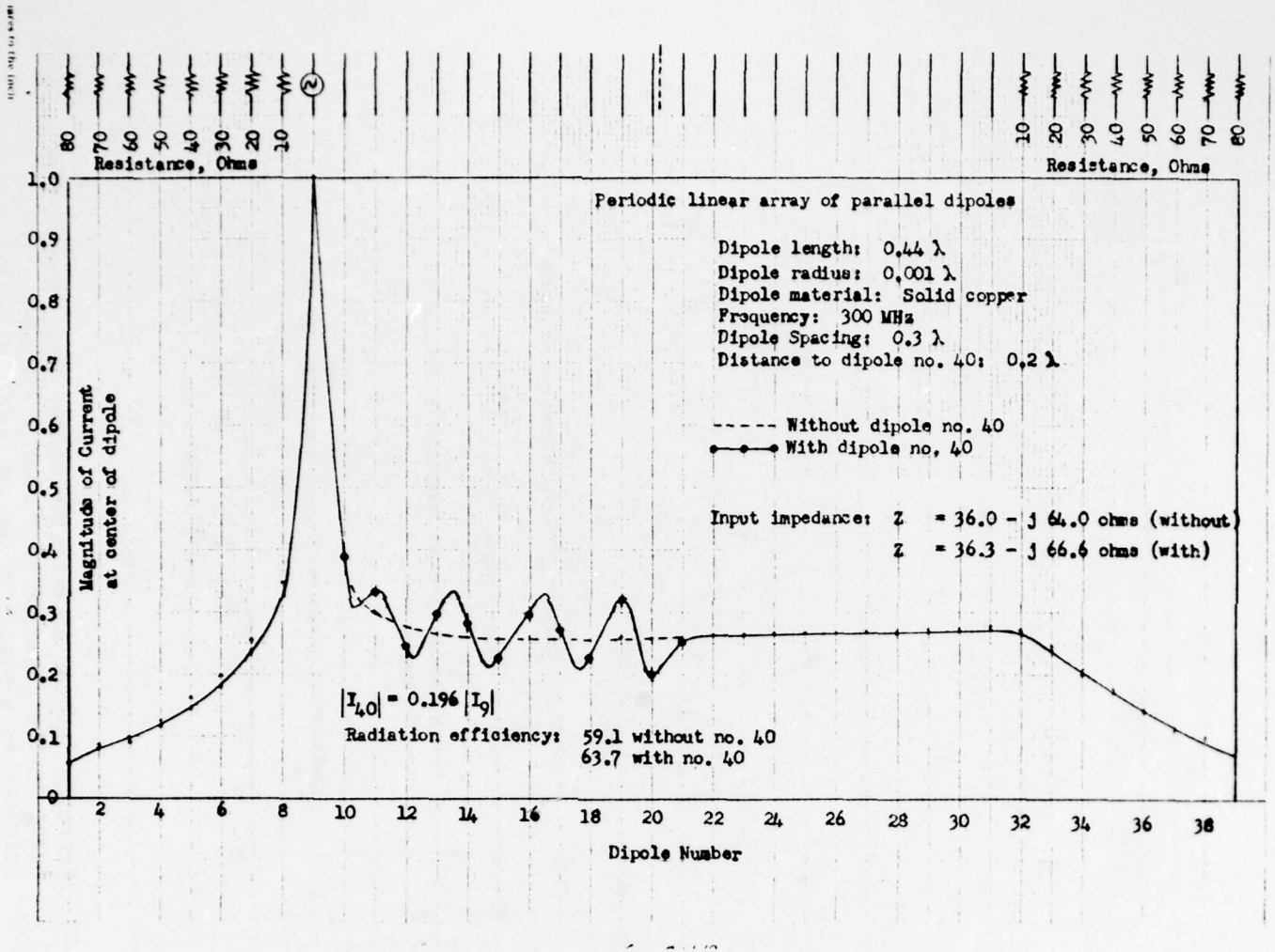

Figure 39. Currents induced on a finite Yagi line in free space in the presence of a nearby intruder (dipole No. 40) of height 0.44λ.

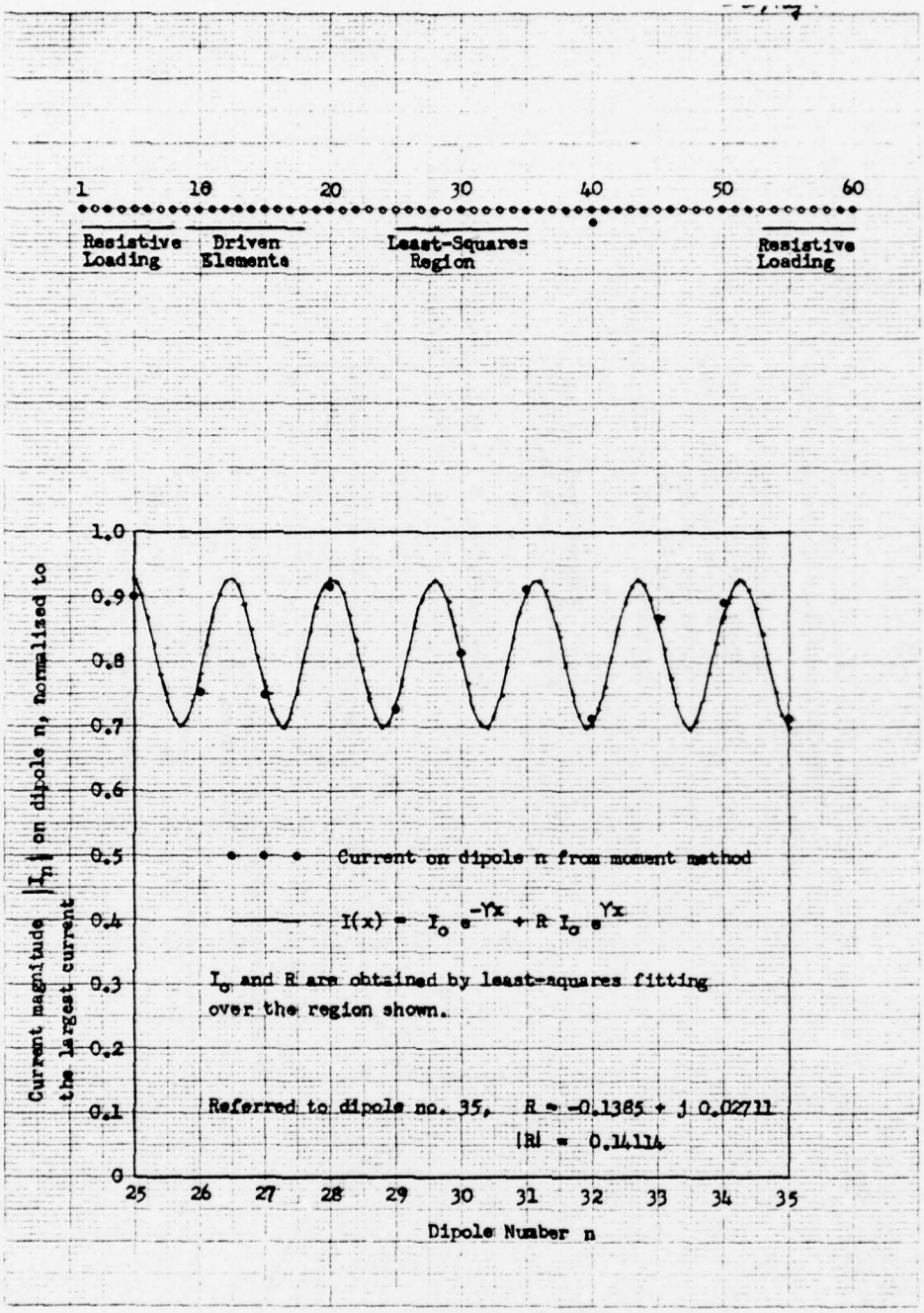

Figure 40. Currents induced on a finite copper Yagi line in free space in the presence of a nearby intruder. The intruder is a dipole of height 0.44λ at a distance x=0.2λ from the 40th dipole in the line. f=300 MHz, line parameters given in Fig. 39.

The dots are the values of the currents as obtained from the method of moments, the solid line is the curve $I_o e^{-\gamma y} + RI_o e^{\gamma y}$, where the values of the two unknowns, I_o and R, were obtained by matching this mathematical form to the actual currents obtained by method of moments. This matching was performed in a least-mean square sense over the 11 dipoles indicated in Figure 40. Comparison of the dots with the solid curve lead us to believe that our representation of the currents as incident and reflected surface waves with reflection coefficient magnitude $|R| \simeq 0.14$ is reasonably accurate.

With the foregoing comments in mind, Figures 41-44 present the magnitude of the surface-wave reflection coefficient of an intruder near an aluminum Yagi in free space at 100 MHz. Two dipole radii, a, and two dipole spacings, s, are considered for a variety of dipole lengths, ℓ. The intruder in all cases is a thin perfectly conducting rod of length 0.44λ (1.32 meters) which is parallel with and symmetrically located with respect to the Yagi dipoles and up to $\lambda/2$ (1.5 meters) away from them. The reflection coefficient in all cases is referenced to the Yagi dipole nearest the intruder. The curves appear to flatten out at distances larger than about 0.3λ, particularly for those combinations of s and ℓ (smaller s, larger ℓ) which correspond to slower surface waves, i.e., more tightly bound waves. This indicates that we are observing the effects of direct radiation from the feed region to the intruder region which corrupts the assumptions upon which our definition of reflection coefficient is based. The results are probably reliable for values of $x/\lambda \leq 0.3$, i.e., within 1 meter of the line.

An additional comment is in order regarding the computational investigation just described, and that involves the radiation efficiency of the entire configuration under consideration. By radiation efficiency we mean the ratio of power radiated to total power supplied by the primary feed. Radiation takes place from the feed region and termination region and, where an intruder is present, from the intruder and intruder region. Figure 39, for example shows that 59.1% of the input power

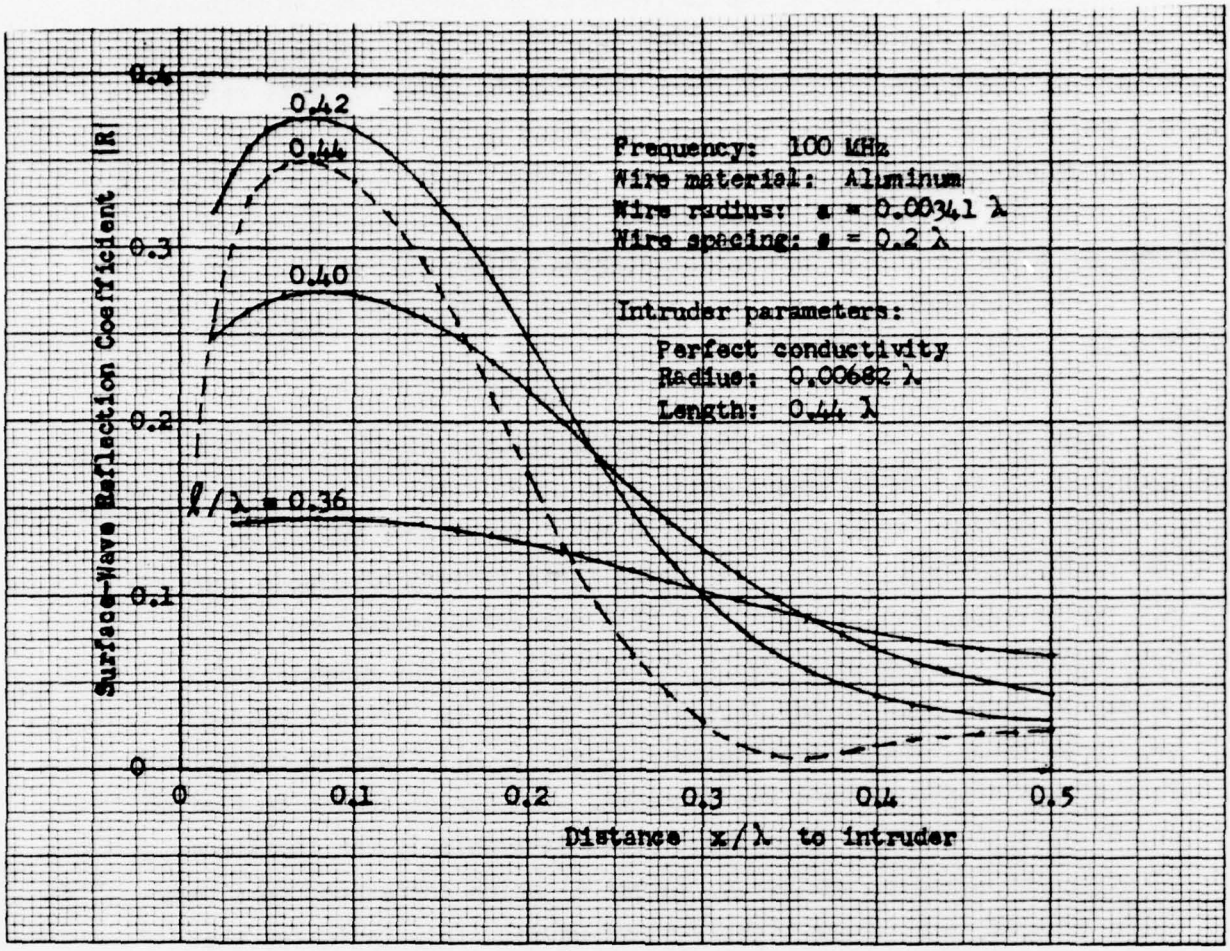

Figure 41. Reflection coefficient of the surface wave on Yagi lines due to an intruder (wire) as a function of intruder distance.

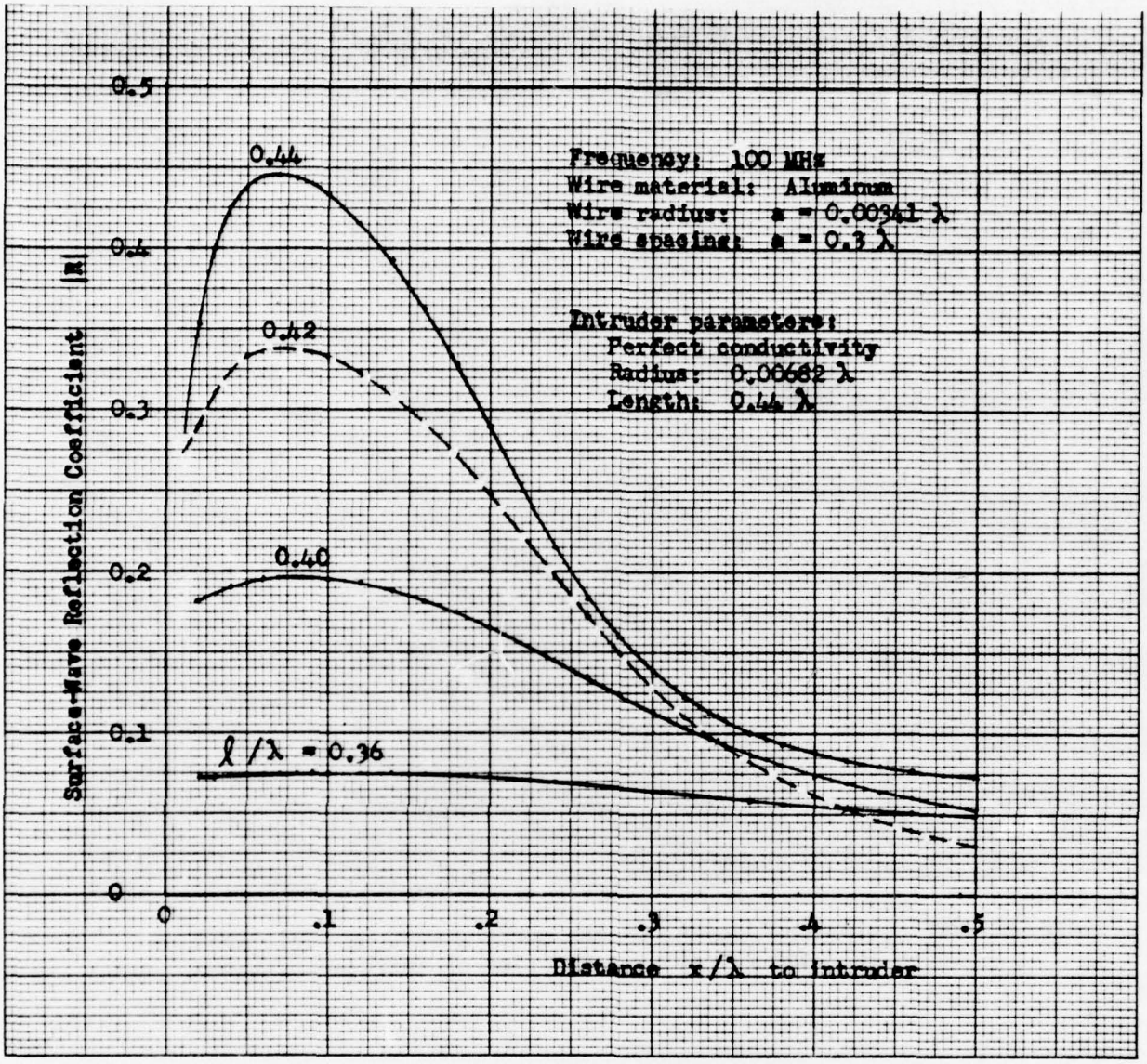

Figure 42. Reflection coefficient of the surface wave on Yagi lines due to an intruder (wire) as a function of intruder distance.

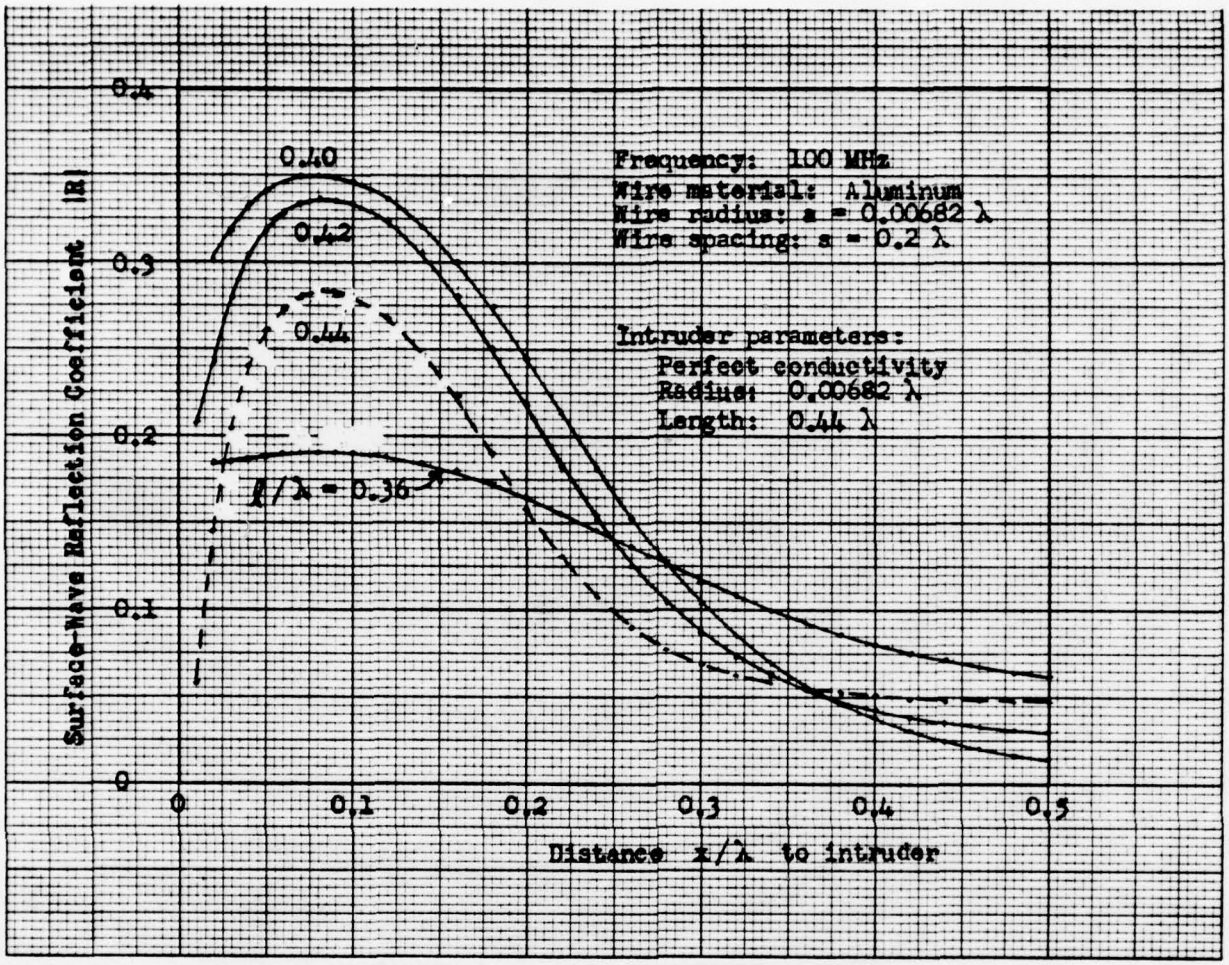

Figure 43: Reflection coefficient of the surface wave on Yagi lines due to an intruder (wire) as a function of intruder distance.

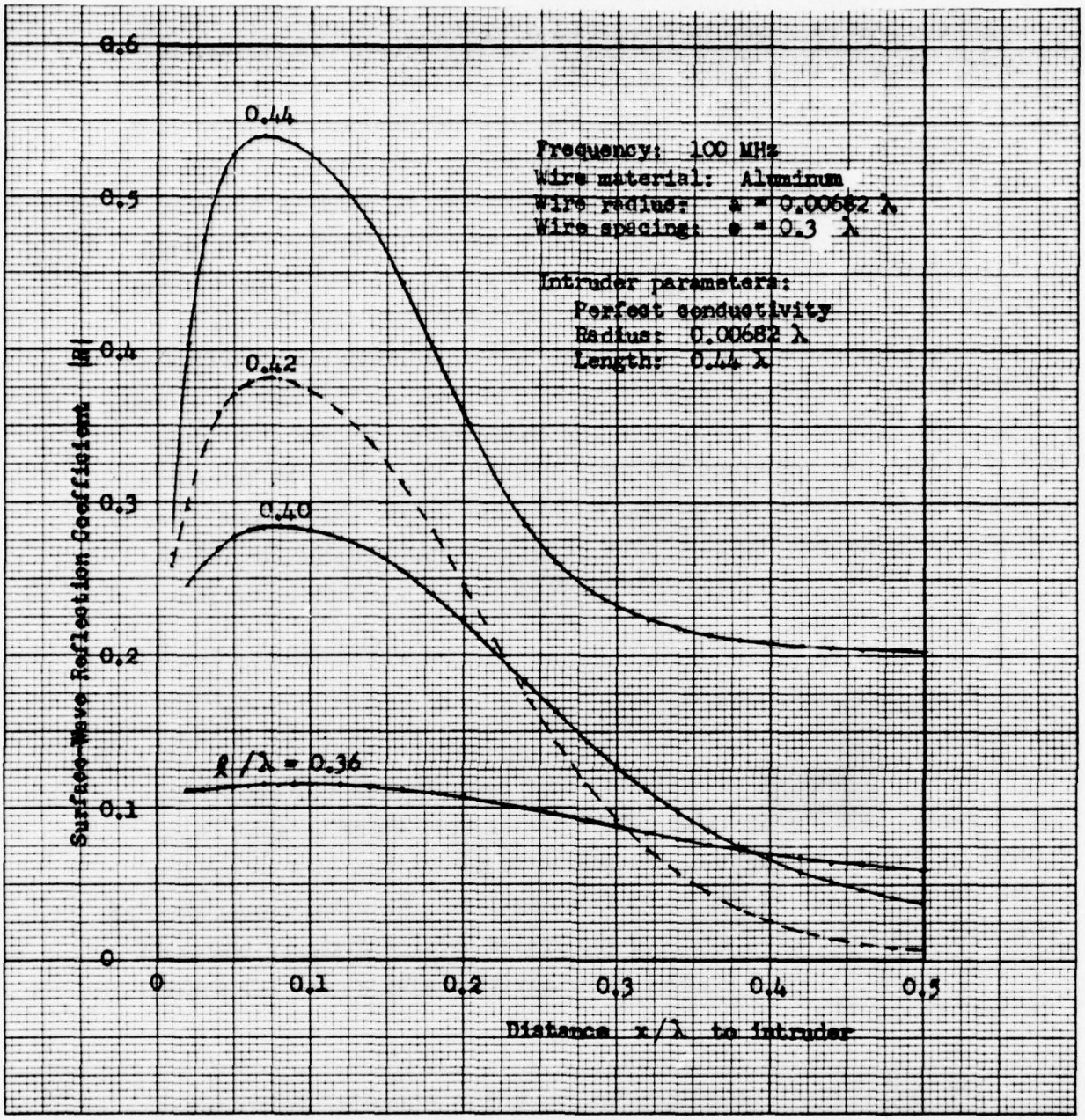

Figure 44. Reflection coefficient of the surface wave on Yagi lines due to an intruder (wire) as a function of intruder distance.

went into radiation and introduction of the intruder raised that to 63.7%. Much of this radiation is due to the feed configuration, in this case a single dipole backed by a linearly tapered resistive load. If a distributed feed, such as that described previously for Figure 40, is used, we would expect a better transfer of power into surface wave fields and less radiation, i.e., a smaller radiation efficiency. This criterion, small radiation efficiency, was, in fact, the one used to arrive at the design consisting of a distributed feed backed by a linearly tapered load used in Figures 40-44. In Figure 45 such a feed together with a linearly tapered load is assumed at the ends of a copper Yagi line in free space whose length is varied to include from 30 to 90 dipoles. The radiation efficiency hovers about 35%. We speculate, though we have not investigated it computationally, that providing more driven elements and including more dipoles in the termination regions will reduce this radiation efficiency further, though never to zero in a practical case.

C. Some Experimental Results

To verify theoretical results, some experimental data were taken on a scaled Yagi transmission line. If the full sized version is assumed to operate at 100 MHz, the scaled model was designed to operate at 2.598 GHz, i.e., it was 25.98 times smaller. Choosing copper dipoles for both the full sized line and the scaled version disturbs the exact scaling insignificantly because conductivity scales almost 1:1 for excellent conductors.

The Yagi dipoles were supported by a thin ribbon of polyfoam (ε_r - 1.05) whose width was about half the dipole length. At the design frequency of 2.598 GHz the dipoles had length 0.44λ (ℓ=2"), diameter 0.0134λ (2a=1/16"), and the dipole spacing was 0.3λ (s=1.36"). This structure was carefully suspended on a system of very fine 1 lb test nylon string zig-zagged across a trough-like wooden structure 2 feet wide, 1 foot deep and 12 feet long. For convenience, the dipoles were

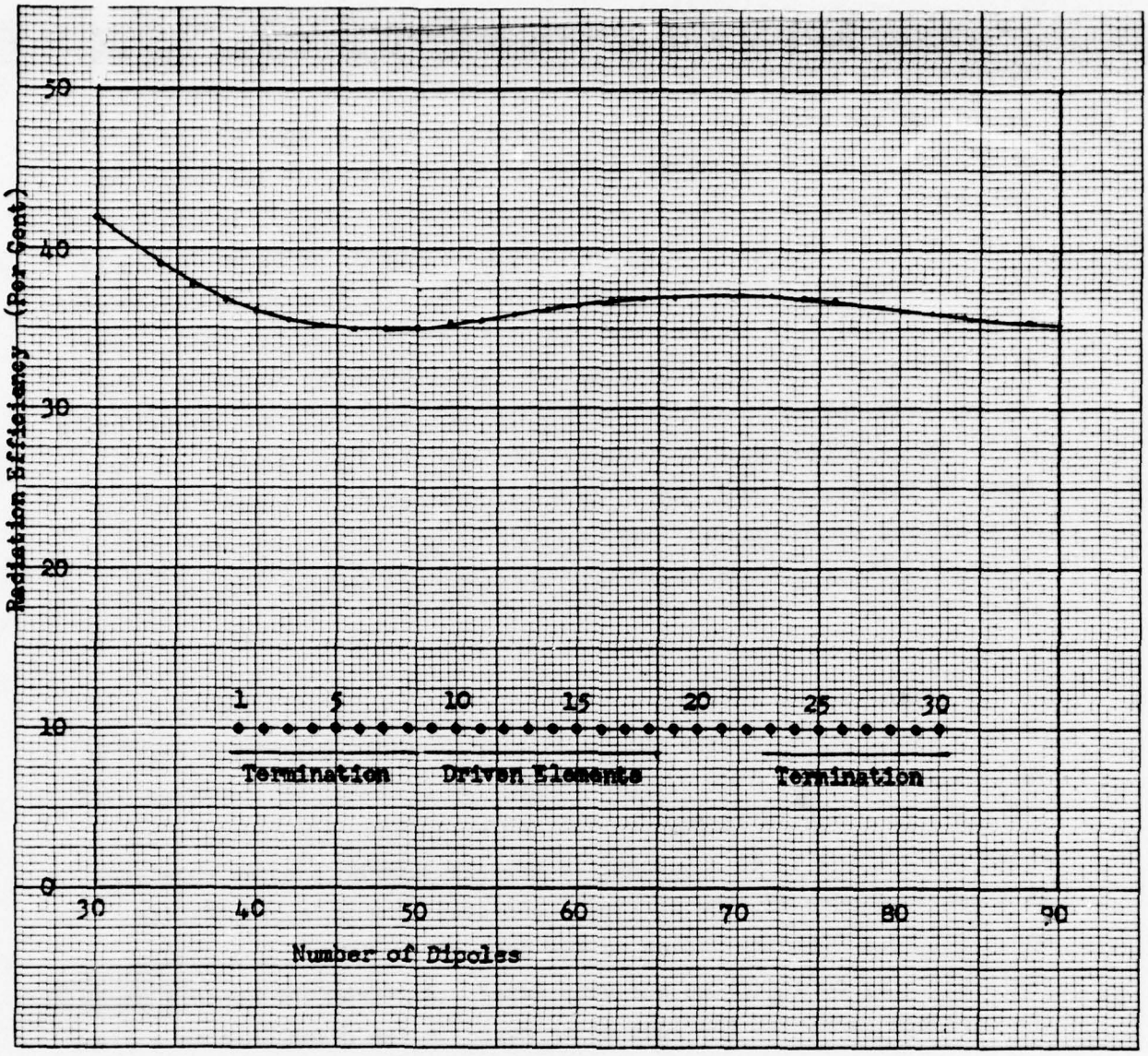

Figure 45. Radiation efficiency of a finite copper Yagi line as a function of its length. f=300 MHz.

oriented horizontally as shown in Figure 46. At one end the line was terminated in a 1 ft x 1.5 ft. short circuiting aluminum plate (not shown); at the other end, the line exited through an aperture in a wall of 8" thick hairflex absorber (shown in the photograph) and under its own weight proceeded to curve gently upward over a 5 foot length toward a log periodic antenna from which it was suspended, as shown in Figure 47. As suggested by our calculated data, the dipole spacing was reduced to 0.2λ (s=0.91") in this curved region to better trap the surface wave as it proceeded from the source to the line beyond the aperture. The log periodic antenna was simply one which was available and worked quite well. As expected the direct radiation from the feed antenna was reduced in the measurement region by this combination of geometrical orientation and absorbing wall and, except for positions very near the aperture, only a surface wave field was detected on the line, as desired.

A balanced loop antenna, 0.5" in diameter, carefully constructed of very fine coaxial cable, served as a probe whose output was carried vertically upward (a line of zero tangential E-field when centered over the Yagi) to slightly larger coaxial cable, thence to a moveable carriage and eventually to a Scientific Atlanta superheterodyne receiver. As shown in Figure 48, the carriage consisted of a pair of modified model railroad flatcars riding on two sets of tracks along a wooden shelf which by construction was very level. A micrometer support on the carriage permitted the loop to be moved in two dimensions in a plane transverse to the surface wave propagation direction. By carefully laying the Yagi line parallel to the tracks and adjusting the tautness of the support strings so that the line maintained a uniform distance below the probe, a type of "slotted line" was formed for the measurement of attenuation and wave velocity.

When centered over the Yagi line and oriented in a plane of a dipole, the loop detected a signal essentially proportional to the longitudinal component of H (H_y) and, being balanced, it was insensitive

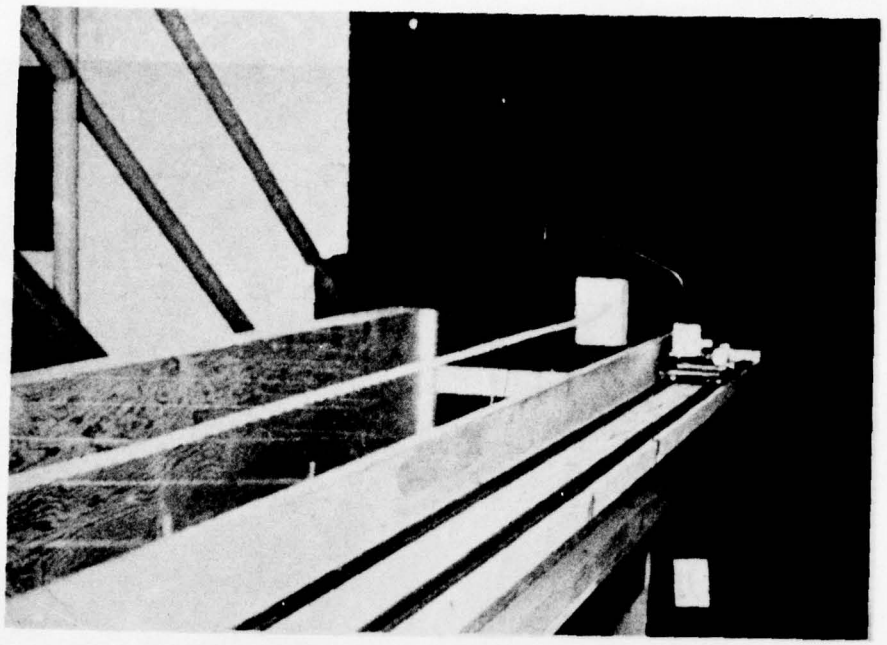

Figure 46. Photograph of experimental Yagi line.

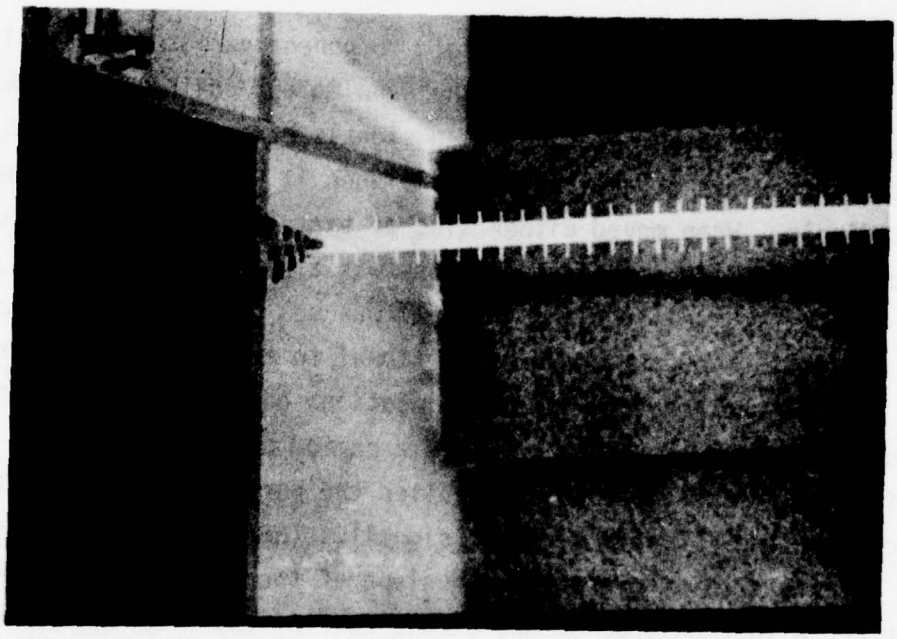

Top→

Figure 47. Photograph of log periodic feed antenna.

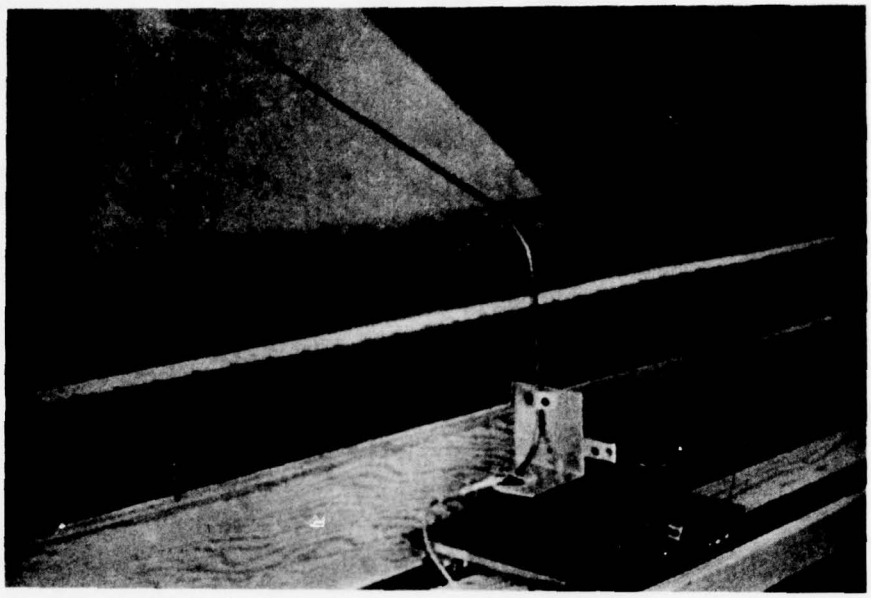

Figure 48. Photograph of carriage and loop probe.

to the electric field. The H_y field component varies greatly along the line, being strongest aside the dipoles and quite weak between them. Thus, the loop as oriented detected signals essentially proportional to the current in a particular dipole when it was located adjacent to that dipole. When moved either side of that location, the signal dropped precipitously. In a sense then, ours was a sampled data system, where the uniform spatial sampling interval was set by the dipole spacing, and the voltage outputs were proportional to the amplitudes of the standing wave at the respective dipole locations on the short circuited line. Since the sampled standing wave has a period different from the sampling period, the recorded samples exhibited the periodicity of a beat wave (much like the FFT of a periodic signal). The period of this beat wave can be extracted by eye as the envelope of the recorded data and it, together with knowledge of the dipole spacing and frequency, permits determination of the wavelength of the surface wave and hence its phase

velocity. As an example of raw data at f=2.519 GHz, Figure 49 shows a graph of bars whose amplitudes are proportional to the log of the power received at 39 dipole stations. The envelope of these bars was sketched by eye and found to have an average period of P=4.5 dipole spacings. It may be shown that the relative velocity is given by the expression

$$\frac{v}{c} = \frac{2s}{c} \frac{f}{1 - 1/P} , \tag{53}$$

and for the line we constructed this becomes,

$$\frac{v}{c} = 0.2309 \times 10^{-9} \frac{f}{1 - 1/P} . \tag{54}$$

Using data such as those shown in Figure 49 and applying Equation (54) we arrive at the experimentally determined values of v/c displayed as dots in Figure 50. Values of v/c predicted by our mathematical model are shown as the dashed curve. They show the same trend but are too high by 15-20%. This difference is at least partly explained by the fact that the dipoles, being rather thick ($\ell/2a=32$), act longer at the test frequency than the 2" they appear to be optically; being effectively longer, the theory indicates that, indeed, the surface wave should be slower than predicted. The difficulty in the theory arises from the current distribution, Equation (9), assumed a priori to exist on each dipole. In this simple model, the dipole is considered to be segmented into two equal parts of length h with piecewise sinusoidal currents on each, matched at the center. A more accurate description of the current would be given by an N-segment model, in which case the current distribution is not assumed a priori but is determined (within the resolution permitted by the N-segment basis set) along with the propagation constant. Because this model better resolves the current distribution near the ends of the dipoles, one might expect it to yield more accurate values of v/c and α. The price one pays for increased N is a more complicated,

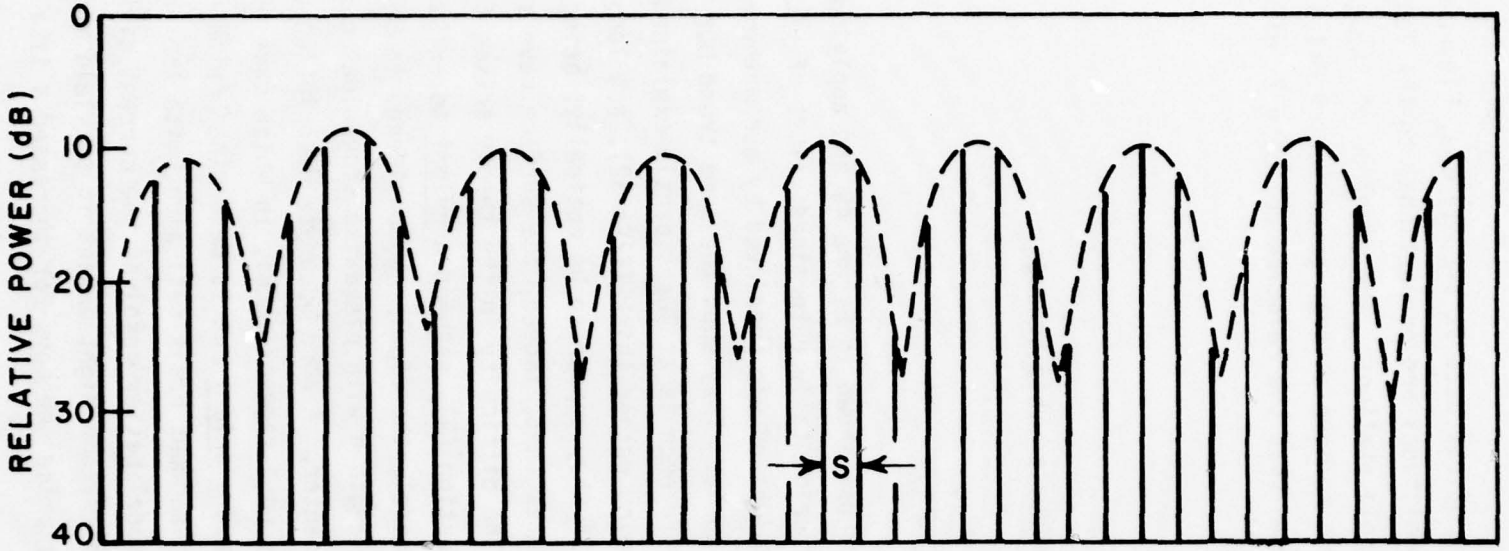

Figure 49. Representation of experimental data recorded for Yagi line at f=2.519 GHz.

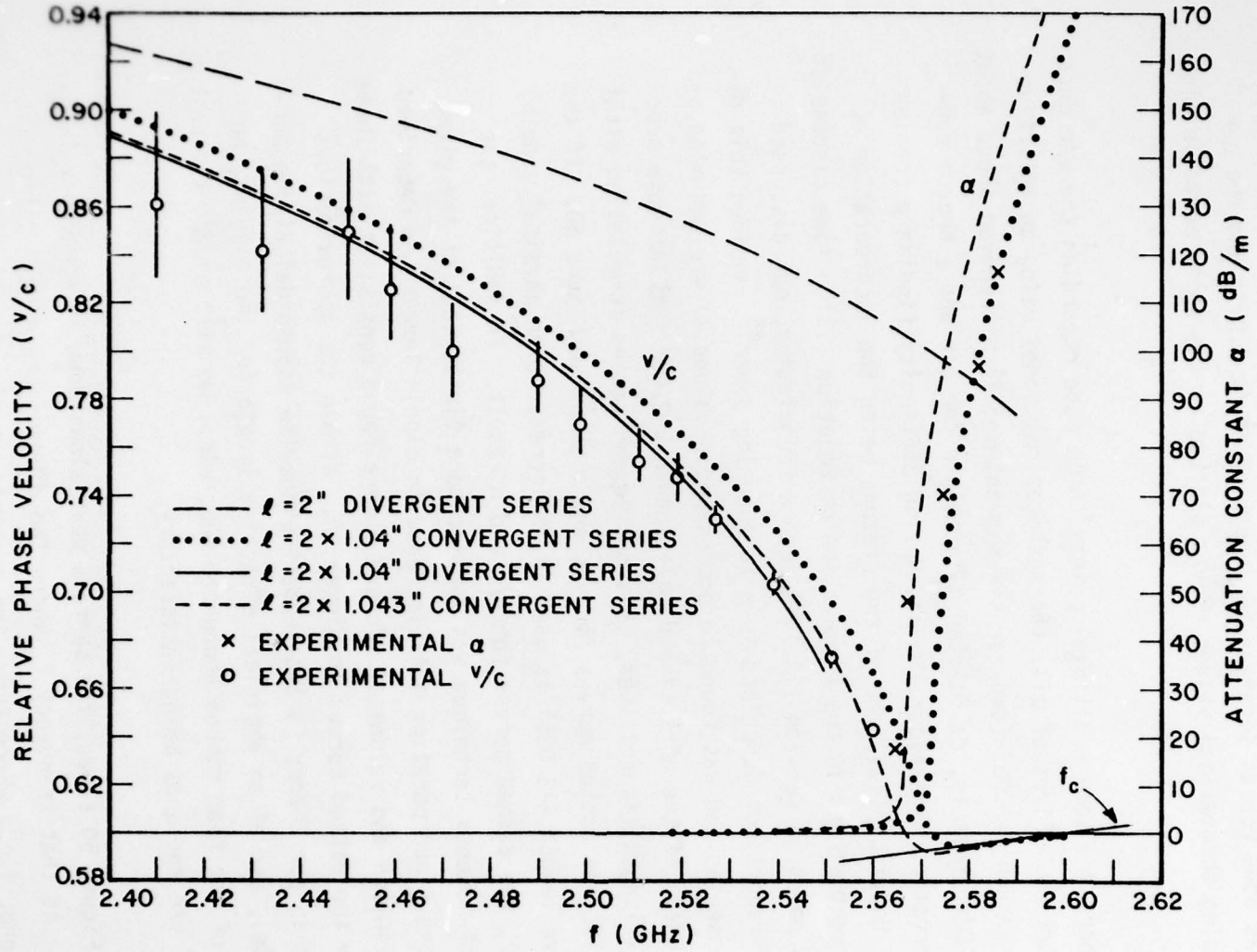

Figure 50. Calculated and experimental values of v/c and α over a frequency band.

slower algorithm for determining the propagation constant. As a compromise alternative, the two segment model can be retained and an effective length, $\ell+\Delta\ell$, can be used rather than ℓ for the dipole length. This was done for an increase in length of 4% (ℓ=2.08") and the corresponding theoretical values of v/c plotted as the solid curve in Figure 50.

There are some additional points to be made regarding the v/c data in Figure 50. First of all, the mathematical model using an effective dipole length ℓ=2.08" (two- or six-segment model) misbehaved above about f=2.55 GHz, that is, calculated data points for v/c and α became randomly erratic. The algorithm was having difficulty finding a complex root of Equation (13), one of the reasons being the incorporation of a divergent series in the formulation of Equation (13). (See discussion of this point in section IIA.) A second formulation, not discussed in this report but described in a forthcoming paper[45], avoided this divergent series and was found to produce good values of v/c and α beyond f=2.55 GHz. If the effective dipole length ℓ=2.08" (4% increase over physical length) is retained, this convergent series formulation with N=2 yields the dotted curves for v/c and α shown in Figure 50. If the effective length ℓ=2.086" is used (4.3% increase over physical length) with N=2, the dashed curves for v/c and α result. In addition, the method-of-moments technique was applied to a finite Yagi of the given dimensions (incorporating a 4% increase in dipole length) as described in section IIB and values of v/c and α were found consistent with those given by the dotted curves in Figure 50. Within the approximations inherent in our theory (a two-segment piecewise sinusoidal dipole current model, use of an empirical effective length for the dipoles, no effects of the foam ribbon accounted for, etc.) we will accept the dashed curve of v/c and α as being satisfactory.

As Figure 50 shows, the surface wave slows down as frequency increases. At that frequency f_c where the dipoles are a half guide wavelength long, i.e., where $\beta s=\pi$, the currents on adjacent dipoles are

180^0 out of phase, which would correspond to waves proceeding in either the +y or -y direction along the Yagi. This nonuniqueness implies that in fact no wave propagates in the +y direction along the line when $\beta s \geq \pi$ and that the frequencies $f_c = \frac{v/c}{2s/c}$ are cutoff frequencies for the surface wave mode in question. These values of f_c are indicated by the sloped line in Figure 50; our theoretical data hugs this line fairly well, with a little undershoot.

The region around the cutoff frequency is the first Bragg interaction region. If the Yagi line were lossless, the surface wave would abruptly change its character at a unique f_c from a propagating wave whose group velocity becomes zero at f_c to an evanescent wave which does not propagate but only attenuates. Since loss must occur in any realistic case, this sharp division between "pass" and "stop" bands is blurred and this is displayed in our theoretical curves by a smooth merging of the two regions.

Experimental data taken over the entire 12 foot line exhibited the influence of loss, i.e., diminishing standing wave ratio as one proceeded from short circuit to source. In the passband frequency range, f=2.41 to 2.5 GHz, this effect was too small and the measurement inaccuracies too great to resolve experimental values of α with confidence. In the stopband above f=2.56 GHz, however, where β remains essentially constant and attenuation is the dominant feature of the Yagi field, instead of standing waves, a severe attenuation of the field was observed as one proceeded away from the source end. Figure 51 shows the recorded bar graph and approximating envelope taken at f=2.574 GHz. Because the vertical scale is in dB the slope of the (approximately) linear envelope is a measure of the attenuation constant α. The crosses in Figure 50 display a few experimental values obtained in this way for comparison with the aforementioned theoretical curves of α.

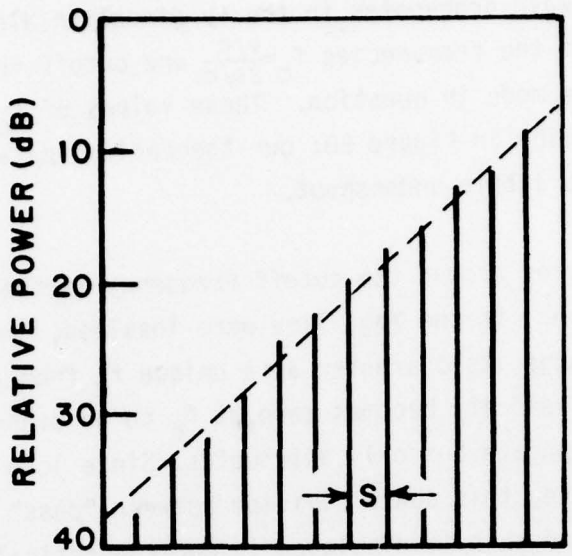

Figure 51. Representation of experimental data recorded for Yagi line at f=2.574 GHz.

A limited amount of experimental data were accumulated for the Yagi line placed near a lossy interface, as shown in Figure 52. The lossy material was hairflex absorber with its backside nearer the line. Typical recorded data in the form of bar graphs are not presented: it may be said, however, that for the high attenuation cases, the data appeared very similar to Figure 51 with very little evidence of a standing wave, making evaluation of v/c impossible; for the low attenuation cases, the data appeared more like Figure 49, with much standing wave evident and attenuation so small that it became difficult or impossible to extract values of α. In between, the recorded data showed an attenuated standing wave near the short circuit, from which v/c could be deduced, and a linear rise near the source end from which α could be extracted.

Figure 52. Photograph of experimental Yagi line with hairflex interface in place.

Figures 53 and 54 show experimental values of v/c and/or α, respectively, obtained in this way at three frequencies in the pass band region for three nominal centerline-to-interface distances, d - 3.175 cm, 3.81 cm and 10 cm. The solid curve in Figure 53 is the same as that in Figure 50 for v/c of the free space case. As expected, we notice that the influence of the lossy interface is primarily on α and very little on v/c, especially for the largest height d=10 cm. The fuzzy nature of the interface made precise evaluation of distance d impossible and, in fact, this distance varied a bit from point-to-point along the line about the nominal values quoted above. Also, we do not know the values of dielectric constant and conductivity of the near side of the hairflex panels. These two intangibles made any theoretical curves generated for the Yagi line over the earth of doubtful value for comparison with experimental data. We did try, however. Using estimated values for hairflex dielectric constant and conductivity of $\epsilon_2=2\epsilon_o$, $\sigma_2=0.01$ Siemens/m, respectively, we calculated v/c and α for a range of heights about the value d=1½" (3.81 cm). Table IV displays some

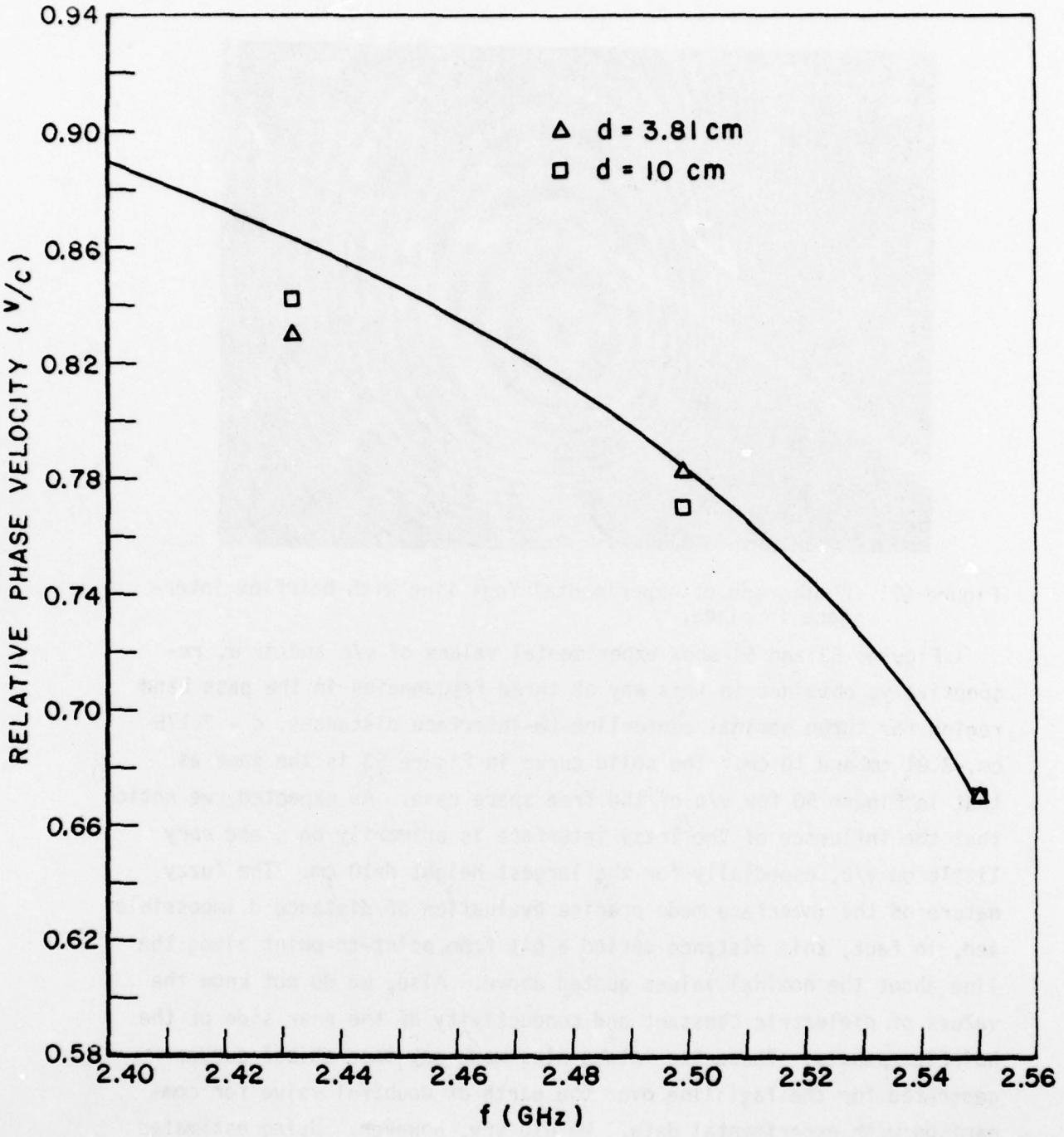

Figure 53. Experimental values of v/c for two nominal heights of Yagi over lossy interface. Solid curve is same theoretical curve as solid curve in Figure 50 for free space case.

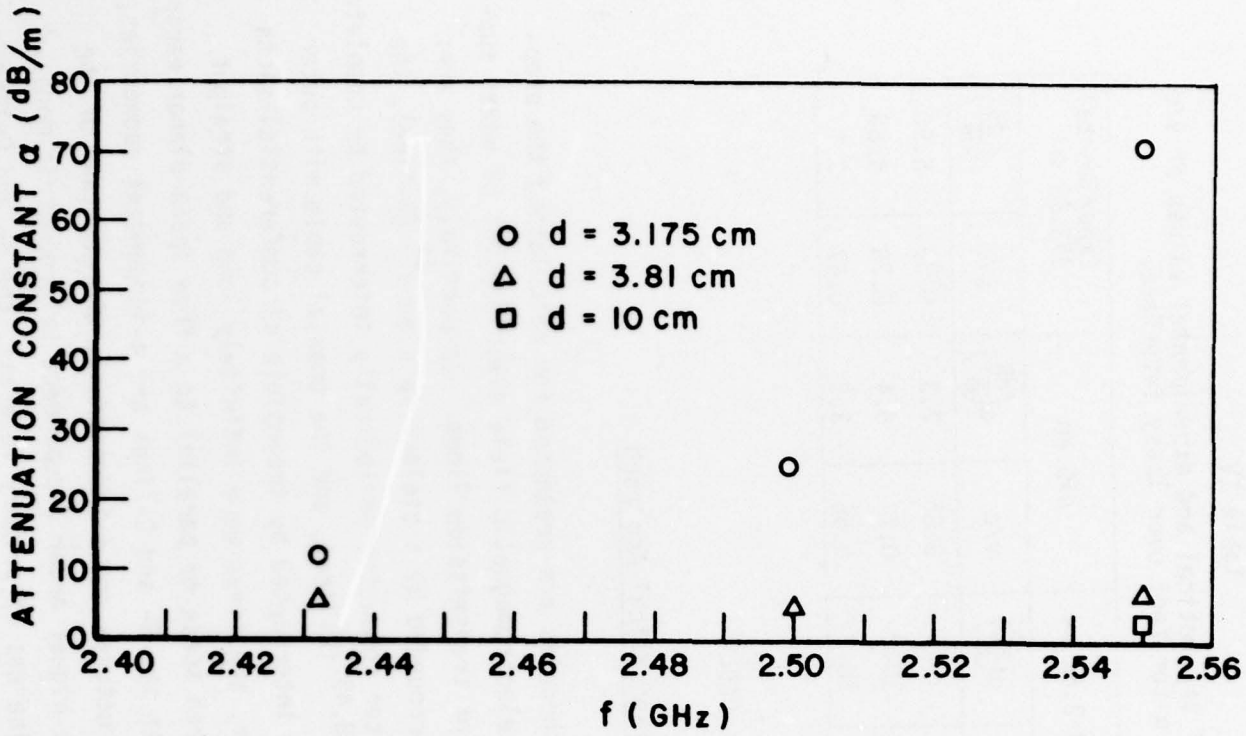

Figure 54. Experimental values of α for three nominal heights of Yagi over lossy interface.

of the results. Increasing σ_2 to 0.02 Siemens/m increased the values of d only slightly.

Table IV

Comparison of theoretical and experimental values of v/c and α for Yagi over lossy interface.

f (GHz)	d=3.81 cm		d=5 cm		Experimental d=3.81 cm	
	v/c	$\alpha\left(\frac{dB}{m}\right)$	v/c	$\alpha\left(\frac{dB}{m}\right)$	v/c	$\alpha\left(\frac{dB}{m}\right)$
2.432	0.82	13.5	0.85	7.3	0.83	5.90
2.499	0.75	10.2	0.77	5.4	0.78	4.86
2.550	0.64	18.8	0.66	3.3	0.67	7.1

III. THE LEAKY COAXIAL CABLE

A. Synopsis of Theoretical Approach

In Reference 46 theories are presented for calculating the propagation constants and electromagnetic field distributions of waves supported by three types of transmission lines. Respectively, they are: the conducting wire surrounded by a dielectric sleeve[47] (G-line), the coaxial cable with center conductor periodically interrupted by complete circumferential slots[48,49] (C-line), and the coaxial cable with outer conductor periodically interrupted by incomplete circumferential slots (R-line). In all cases, the lines were infinitely long and straight and reside either in free space or parallel to a free space-planar earth interface. Because both the G- and C-lines are ϕ-indpendent geometries, their assumed field structures are ϕ-independent, whereas that of the R-line must incorporate higher order ϕ-dependent trigonometric modes. Thus, although the R-line was of primary interest, the G- and C-lines served as stepping stones to the more intricate R-line analysis. Additionally, independently derived theory and calculations existed for the G-line over earth[50-52] which could serve as a check case.

Since all three transmission lines are essentially cylindrical in their geometry, the functions best suited to the expansion of their fields are the cylindrical wave functions, which serve quite well in the free space cases. The presence of a flat earth interface, however, complicates matters because the cylindrical wave functions are inappropriate forms for matching boundary conditions on planar surfaces; thus, more natural functions would be plane wave functions. As was done for the Yagi line the presence of the flat earth is accommodated mathematically, first by solving for the fields of the free space configuration in terms of cylindrical wave functions, then, by transforming each of these into continuous spectra of incident plane waves (Fourier integral expansion) each of whose interaction with the earth is described compactly by familiar Fresnel reflection and transmission coefficients and, lastly, by forcing the sum of the incident and reflected fields to satisfy a boundary condition back on the transmission line proper. Since the transformations of cylindrical wave functions into plane wave functions are common to all three transmisison line analysis and are not all found in the literature, their derivations are given in Reference 46.

To lend confidence to the analyses of the three lines discussed above, in each case an infinite array of parallel lines (G-, C-, or R-lines), in free space and in the presence of the flat earth, was analyzed using the same methodology but now involving the transformation of sums of cylindrical waves into discrete spectra of plane waves (Fourier series expansion). By separating the lines in the array sufficiently, results for the array approach those of the isolated line, providing a necessary, but not sufficient, check on the relevant mathematics and computer codes.

Because the formulation of the R-line theory is long and complicated, rather than repeat it here, we refer the reader to Reference 46 and pass on to a few numerical results.

B. Some Calculated Results

For the G-line configuration shown in Figure 55, curves of attenuation constant α vs frequency are shown in Figures 50 and 57 for free space and d=5 meters over the earth, respectively. The phase constants $\beta=w/v$ for the two cases are indistinguishable and are shown in Figure 58. A typical pattern of the longitudinal component of the electric field, E_z, shown in Figure 59 on a polar plot with linear scale, displays distorting effect of the ground at 100 MHz.

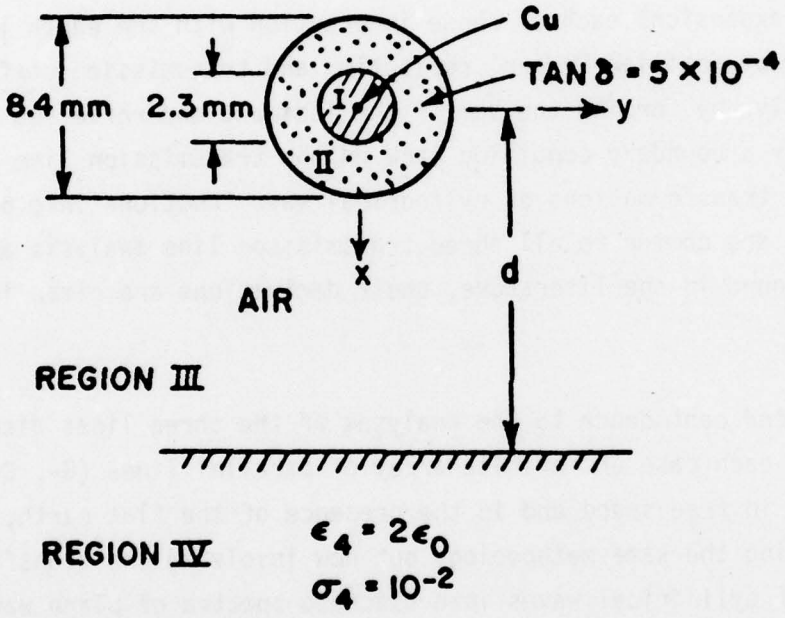

Figure 55. Parameters used for numerical examples. The conductivity of copper was assumed to be 57 Megasiemens/m.

For the C-line configuration shown in Figures 60 and 61, curves of the attenuation constant α vs frequency are shown in Figures 62 and 63 for free space and d=4 meters over the earth, respectively. The phase constants are shown in Figure 64. A polar pattern of E_z is shown in Figure 65.

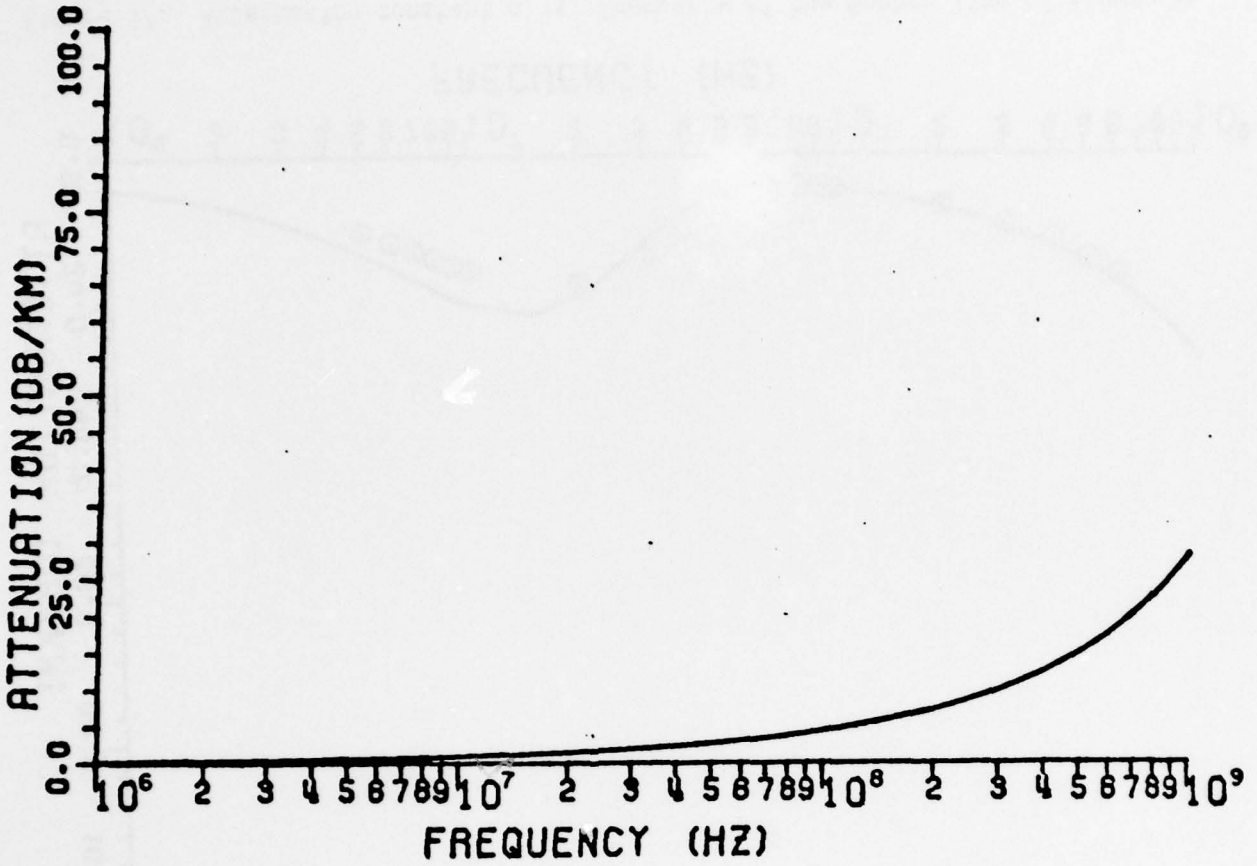

Figure 56. Attenuation constant α vs. frequency of the Goubau line of Figure 55 with $d=\infty$ (free space).

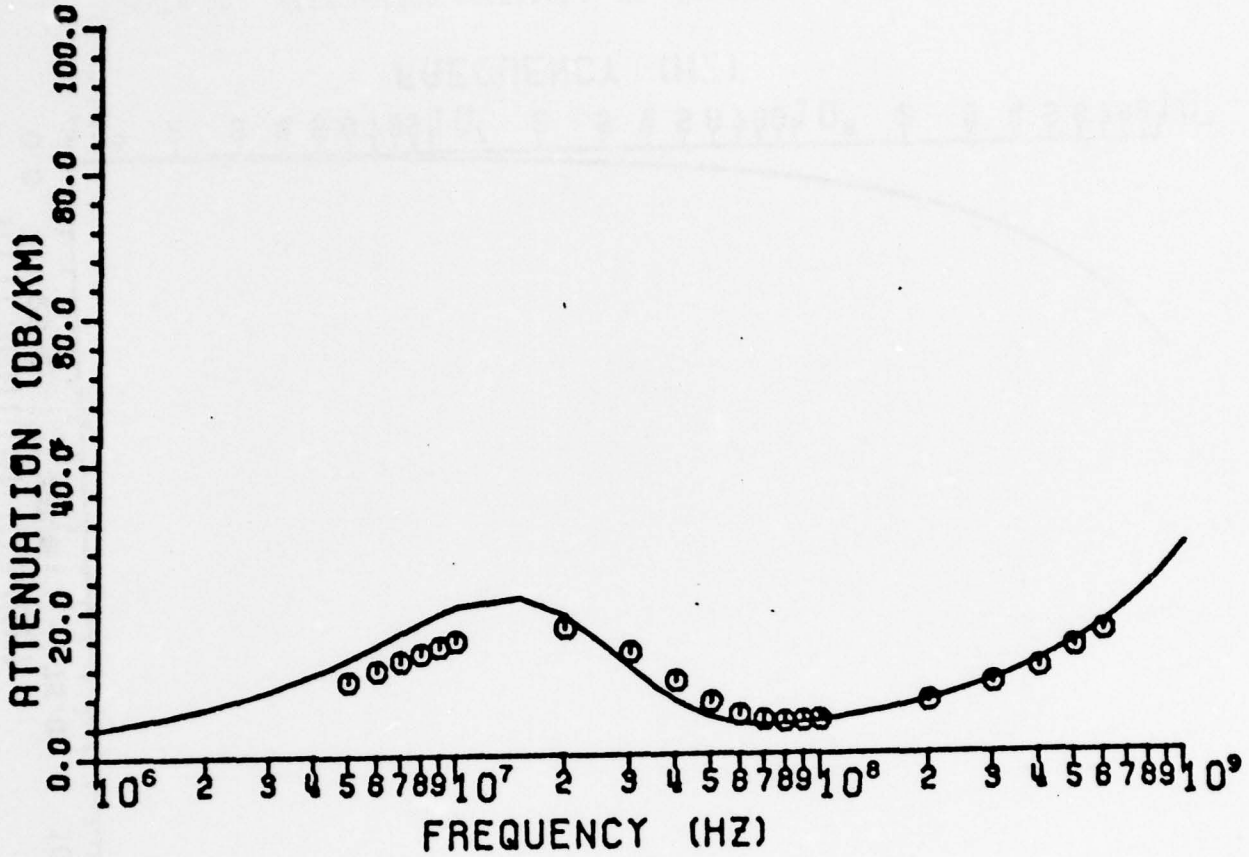

Figure 57. Attenuation constant α vs. frequency of the Goubau line of Figure 55 with d=5 meters. The circled data are calculated using the theory of Chiba found in Reference 51.

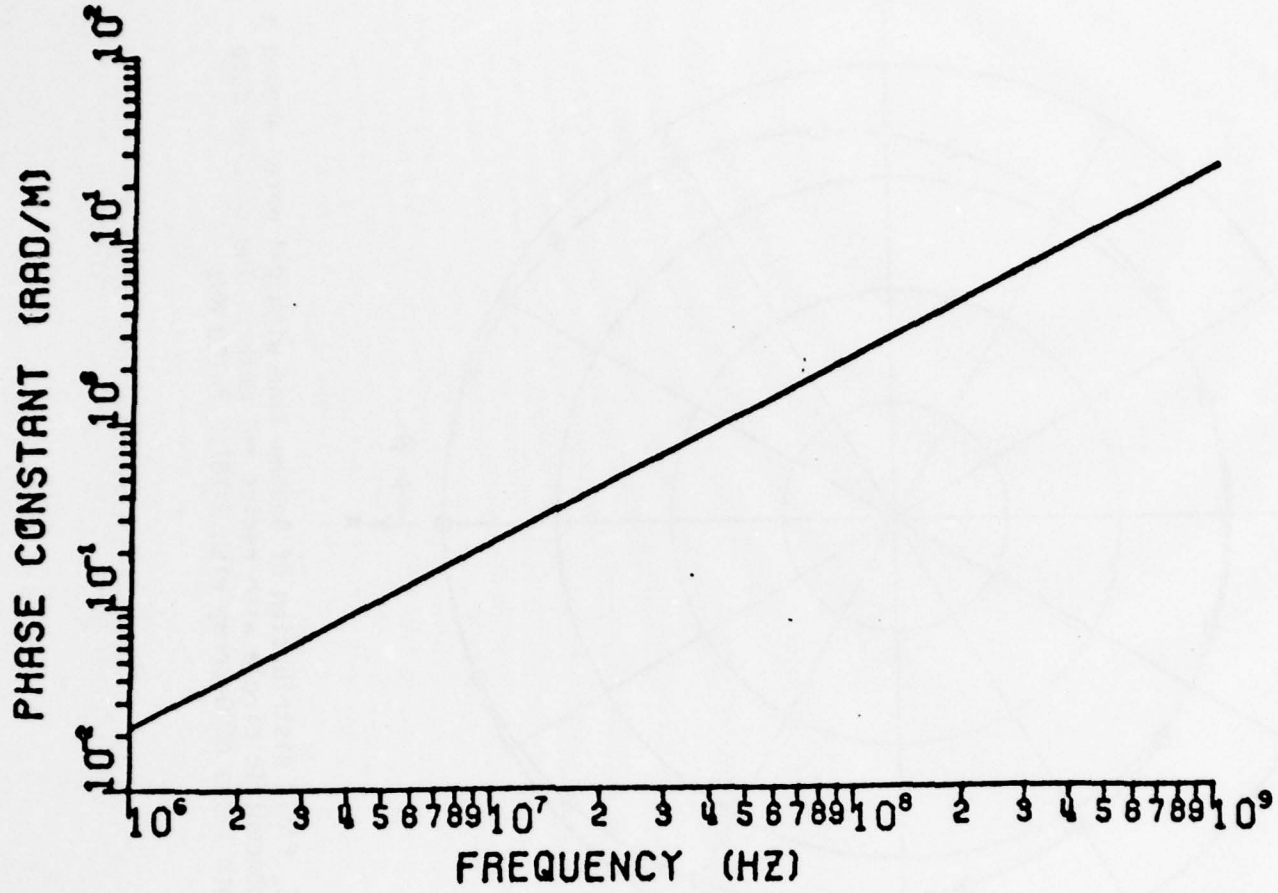

Figure 58. Phase constant β vs. frequency of the Goubau line of Figure 55 with d=∞ (free space).

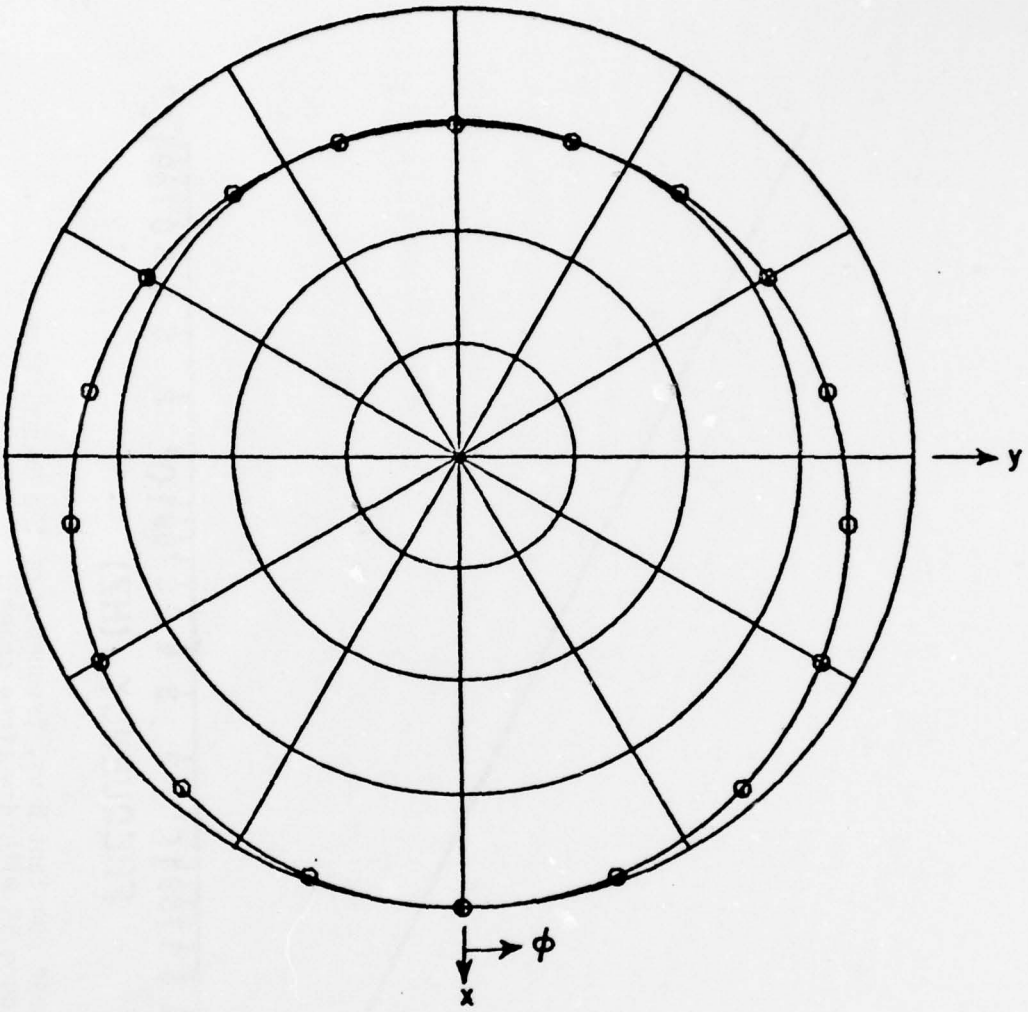

Figure 59. E_z field distribution of Goubau line with d=4 meter around a concentric circle with radius r=1 meter. The circled data are those of G-array with $S \geq 10\lambda$. f=100 MHz.

AD-A074 051 OHIO STATE UNIV COLUMBUS ELECTROSCIENCE LAB F/G 15/3
RADIATIVE TRANSMISSION LINE ANALYSIS.(U)
JUN 79 R J GARBACZ, J RICHMOND, B TRAN F19628-77-C-0069
UNCLASSIFIED ESL-784659-5 RADC-TR-79-158 NL

2 OF 2
AD
A074051

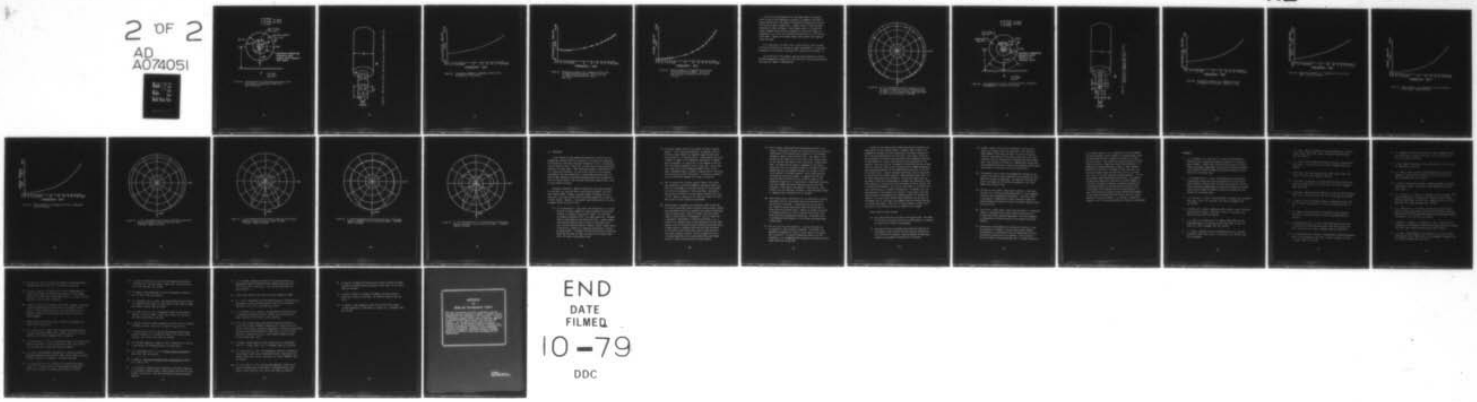

END
DATE
FILMED
10-79
DDC

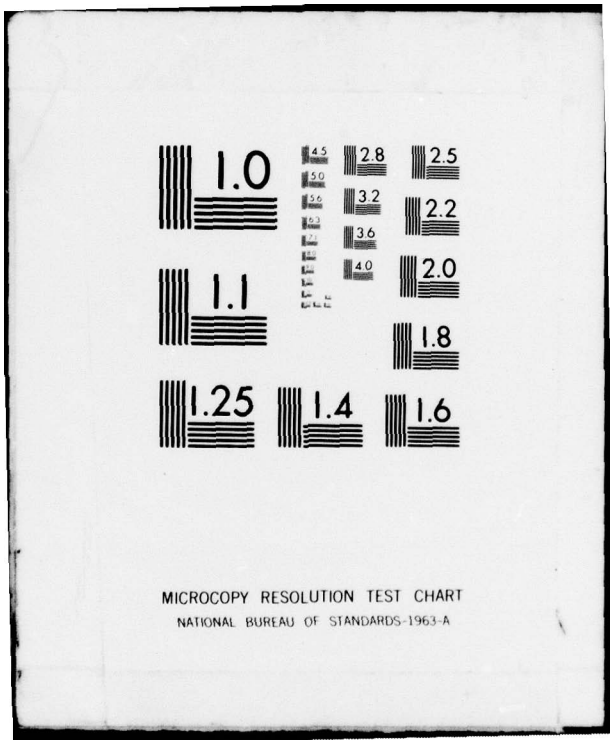
1.0
1.1
1.25
1.4
1.6
1.8
2.0
2.2
2.5
2.8
3.2
3.6
4.0
4.5
5.0
5.6
6.3
7.1
MICROCOPY RESOLUTION TEST CHART
NATIONAL BUREAU OF STANDARDS-1963-A

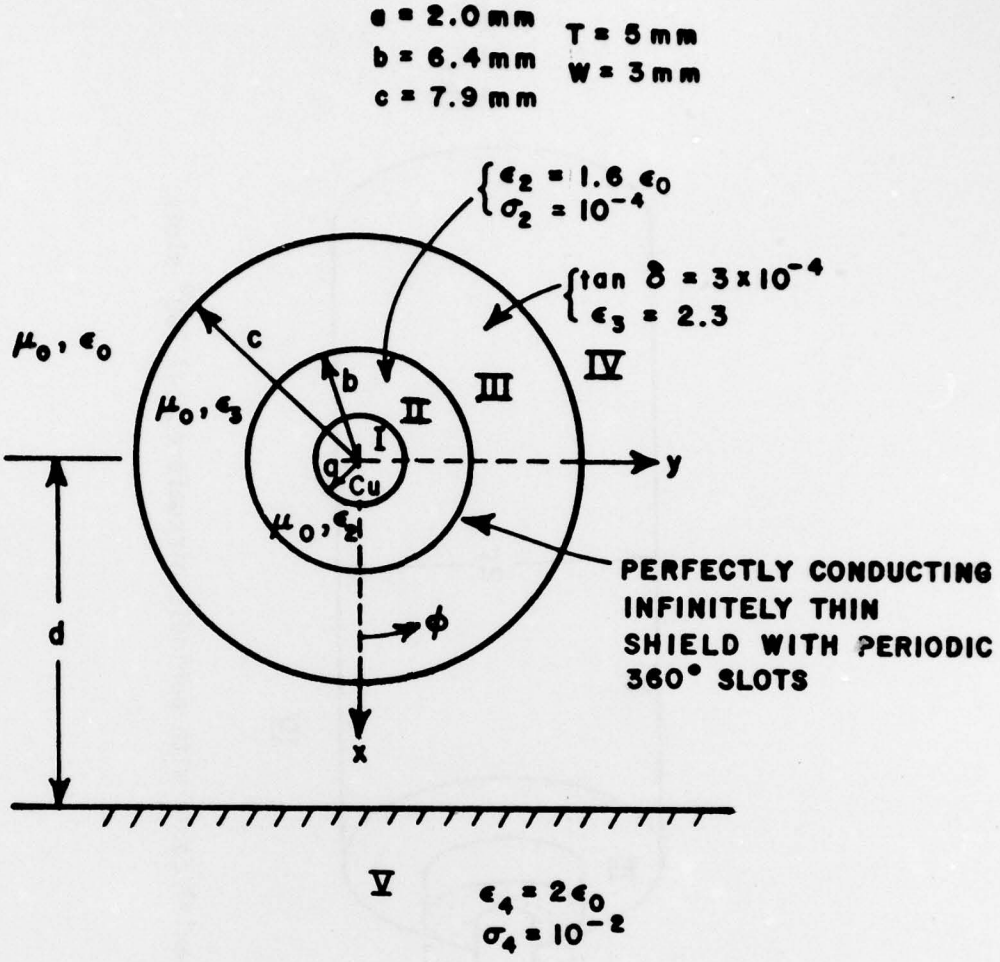

Figure 60. Cross-section of an infinitely long coaxial cable with periodic circumferential 360^0 slots over a flat earth.

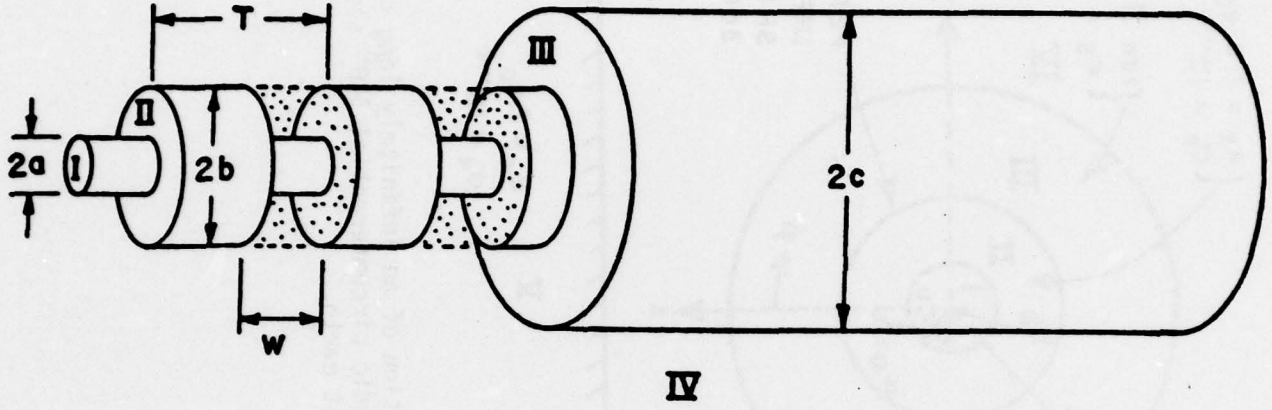

Figure 61. Side view of a coaxial cable with periodic circumferential 360^{o} slots.

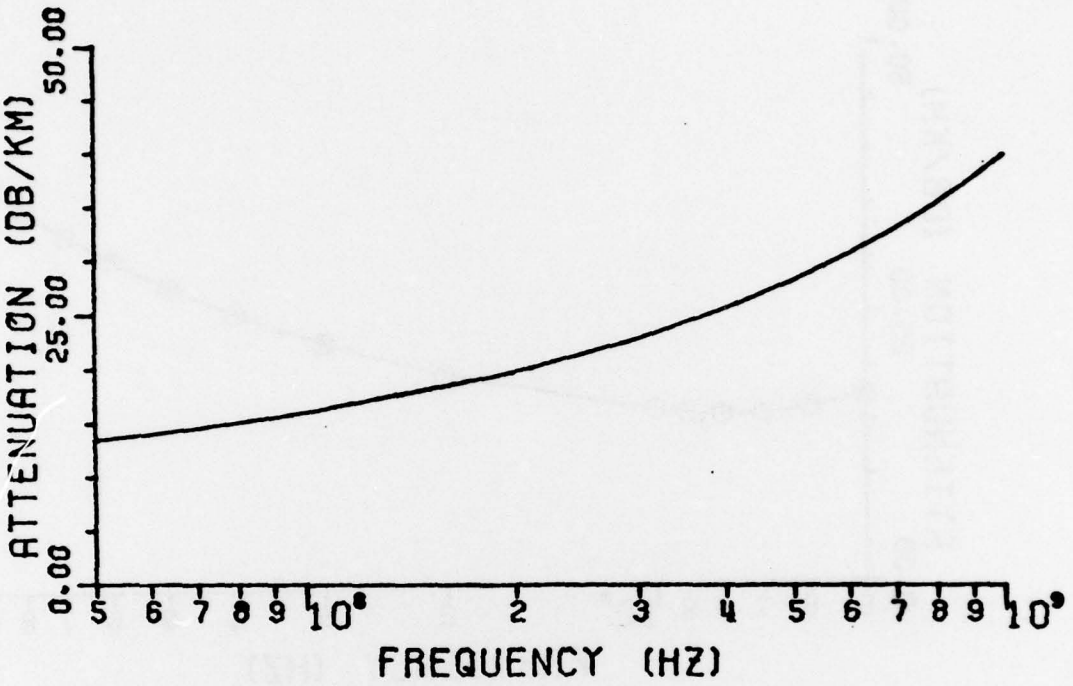

Figure 62. Attenuation constant vs. frequency of the C-line of Figure 60 in free space.

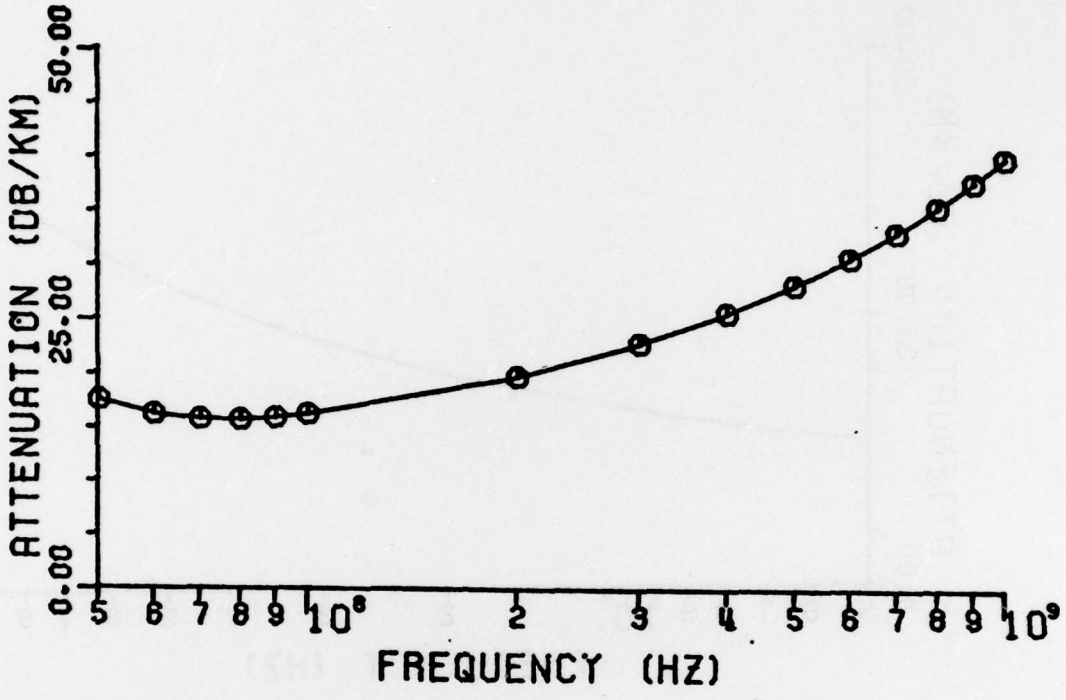

Figure 63. Attenuation constant α vs. frequency of the C-line of Figure 60 with d=4 meters. The circled data are those calculated for the C-array with $S \geq 10$.

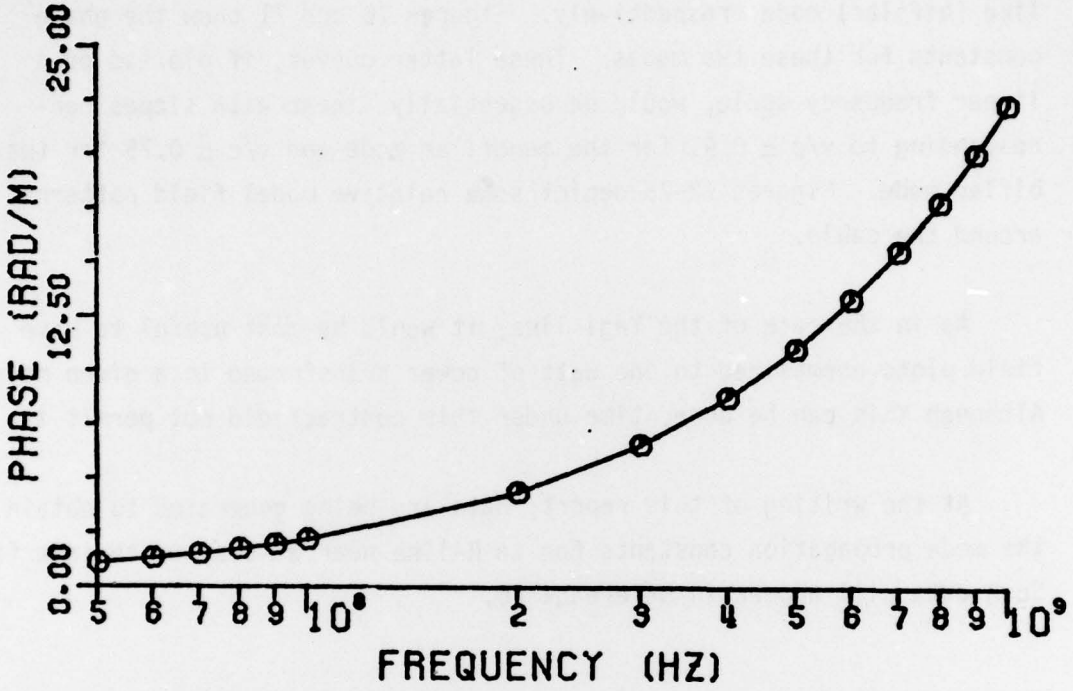

Figure 64. Phase constant β vs. frequency of the C-line of Figure 60 with d=4 meters. The circled data are those calculated for the C-array with $S \geq 10$.

For the R-line configuration in free space shown in Figures 66 and 67 curves of the attenuation constant α vs frequency are shown in Figures 68 and 69 for the Goubau-like (monofilar) mode and the coaxial-like (bifilar) mode, respectively. Figures 70 and 71 show the phase constants for these two modes. These latter curves, if plotted on a linear frequency scale, would be essentially linear with slopes corresponding to $v/c \simeq 0.91$ for the monofilar mode and $v/c \simeq 0.75$ for the biflar mode. Figures 72-75 depict some relative model field patterns around the cable.

As in the case of the Yagi line, it would be most useful to have field plots normalized to one watt of power transformed in a given mode. Although this can be done, time under this contract did not permit it.

At the writing of this report, data are being generated to obtain the mode propagation constants for an R-line near a lossy earth interface. Such data will appear in Reference 46.

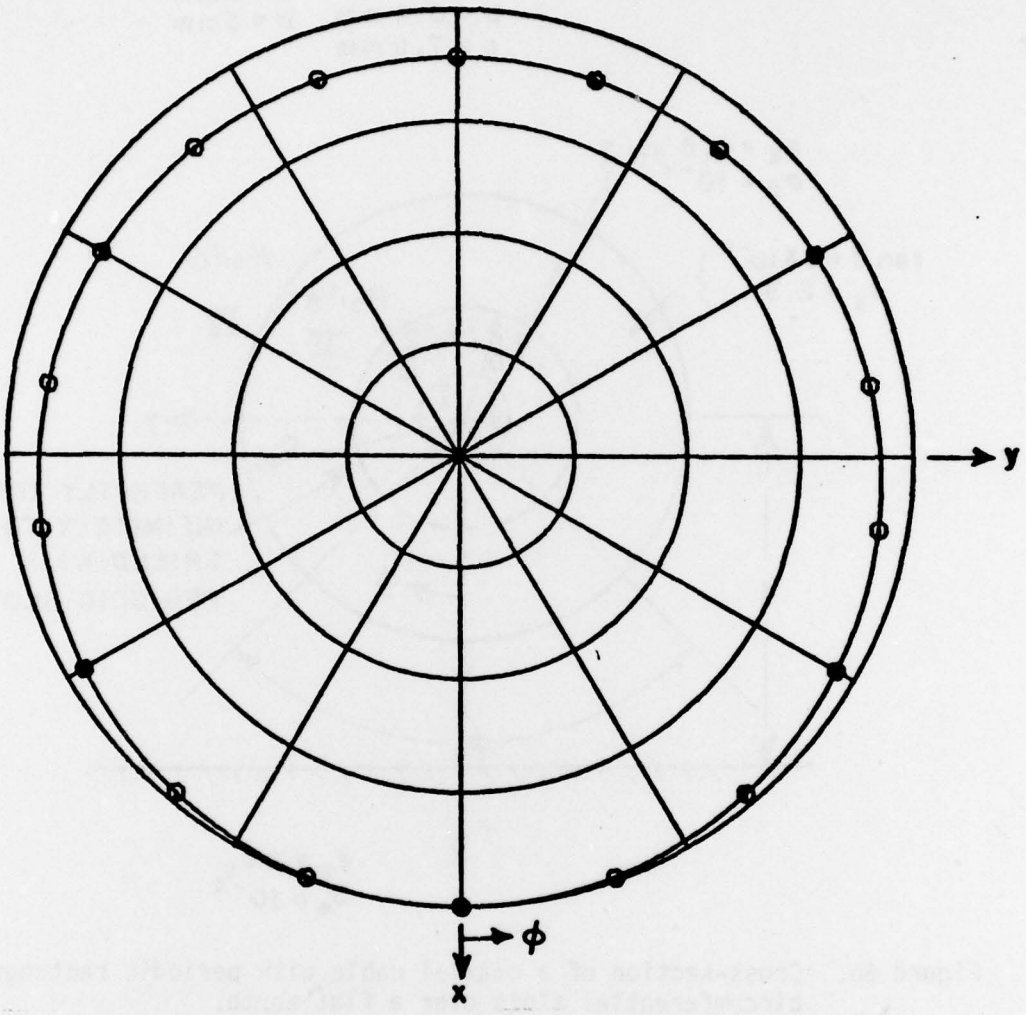

Figure 65. E_z field distribution around a concentric circle of radius r=1 meter of a C-line of Figure 60 with d=4 meters. The circled data are those calculated for the C-array with $S \geq 10\lambda$. f=100 MHz.

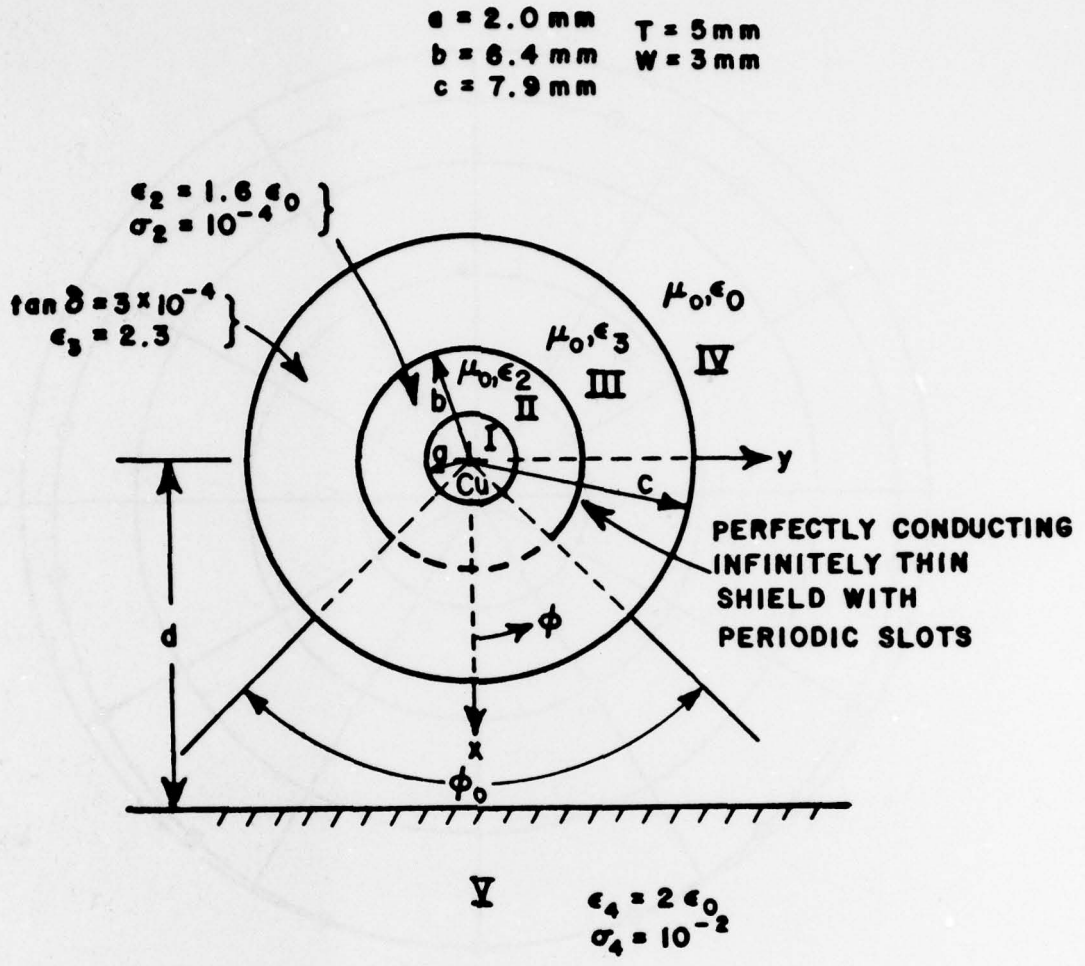

Figure 66. Cross-section of a coaxial cable with periodic rectangular circumferential slots over a flat earth.

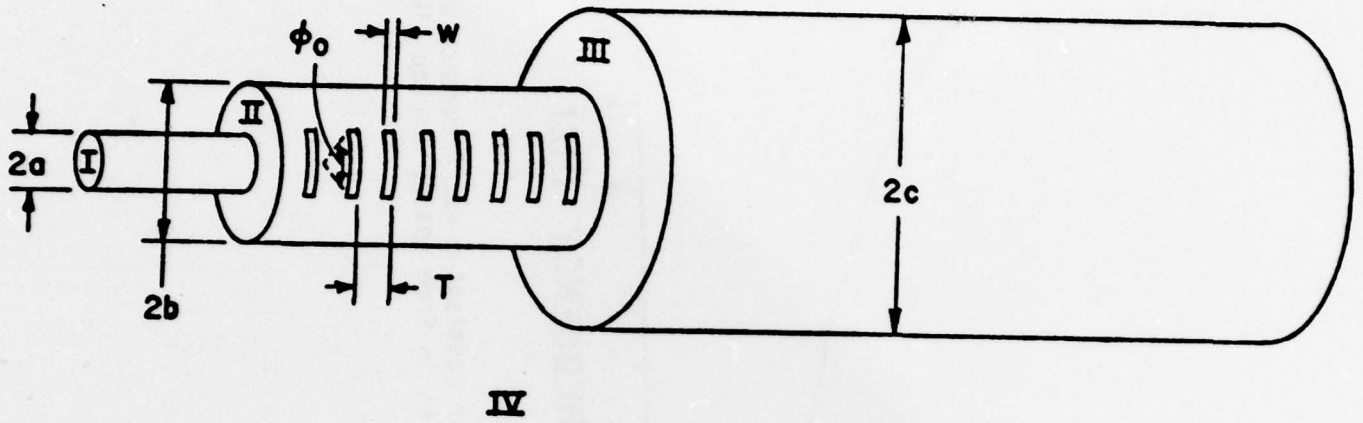

Figure 67. Side view of a coaxial cable with periodic rectangular circumferential slots.

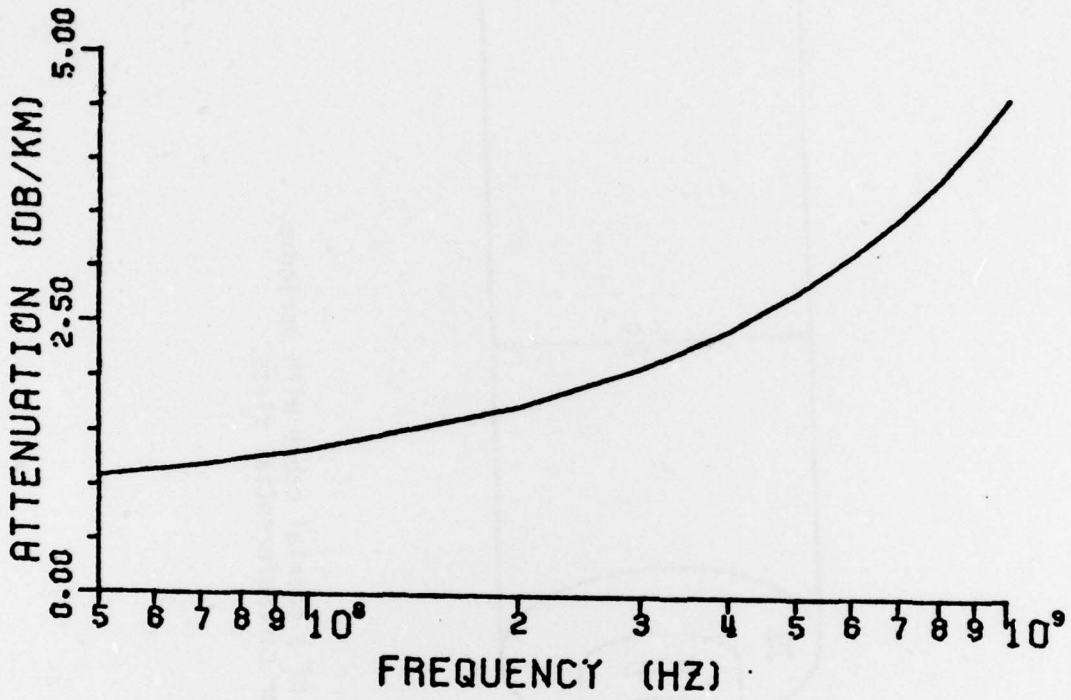

Figure 68. Attenuation constant α vs. frequency of R-line of Figure 66 in free space. Goubau-like mode.

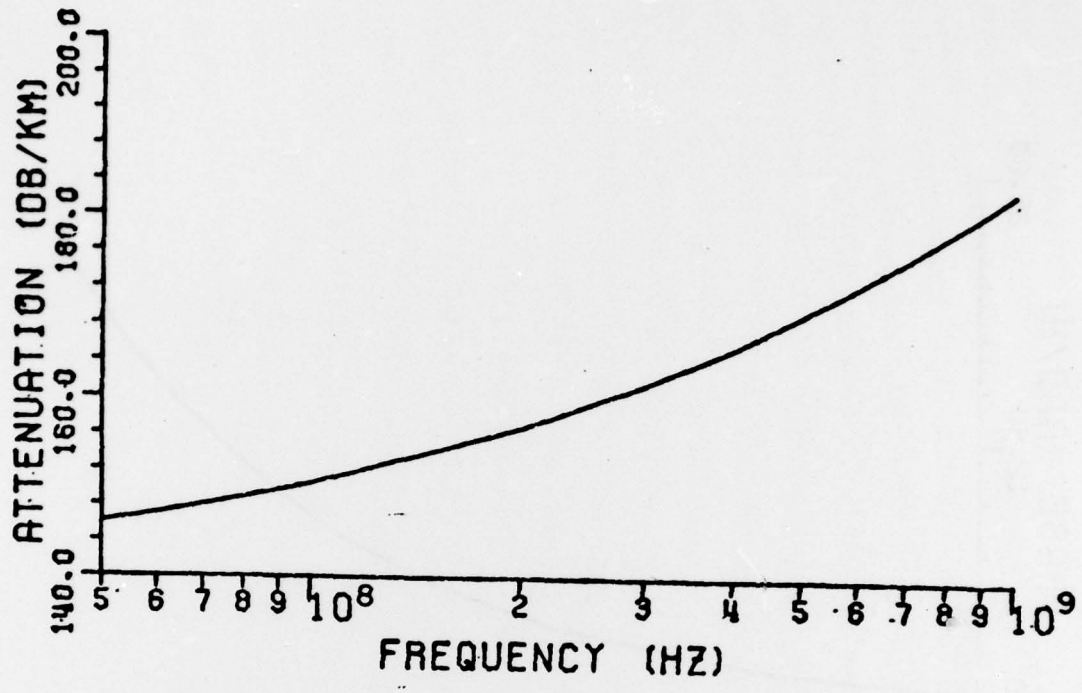

Figure 69. Attenuation constant α vs. frequency of R-line in free space. Coaxial-like mode.

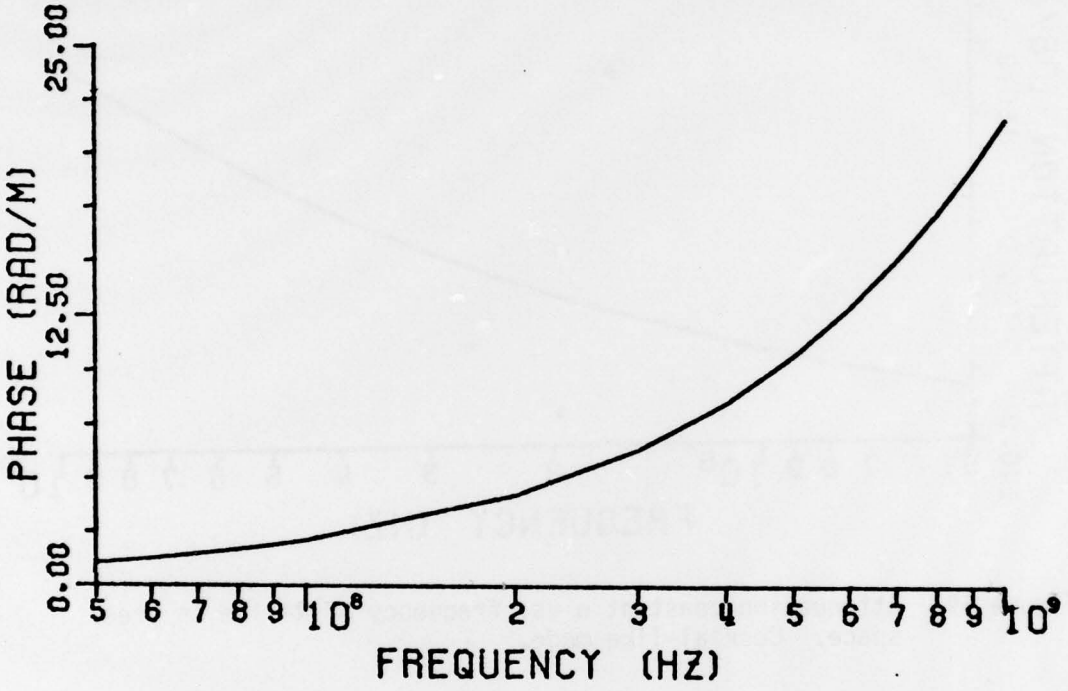

Figure 70. Phase constant β vs. frequency of R-line of Figure 66 in free space. Goubau-like mode.

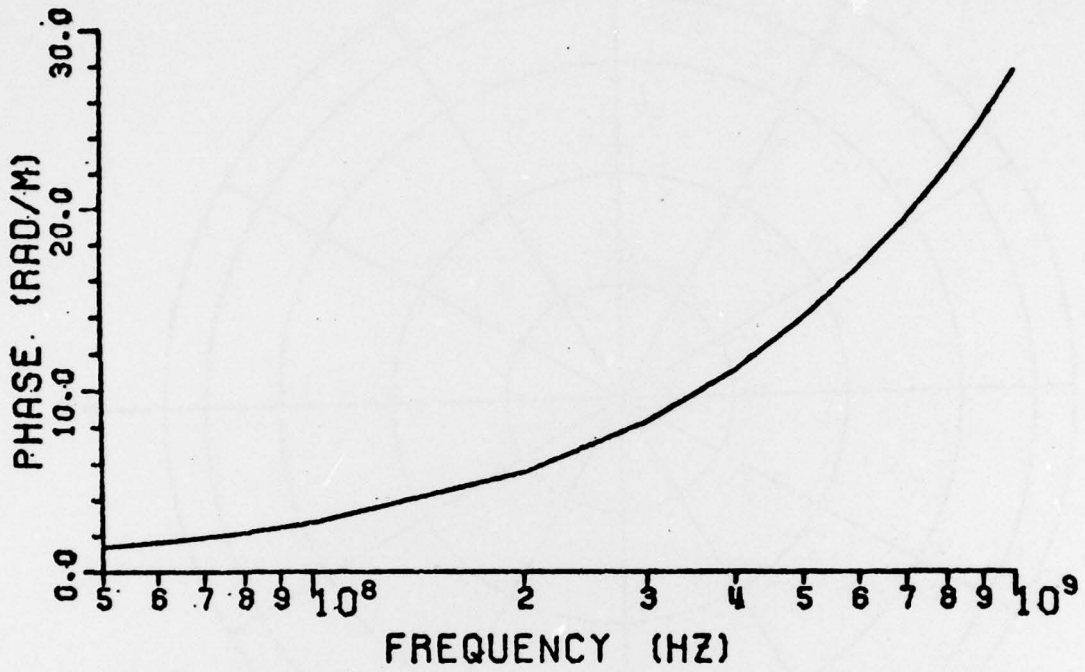

Figure 71. Phase constant β vs frequency of R-line in free space. coaxial-like mode.

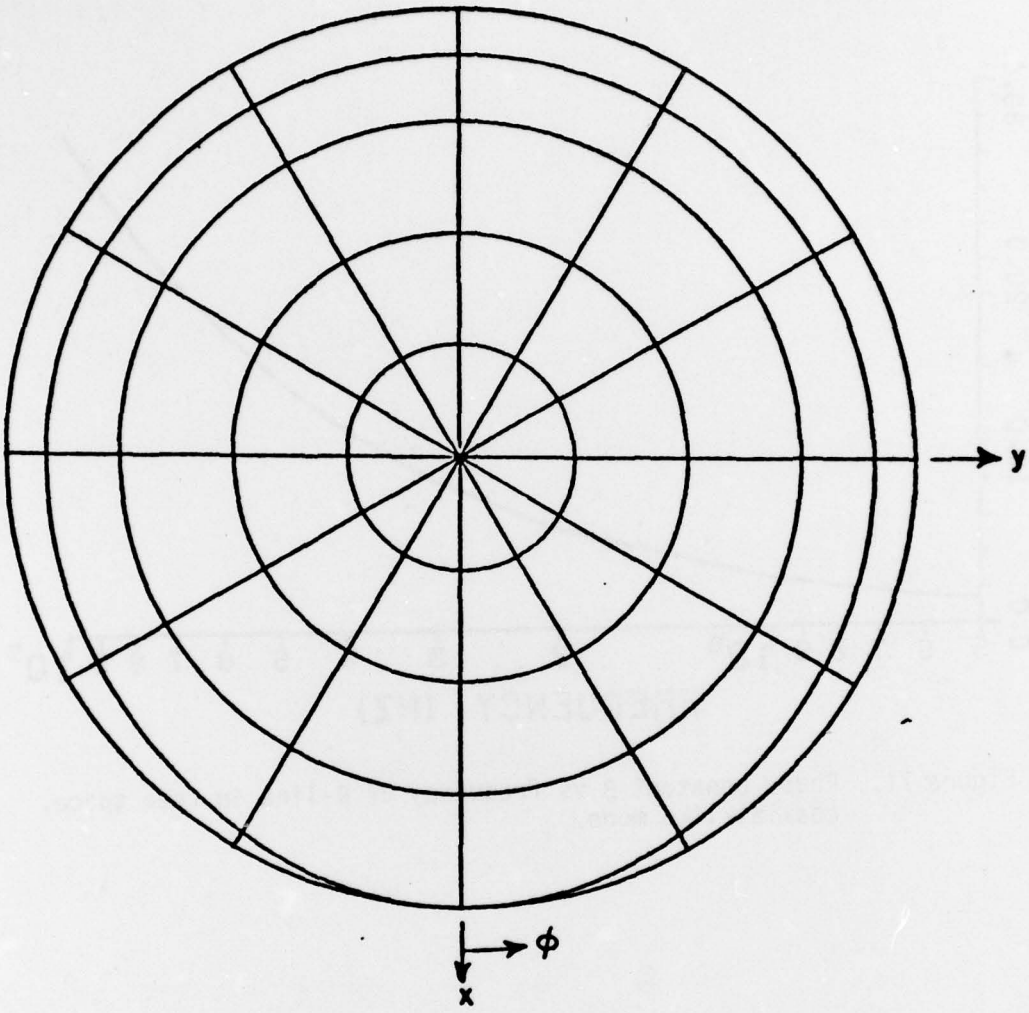

Figure 72. E_z field distribution of R-line of Figure 66 in free space around a concentric circle of radius r-1 meters. f=100 MHz. Goubau-like mode.

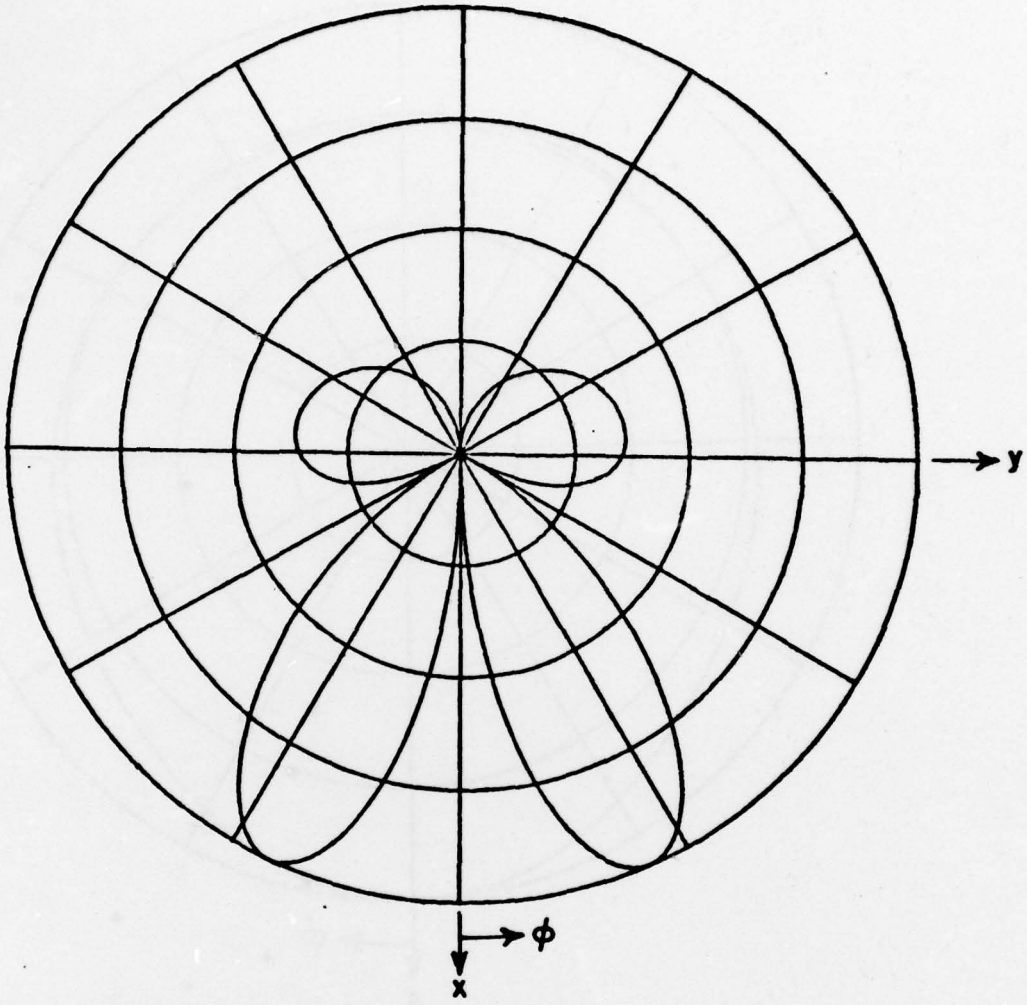

Figure 73. H_z field distribution of R-line of Figure 66 in free space around a concentric circle of radius r=1 meter. f=100 MHz. Goubau-like mode.

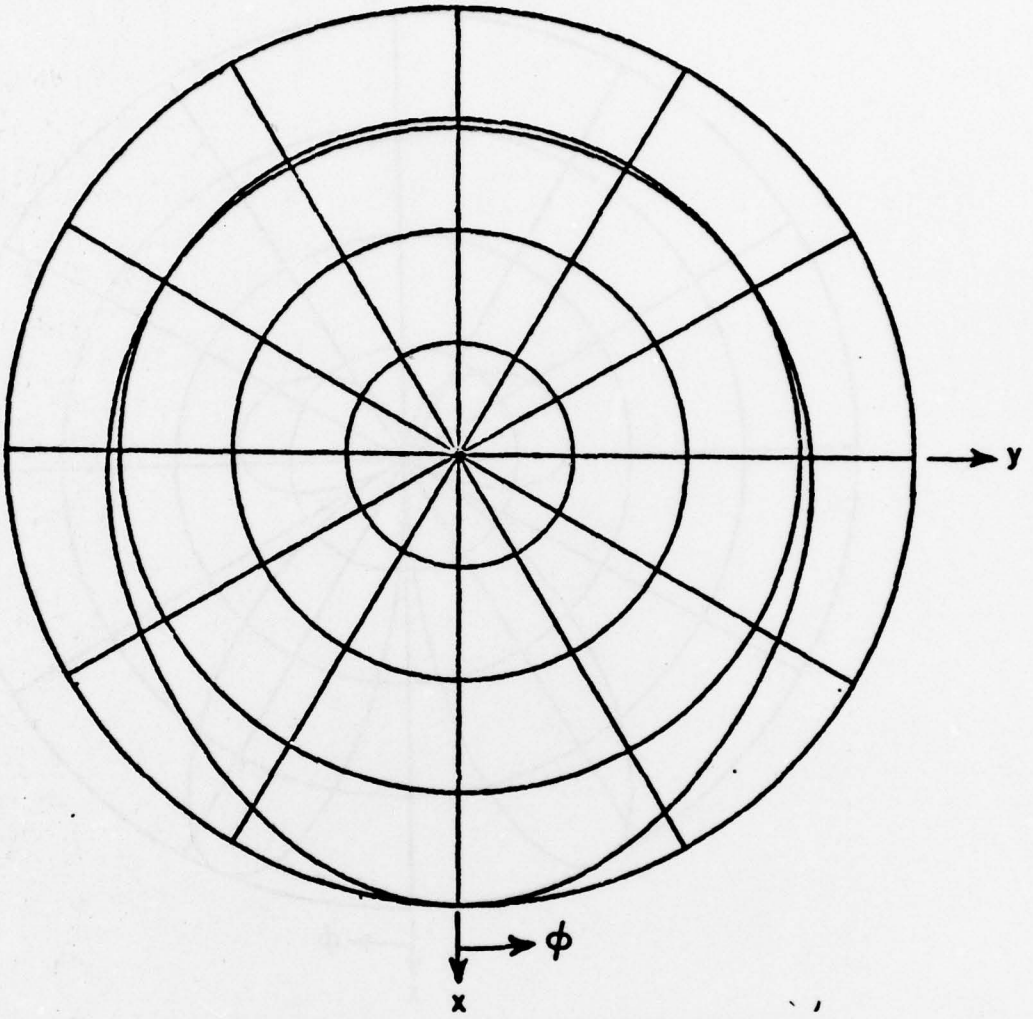

Figure 74. E_z field distribution of R-line of Figure 66 in free space around a concentric circle of radius r=1 meter. f=100 MHz. Coaxial-like mode.

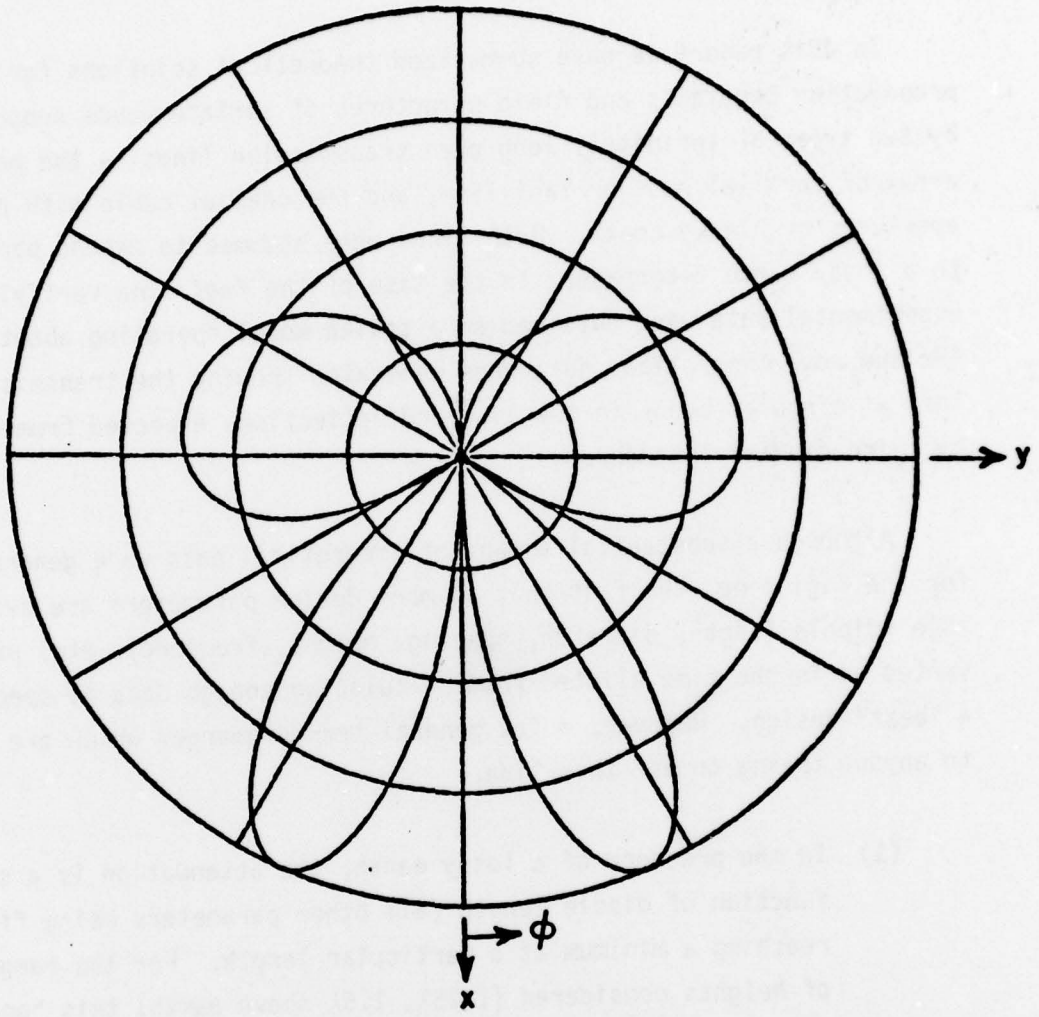

Figure 75. H_z field distribution of R-line of Figure 66 in free space around a concentric circle of radius r=1 meter. f=100 MHz. Coaxial-like mode.

IV. DISCUSSION

In this report we have summarized theoretical solutions for the propagation constants and field structures of surface waves supported by two types of infinitely long open transmission lines -- the periodic array of parallel rods or Yagi line, and the coaxial cable with periodic apertures or "leaky coax". Both lines were assumed to extend parallel to a lossy earth interface. In the case of the Yagi line verifying experimental data were obtained on a scaled model operating about 2.5 GHz and some theoretical data were generated showing the transmission loss at circular bends in the line and reflections expected from a nearby (wire dipole) intruder.

Although a substantial amount of theoretical data were generated for the Yagi line, the fact that so many design parameters are available (dipole length, diameter, spacing, height, frequency, etc) prevented us in the time alloted from calculating enough data to specify a "best" design. However, a few general trends emerged which are useful to anyone trying to use this line.

(1) In the presence of a lossy earth, the attenuation is a strong function of dipole length (all other parameters being fixed), reaching a minimum at a particular length. For the range of heights considered (1.25λ, 1.5λ above earth) this "optimum" dipole length appears to be about 0.4λ-0.44λ. Longer lengths slow down the wave and bind it closer to the dipole structure, causing primarily metallic losses; shorter lengths speed up the wave or extend it so that more attenuation is caused by earth losses. It appears that the wave should be travelling about 90% the speed of light to achieve this minimum attenuation (all other things being fixed).

(2) All dipole lengths given in this report are metric lengths. However, it was found experimentally, as expected, that the effective dipole lengths are somewhat longer and they must be accounted for in accurate design. Unfortunately, the exact increase in length is not completely understood; it depends upon rod diameter, of course, but it also depends on the current distribution assumed to exist on the rods. In our case, with rather thick rods (length-to-diameter ratio of 32:1) about a 4%-4½% increase in length is appropriate for the piecewise sinusoidal current distribution. A cosine on a pedestal current distribution demands an increase of about 3%.

(3) The rod spacing also strongly controls speed, field extent and attenuation. We would recommend a spacing of about one third of a wavelength in straight sections of line and about one fifth of a wavelength in curved sections. Decreasing the spacing any further on curves reduces shedding loss very little. Tapers in spacing at the input and output of a curve were found to effect negligible improvement.

(4) We found that a reasonably low reflection load for the Yagi line could be provided simply by center-loading several dipoles (we considered 8 typically) extending over several wavelengths with resistances which linearly increase from low to high values in the direction of propagation. We also found that a substantial improvement in radiation efficiency, i.e., a reduction of radiated energy to the advantage of surface wave energy, could be effected by phasing several center-fed dipole voltage sources in adjacent rods such that they correspond to the speed of the surface wave natural to the structure and induce constant currents. We also suggest the use of a matched termination as discussed above behind the phased source to reduce radiation from the source region.

(5) Wire intruders (about man-high) encroaching parallel to the array in free space displayed (for the designs chosen) reflection coefficients of the surface wave of about 0.1 at an intruder distance of about 1 meter from the line. This number is normalized to the region on the line local to the intruder; back at the receiver, the effect of this reflection is much attenuated. We looked at the change in impedance at the source dipole due to a wire intruder and even at very short distances between the two, the impedance change is so slight as to be a poor measure of intruder presence. Earth losses would deteriorate the situation further. It appears that the Yagi structure would not serve well as a barrier sensor of any substantial length if it is operated as a single mode structure. Like most schemes which have found some success over long distances, it may require two parallel lines, one for transmitting, one for receiving, to effect a large percentage change in impedance upon introduction of an intruder.

(6) Earth losses cause a precipitous rise in attenuation, becoming reasonable only for line heights above the earth which are not practical at 100 MHz. A more practical version would use a metallic ground screen which would shield the wave at least partially from the earth. Dipoles of length $h=\ell/2$ would be attached vertically to this screen and form a Yagi array which could not be penetrated from below. At 100 MHz, such a configuration would appear as 2 foot high rods spaced about a meter apart.

(7) The Yagi line is quite dispersive, so pulse distortion can be expected if short pulses are required. At 100 MHz a 5% bandwidth corresponds to a 200 ft. pulse, which is an acceptable resolution. To minimize dispersive effects over this bandwidth, it is recommended that designs be used where relative phase velocities exceed 0.80.

A theory of the single coaxial cable with periodic apertures was completed during the contract period. Computer codes to obtain the propagation constants and field structures of the modes supported by this line were generated only for the line in free space; difficulty was encountered in finding roots associated with propagation constants in the presence of a lossy interface and at the termination of this contract it was not clear to us whether this difficulty was due to poor choice of starting values for the iterative search scheme we employed, poor convergence behavior of the computational algorithm, or an error in the code itself. Certain necessary conditions, such as consistancy of results with and without earth for large distances above earth, or for high frequencies, were satisfied. For the free space case, the two modes on the cable corresponded to a Goubau-like (monofilar) eigenmode supported by the metallic shield and outer dielectric sheath, and a coaxial-like eigenmode. The first of these modes is relatively loss-free, suffering only 1-2 dB/Km of attenuation. If however, the line were operated in the presence of or buried in lossy earth, this mode would be greatly attenuated and be rendered useless for intruder detection. The coaxial mode suffers high attenuation, of the order of 150 dB/Km, even in free space, but probably would not suffer much more in an earth environment. Most of its field, however, resides inside the coaxial cable and would be poorly coupled to an intruder.

Future efforts should include:

(1) The study of the Yagi line over a wire mesh screen. The width of the screen, the mesh size and its effectiveness in screening the lossy earth should be investigated.

(2) The possibility of a multimode Yagi-structure should be investigated so that one mode could be used for transmission and the other for reception, coupling between the two being caused by the asymmetry introduced by an intruder.

(3) Perhaps a hybrid line could be considered, consisting of a leaky coax attached along the centerline of the Yagi line. Under symmetry conditions, the Yagi line should not be sensitive to the presence of the coaxial cable and so its field structure should be substantially unchanged from that studied here. How severely an intruder (or imperfections) would upset this decoupling and cause a signal to be received on the coaxial cable would be a measure of the line's sensitivity.

(4) The computer code to obtain the propagation constants of the coaxial cable with periodic apertures in the presence of earth should be brought to completion. We simply did not have the time to overcome the difficulties encountered in this task before the contract's end.

(5) The case of two parallel leaky coaxial cables, in free space and near earth, should be formulated since it is this geometry which has been experimentally successful. Once this theory is developed, it makes sense to then introduce intruder obstacles between and above the lines to estimate coupling losses and sensitivity.

(6) The case of a leaky coaxial cable along the edge of a conducting septum, to represent such a cable running along the top of a chain-link fence, should be developed. Since earth appears so deleterious, raising the cable in this manner may provide benefits.

(7) Although not investigated at all during this contract it may be profitable to consider a barrier sensor which combines the benefits of a relatively loss-free transmission line with the detection sensitivity of an antenna. We are thinking here of a type of line which guides the r.f. energy essentially

as a closed structure, i.e., insensitive to the environment, including intruders, from a source to a distant region along the line where the line is caused to radiate, or at least extend its field. This "aperture" would be caused to "slide" along the line at a speed much slower than the speed of r.f. propagation, thereby performing a type of linear scanning. What sort of structure is suitable to serve this dual role and how one might signal the structure to act as a closed feed line or as a small aperture are open questions. It certainly offers some interesting possibilities - for example, an open-loop system could cause each individual element in a periodic structure to maintain a radiating condition for a specified duration, at the end of which it would signal its neighbor to do likewise much like a domino effect. A more sophisticated and complex system incorporating feedback to the signalling mechanism could slow or stop the sliding aperture to track an intruder. The concept is attractive; whether or not it can be made practical should be investigated.

REFERENCES

1. J. H. Richmond, H. B. Tran, and T. B. Crane, "Surface Waves on Periodic Array of Imperfectly Conducting Dipoles in Free Space," Report 784659-1, January 1978, The Ohio State University Electro-Science Laboratory, Department of Electrical Engineering; prepared under Contract F19628-77-C-0069 for Electronic Systems Division, Hanscom Air Force Base, Mass.

2. J. H. Richmond and H. B. Tran, "Surface Waves on Periodic Array of Imperfectly Conducting Vertical Dipoles Over the Flat Earth," Report 784659-2, February 1978, The Ohio State University Electro-Science Laboratory, Department of Electrical Engineering; prepared under Contract F19628-77-C-0069 for Electronic Systems Division, Hanscom Air Force Base, Mass.

3. C. C. Lee and L. C. Shen, "Traveling Waves in Coupled Yagi Structures," IEEE Trans. on Mic. Th. and Tech., Vol. MTT-25, November 1977, pp. 931-933.

4. N. Amitay and H. Zucker, "Attenuation Due to Ohmic Losses in Periodic Dipole and Slot Arrays," IEEE Trans. on Mic. Th. and Tech., Vol. MTT-20, February 1972, pp. 148-155.

5. L. C. Shen, H. D. Cubley and D. S. Eggers, "Measurement of the Propagating Waves on a Yagi-Uda Array," IEEE Trans. on Ant. and Prop., Vol. AP-19, November 1971, pp. 776-779.

6. L. C. Shen, "Characteristics of Propagating Waves on a Yagi-Uda Structure," IEEE Trans. on Mic. Th. and TEch., Vol. MTT-19, June 1971, pp.536-562.

7. L. C. Shen, "Numerical Analysis of Wave Propagation on a Periodic Linear Array," IEEE Trans. on Ant. and Prop., Vol.AP-19, March 1971, pp. 289-292.

8. L. C. Shen, "Possible New Applications of Periodic Linear Arrays," IEEE Trans. on Ant. and Prop., Vol. AP-18, September 1970, pp. 698-699.

9. R. Mailloux, "The Long Yagi-Uda Array," IEEE Trans. on Ant. and Prop., Vol. AP-14, March 1966, pp. 128-137.

10. R. Mailloux, "Excitation of a Surface Wave Along an Infinite Yagi-Uda Array," IEEE Trans. on Ant. and Prop., Vol. AP-13, September 1965, pp.719-724.

11. R. Mailloux, "Antenna and Wave Theories of Infinite Yagi-Uda Arrays," IEEE Trans. on Ant. and Prop., Vol. AP-13, July 1965, pp. 499-506.

12. J. Shefer, "Periodic Cylinder Arrays as Transmission Lines," IEEE Trans. on Mic. Th. and Tech., Vol. MTT-11, January 1963, pp. 55-61.

13. E. K. Damon, "The Near Fields of Long End-Fire Dipole Arrays," IEEE Trans. on Ant. and Prop., Vol. AP-10, September 1962, pp. 511-523.

14. F. Serracchioli, and C. A. Levis, "The Calculated Phase Velocity of Long End-Fire Uniform Dipole Arrays," IRE Trans. on Ant. and Prop., Vol. AP-7, Spl. Suppl., December 1959, pp. S424-S434.

15. H. W. Ehrenspeck and H. Poehler, "A New Method for Obtaining Maximum Gain from Yagi Antennas," IRE Trans. on Ant. and Prop., Vol. AP-7, October 1959, pp. 379-386.

16. D. L. Sengupta, "On the Phase Velocity of Wave Propagation Along an Infinite Yagi Structure," IRE Trans. on Ant. and Prop., Vol. AP-7, July 1959, pp. 234-239.

17. H. Yagi, "Beam Transmission of Ultra Short Waves," Proc. IRE, Vol. 16, June 1928, pp. 715-741.

18. D. C. Chang, "Theory on Small Radiating Apertures in the Outer Sheath of a Coaxial Cable," IEEE Trans. on Ant. and Prop., Vol. AP-26, September 1978, pp. 674-682.

19. S. Plate, D. Chang and E. Kuester, "Propagating Modes on a Buried Leaky Coaxial Cable," Interim Tech. Rept. RADC-TR-78-77, March 1978, A057253.

20. J. L. Poirier, N. V. Karas, J. A. Antonucci, and M. Szczytko, "VHF Intrusion Detection: A Technique for Parked Aircraft," Report RADC-TR-77-384, RADC, Air Force Syst. Command, Griffiss Air Force Base, New York, 13441, November 1977, A051144.

21. R. K. Harman and N. A. M. Mackay, "Ported Coaxial Cable Sensor," Report on Sensor Technology for Battlefield and Physical Security Applications," Mobility Equipment Research and Development Command, Fort Belvoir, Va., July 1977, pp. 393-413.

22. A. Hessel, S. Choudhary, L. Felsen and S. Shin, "The Analysis of Propagation on Periodically Slotted Coaxial Cable Above Lossy Ground," Final Tech. Rept. RADC-TR-77-85, February 1977, A040044.

23. J. R. Wait, "Electromagnetic Field Analysis for a Coaxial Cable with Periodic Slots," IEEE Trans. on Electromagnetic Compatibility, Vol. ENC-19, February 1977, pp. 7-13.

24. D. Cree and L. Giles, "Practical Performance of Radiating Cables," The Radio and Elect. Eng., Vol. 45, May 1975, pp.221-223.

25. P. Yoh, R. Esposito, R. Gagnon, and R. Kodis, "Measurements of Leaky Coaxial Cables and Possible Applications to Train Communication," Final Report No. FRA-ORD and D-75-43, U. S. Dept. of Transportation, Fed. Rail Admin., May 1974.

26. A pair of leaky coaxial cables has been found to detect the passage of humans through tunnels buried in sand to a depth of about 4 meters. Private conversation with J. D. Oates. Assist. Dir. of Research, Internal Security, Parten Down, Salisbury, Wilshire, United Kingdom.

27. Andrew Corporation, General Edition Catalog 27, Antennas/Transmission Lines, 1971, p. 53.

28. D. B. Seidel and J. R. Wait, "Role of Controlled Mode Conversion in Leaky Freder Mine Communication Systems," IEEE Trans. on Ant. and Prop., Vol. AP-25, September 1978, pp. 690-694.

29. D. B. Seidel and J. R. Wait, "Transmissson Modes in a Braided Coaxial Cable and Coupling to a Tunnel Environment," IEEE Trans. on Mic. Th. and Tech., Vol. MTT-26, July 1978, pp. 494-499.

30. J. R. Wait, "Electromagnetic Guided Waves in Mine Environments," Workshop Proceedings, Boulder Colo., March 28-30, 1978, U.S. Bureau of Mines, Contract No. H0155008. (Available from NTIS)

31. J. R. Wait, and D. A. Hill. "Analysis of the Dedicated Communication Line in a Mine Tunnel for a Shunt-loaded Trolley Wire," IEEE Trans. on Comm., Vol. COM-26, March 1978, pp. 355-361.

32. J. R. Wait, "Quasi-Static Limit for the Propagating Mode Along a Thin Wire in a Circular Tunnel," IEEE Trans. on Ant. and Prop., Vol. AP-25, May 1977, pp. 441-443.

33. P. Delogue, "Basic Mechanisms of Tunnel Propagation," Radio Sci., Vol. 11, April 1976, pp. 295-303.

34. S. F. Mahmoud, and J. R. Wait, "Calculated Channel Characteristics of a Braided Coaxial Cable in a Mine Tunnel," IEEE Trans. on Comm., Vol. COM-24, January 1976, pp. 82-87.

35. J. R. Wait and D. A. Hill, "Propagation Along a Braided Coaxial Cable in a Circular Tunnel," IEEE Trans. on Mic. Th. and Tech., Vol. MTT-23, May 1975, pp. 401-405.

36. L. Deryck, "Control of Mode Conversions on Bifilar Line in Tunnels," The Radio and Elect. Eng., Vol. 45, May 1975, pp. 241-247.

37. J. R. Wait and D. A. Hill, "Guided Electromagnetic Waves Along an Axial Conductor in a Cylindrical Tunnel," IEEE Trans. on Ant. and Prop., Vol. AP-22, July 1974, pp. 627-630.

38. The 1976 URSI Symposium in Amherst, Mass., Commission C/E, Session II was devoted to Telecommunications via Leaky Cables.

39. S. S. Schelkunoff and H. T. Friis, Antenna Theory and Practice, John Wiley, 1952, pp. 408-411.

40. A. Papoulis, The Fourier Intregral and its Applications, McGraw-Hill, 1962, p. 44.

41. J. H. Richmond, "Radiation and Scattering by Thin-Wire Structures in the Complex Frequency Domain," NASA-CR-2396, May 1974 (for sale by NTIS, price $3.25). Also OSU ElectroScience Laboratory Report 2902-10.

42. J. H. Richmond, "Computer Program for Thin-Wire Structures in a Homogeneous Conducting Medium," Report NASA-CR-2399, June 1974. (For sale by NTIS, price $3.75). Also OSU ElectroScience Lab. report 2902-12.

43. Status report dated 30 June 1978 on Contract F19628-77-C-0069.

44. R. J. Lytle, "Measurement of Earth Medium Electrical Characteristics: Techniques, Results, and Applications," IEEE Trans. on Geodetic Electronics, Vol. GE-12, July 1974, pp. 81-101.

45. J. H. Richmond and R.J. Garbacz, "Surface Waves on Periodic Array of Imperfectly Conducting Vertical Dipoles over the Flat Earth," paper submitted to IEEE Trans. on Ant. and Prop.

46. H. B. Tran, "Surface Waves on Periodic Horizontal Structures on a Flat Earth," Report 784659-4, December 1978, The Ohio State University ElectroScience Laboratory, Department of Electrical Engineering; prepared under Contract F19628-77-C-0069, Dept. of the Air Force, Electronic Systems Division, Air Force Systems Command, Hanscom Air Force Base, Mass. 01731.

47. G. Goubau, "Surface Waves and Their Application to Transmission Lines," J. of Appl. Phys., Vol. 21, November 1950, pp. 1119-1128.

48. J. R. Wait and D. A. Hill. "Electromagnetic Fields of a Dielectric Coated Coaxial Cable with an Interrupted Shield - Quasi-Static Approach," IEEE Trans. on Ant. and Prop., Vol. AP-23, September 1975, pp. 679-682.

49. J. R. Wait and D. A. Hill, "On the Electromagnetic Field of a Dielectric Coated Coaxial Cable with an Interrupted Shield," IEEE Trans. on Ant. and Prop., Vol. AP-23, July 1975, pp. 470-479.

50. H. Kikuchi, "Propagation Characteristics Along a Dielectric Coated Cylindrical Conductor Above the Ground," Proc. IEEE, Vol. 66, March 1978, pp. 351-352.

51. H. Chiba, "Studies in Overhead Wire-Goubau Line Above Ground," IEEE Trans. on Mic.Th. and Tech., Vol. MTT-25, February 1977, pp. 83-93.

52. H. Kikuchi, "Wave Propagation Along Infinite Wire Above Ground at High Frequencies," Electrotech. J. Japan, Vol. 2, December 1956, pp. 773-778.

MISSION
of
Rome Air Development Center

RADC plans and executes research, development, test and selected acquisition programs in support of Command, Control Communications and Intelligence (C^3I) activities. Technical and engineering support within areas of technical competence is provided to ESD Program Offices (POs) and other ESD elements. The principal technical mission areas are communications, electromagnetic guidance and control, surveillance of ground and aerospace objects, intelligence data collection and handling, information system technology, ionospheric propagation, solid state sciences, microwave physics and electronic reliability, maintainability and compatibility.

Printed by
United States Air Force
Hanscom AFB, Mass. 01731